Lehigh University
Lehigh Preserve

Fritz Laboratory Reports

Civil and Environmental Engineering

1982

A study of the defects and electroslag welds in the I-79 bridge at meadville, September 1982

John W. Fisher

Alan W. Pense

John D. Wood

Rajen Dias

Follow this and additional works at: http://preserve.lehigh.edu/engr-civil-environmental-fritz-lab-reports

Recommended Citation

Fisher, John W.; Pense, Alan W.; Wood, John D.; and Dias, Rajen, "A study of the defects and electroslag welds in the I-79 bridge at meadville, September 1982" (1982). *Fritz Laboratory Reports.* Paper 514.
http://preserve.lehigh.edu/engr-civil-environmental-fritz-lab-reports/514

This Technical Report is brought to you for free and open access by the Civil and Environmental Engineering at Lehigh Preserve. It has been accepted for inclusion in Fritz Laboratory Reports by an authorized administrator of Lehigh Preserve. For more information, please contact preserve@lehigh.edu.

LEHIGH UNIVERSITY LIBRARIES
3 9151 00942857 0

Lehigh University

Cracking in Electroslag Welds at Meadville

A STUDY OF THE DEFECTS AND ELECTROSLAG WELDS IN THE I-79 BRIDGE AT MEADVILLE

FRITZ ENGINEERING
LABORATORY LIBRARY

by

John W. Fisher

Alan W. Pense

John D. Wood

Rajen Dias

Sainath Venkatachalam

September 1982

Report No. 455-1(82)

Fritz Engineering Laboratory

Technical Report Documentation Page

1. Report No.	2. Government Accession No.	3. Recipient's Catalog No.
FHWA/PA 82-009		

4. Title and Subtitle

A STUDY OF THE DEFECTS AND ELECTROSLAG WELDS IN THE I79 BRIDGE AT MEADVILLE

5. Report Date: June 1982

6. Performing Organization Code:

7. Author(s): John W. Fisher, Alan W. Pense, John D. Wood, Rajen Dias, Sainath Venkatachalam

8. Performing Organization Report No.: Fritz Lab. No. 455-1(82)

9. Performing Organization Name and Address

Fritz Engineering Laboratory, #13
Whitaker Laboratory, #5
Lehigh University
Bethlehem, Pennsylvania 18015

10. Work Unit No. (TRAIS):

11. Contract or Grant No.: 78-13 (FCP No. 63352-A)

12. Sponsoring Agency Name and Address

Pennsylvania Department of Transportation
P.O. Box 2926
Harrisburg, PA 17120

U. S. Department of Transportation
Federal Highway Administration
Washington, D.C. 20590

13. Type of Report and Period Covered: Final Report June 1977 to December 1981

14. Sponsoring Agency Code:

15. Supplementary Notes

Prepared in cooperation with the Pennsylvania Department of Transportation and the United States Department of Transportation, Federal Highway Administration.

16. Abstract

This report presents the results of a detailed investigation of the fatigue and fracture characteristics of samples removed from cracked electroslag weldments of the I79 bridges at Meadville, Pennsylvania. Fatigue crack propagation behavior, fracture toughness, tensile and chemical analyses, metallographic and fractographic studies were carried out on the segments removed from the electroslag groove welds.

The results show that the fatigue crack growth characteristics of the electroslag weldments were about the same as the upper bound growth rate of ferrite-pearlite steels. Hence, the electroslag weldments were comparable to structural steels and other weld processes. The fracture toughness of the weldments was found to be equal or exceed 100 ksi $\sqrt{\text{in.}}$ which would permit nearly full flange thickness cracks to develop without brittle fracture.

Metallographic and fractographic studies were carried out to identify the causes of the cracks in the bridge structure. The cracks were found to result from copper melting from the shoes and contaminating the weld pool. This caused solidification cracking along or near the fusion line at the time of welding. The fractographic studies indicated that some of the crack had grown by fatigue. It was found that the defects and cracks that remain in unspliced joints do not pose a threat to the fatigue and fracture resistance of these joints for the next twenty years at current traffic levels.

17. Key Words	18. Distribution Statement
Cracks, Crack growth rate, Electroslag welds, Fatigue, Fracture toughness, Groove welds, Steel bridges, Metallography, Inspection, Fractography	

19. Security Classif. (of this report)	20. Security Classif. (of this page)	21. No. of Pages	22. Price
		118	

Form DOT F 1700.7 (8-72) Reproduction of completed page authorized

COMMONWEALTH OF PENNSYLVANIA

Department of Transportation

Office of Research and Special Studies

Project 78-13

A STUDY OF THE DEFECTS AND ELECTROSLAG WELDS IN THE I79 BRIDGE AT MEADVILLE

by

John W. Fisher

Alan W. Pense

John D. Wood

Rajen Dias

Sainath Venkatachalam

Prepared in cooperation with the Pennsylvania Department of Transportation and the U. S. Department of Transportation, Federal Highway Administration. The contents of this report reflect the views of the authors who are responsible for the facts and the accuracy of the data presented herein. The contents do not necessarily reflect the official views or policies of the Pennsylvania Department of Transportation or the U. S. Department of Transportation, Federal Highway Administration. This report does not constitute a standard, specification, or regulation.

Lehigh University

Office of Research

Bethlehem, Pennsylvania

June 1982

Fritz Engineering Laboratory Report No. 455-1(82)

TABLE OF CONTENTS

ACKNOWLEDGMENTS

This study was carried out as Pennsylvania Department of Transportation Project No. 78-13 under the sponsorship of the Pennsylvania Department of Transportation and the U. S. Department of Transportation - Federal Highway Administration. The work was carried out at the Fritz Engineering Laboratory and the Whitaker Laboratory of Lehigh University.

The authors wish to acknowledge the assistance provided by the Pennsylvania Department of Transportation throughout this study. Records and details were provided that greatly assisted with the evaluation. Particular thanks are due B. F. Kotalik, Bridge Engineer, for his encouragement and support. Thanks are also due Dr. G. R. Irwin for helpful suggestions and fruitful discussions.

The photographic coverage was provided by Mr. Richard Sopko and the figures by Mr. John Gera and Mrs. Sharon Balogh. The manuscript was typed by Mrs. Ruth Grimes and Mrs. Phyllis Sanko.

1. INTRODUCTION

When a girder in the I79 Glenfield Bridge near Pittsburgh was discovered to have cracked at an electroslag welded splice[1], and subsequent examination of the Brady Street Bridge electroslag weldments revealed numerous cracks[2], other bridges with electroslag welded tension splices were considered suspect[3]. As a result, the Pennsylvania Department of Transportation had other electroslag welded bridges that were known to exist in Pennsylvania examined.

Detailed nondestructive inspections and limited metallographic and material fracture toughness studies were initiated and carried out on three bridges in Pennsylvania[4]. They included the I-79 multiple girder bridges at Meadville in Crawford County which were composed of three simple-span bridges with seven girders in both the northbound and southbound structures. The Meadville Bridges were the first bridge members fabricated with electroslag welds in Pennsylvania. Three of the six spans contained electroslag weldments. Construction had started in 1968, and the structure was opened to traffic in October 1970

Figure 1a shows the Meadville steel framing plan for the southbound structure. Electroslag welds were provided at each flange splice. Since the spans are all simple span structures, only the bottom flange splices are of concern. Figure 1b shows the electroslag groove weld detail used in the Meadville girder groove welds.

The flange thicknesses at the two pairs of groove weld transitions in Span 2 were 1-1/16 in. to 1-7/16 in. and 1-7/16 in. to 1-3/4 in. In

Span 3, the flange thicknesses were 1 in. to 1-1/2 in. and 1-1/2 in. to 1-3/4 in. Figure 1c shows the framing plan for north and southbound spans. The northbound girders were numbered from 1 to 7 in Span 2 and from 8 to 14 in Span 3. Only Span 2 of the southbound structures contained electroslag welds.

Field and laboratory studies revealed significant evidence of defects and cracks in the electroslag welds of the Crawford County Bridges at Meadville[4]. Figure 2 shows the flange tip of northbound girder G1 weld W4A and indicates that slag was left embedded in the flange tip near the fusion line. This was typical of many of the flange tip indications that were observed in the electroslag weldments. Figure 3 shows a lack-of-fusion crack that was found in northbound girder G5 at weld W3B. The most common type of cracking that was detected at the electroslag groove welds is shown in Figs. 4 and 5. These electroslag weld cracks were generally found near the fusion line. They most often occurred on the thin plate side at either the top or bottom surface of the flange. Generally, these cracks followed the grain boundaries and were near the fusion line in the melt-back region of the flange.

The ultrasonic and radiographic nondestructive examination revealed that 48 of the 84 groove welded joints that existed in the bridge tension flanges had detectable signs of cracking in and near the boundaries of the electroslag weldments[4]. Table 1 provides a summary of tension flange groove welded joints with defects. Twenty-two of these defective joints were found to require immediate attention and retrofitting. These joints were retrofitted as Phase I of the retrofit work[4].

The work presented in this report was designed to study the causes of the cracking that developed in the electroslag welds of the Crawford County Bridges. The results of this study were needed to determine what course of action must be taken for the remaining 62 joints that were not retrofitted during Phase I of the retrofit contract.

Most of the cracking was concentrated along the stress concentration line where a tapered transition was used to make the groove welded joint thickness transition. This suggested that fatigue cracking has played a role in the crack formation.

The objectives of this study were:

1. To carry out detailed metallographic and fractographic studies of the cracks contained in the sample cores removed from the Crawford County structures during Phase I of the retrofit work.
2. To carry out basic fatigue crack initiation and crack growth studies on the specimens removed from the structure.
3. To conduct appropriate fracture toughness tests on material in and adjacent to the electroslag weldments. Detailed chemical analysis and other material properties were to be examined in order to assist in evaluating the causes for cracking.
4. To provide recommendations after completing these studies for whatever corrective action and retrofitting is deemed necessary on the remaining 62 electroslag tension flange weldments.

To carry out the objectives of this study, sample cores were removed from 15 of the 22 electroslag welded joints that were bolt spliced in Phase I of the retrofit contract.

Figures 6, 7 and 8 show cores taken from three of the more seriously cracked joints after metallographic preparation and etching of their exterior surface. These cores show the typical fusion line cracking that was commonly found in the electroslag welded joints. Figure 9 shows the core removed from northbound girder G5 weld W3B with the lack-of-fusion crack. As is apparent in this figure, the crack has initially formed at the tip of the flange (flat edge of core), along the fusion line, and then has propagated into the flange. Figures 10 and 11 show a similar condition in the core removed from the northbound girder G4 weld W2A, where a repair weld has been made at the location of the crack.

2. GENERAL SPECIMEN PREPARATION

Fifteen sample cores were removed from the 22 joints that were bolt-spliced in Phase I of the retrofit contract. These sample cores were 4 in. in diameter. The cores were usually centered on the cracks that were observed in order to facilitate testing of the sample. The core samples were removed at the characteristic types of cracks summarized in Table 2. The cores are identified from "A" to "O", in decreasing order of severity of cracking. The girder identity and several core locations can be seen in Fig. 1c. The flange plate thickness on each side of the electroslag weld is shown in Table 2.

The core surfaces were initially metallographically prepared in order to observe the macroscopic and microscopic features of the weldment and the nature of the cracks. The surfaces were ground flat and parallel Extensive photographic evidence was obtained, as can be seen in Figs. 6 to 11. The cores were then press-fitted into machined holes in A36 steel plates and then electron-beam-welded (EBW) into the plates, as shown in Fig. 12. Electron beam welding (EBW) was chosen because of the small width of the weld. This procedure increased the size of the specimen by the additional steel around the cores, to allow for preparation of more samples.

Each plate was then saw cut perpendicular to the welding direction into six or seven rectangular bars of approximately 0.5 in. (13 mm) thickness, as shown in Fig. 13. These bars were then identified by Nos. 1 to 7, along with the core identification letter "A" to "O". Selected bars were notched in the electroslag weld with an electric

discharge machine (EDM) to obtain a good stress concentration to start fatigue cracks. All notches were oriented parallel to the welding direction and along the weld center line or near the fusion line, so that the fatigue crack propagated in the same direction as cracks in the tension flanges in the bridge. Figure 14 shows a schematic of the rectangular bar and the orientation of test samples that were fabricated from these bars. After the EDM notch was completed, one side of each specimen was metallographically ground and polished in order to facilitate observation on the crack. Scribe lines were placed on the polished side to facilitate crack growth measurements.

After fatigue-crack-propagation data was obtained, the cracked specimens were used to obtain fracture toughness data using a three-point bending test. Knife edges were adhesively bonded on either side of the EDM notch in order to hold a clip gauge for the displacement measurements. After the fracture toughness tests, the specimens were used to carry out fractographic studies on the crack surfaces.

3. CHEMISTRY AND TENSILE PROPERTIES

The chemical analysis carried out on the base plate and in zone I and zone II of the weld are summarized in Table 3. The chemical compositions that are reported here depict the overall alloy concentrations and do not give any indication of the manner in which the various elements are dispersed throughout the microstructure. Zone I and zone II weld metal have virtually identical alloy compositions and the chemistry of the weld metal is similar to that of the base plate. (See Fig. 40)

Standard 6.35 mm (.25 in.) buttonhead tension specimens were machined from a selected sample of the cores. The direction tested is shown in Fig. 14. This orientation is the normal direction of applied stress under bridge service loading conditions. The specimens provided for a 25.4 mm (1 in.) gauge length. The standards of ASTM Specification E8[22] were followed in all testing. Tests were run on a 44.5 KN (10,000 lb.) capacity Instron Universal tester.

All tensile tests were conducted at room temperature, and the results are tabulated in Table 4. All weldments tested met the minimum tensile property standards which require the deposited electroslag weld metal to match the properties specified for the base plate (in this case, the base plate was A-36 steel). Two of the specimens failed outside the gauge length and in the base metal, indicating that the weld was stronger than the base plate. The failure of these two specimens was a typical cup and cone type of fracture. The other specimens, which fractured in the weld, had a jagged appearance, since failures were along the columnar grains. Failures were noticed to occur in both zone I and zone II region of the weldment, and their tensile properties were similar.

4. CRACK GROWTH STUDIES

Fatigue behavior and the resulting propagation of cracks is of major concern in the use of electroslag welding in bridges. The fatigue life of a structural component can be considered to be composed of three stages: (1) Fatigue crack initiation, (2) Fatigue crack propagation, and (3) Fracture. Welded joints, regardless of the type of weld and fabrication techniques, have microdiscontinuities. These defects, accompanied by the high stress concentration at geometric details at weld toes and weld ends, can restrict the useful life of the structure if they propagate to a critical size and result in fracture failure. Linear elastic fracture mechanics (LEFM) has been found to be as very successful approach to study fatigue crack initiation and propagation (FCP).

The FCP behavior of steel can be divided into the three regions shown in Fig. 15. The behavior in Region A is associated with a "Fatigue Crack Growth Threshold," i.e. the cyclic stress intensity factor range, ΔK_{Th}, below which cracks do not propagate under large numbers of cyclic stress fluctuations[5]. Region B represents the FCP behavior about ΔK_{Th}, which can be represented by an empirical relationship proposed by Paris[6].

$$\frac{da}{dN} = A\Delta K^n \qquad (1)$$

where a = crack length

N = number of cycles

Δ = stress intensity factor fluctuation

A and n are material constants

Region C is an accelerated crack growth condition that develops before fast fracture.

The fatigue crack propagation studies in this report focused on the characteristics of: (1) The crack growth rate in Region B of FCP behavior (Fig. 15), and (2) the fatigue-crack-growth threshold in Region A.

4.1 Test Setup and Procedure

Cyclic load tests were carried out on two types of specimens: naturally-cracked specimens and EDM notched specimens. Due to material limitations, four-point-bend specimens were utilized for the testing. The Four-point-bend specimen was preferred over three-point-bend specimens, because it provided a uniform moment zone, which allowed the crack to propagate without being influenced by the crack path, the changing bending stress distribution and the different sections of the sample. A schematic of the specimen is shown in Fig. 16. The natural-crack specimens usually had cracks that were at or adjacent to the fusion line and propagated into the weld. The EDM notches were either placed at the weld centerline or adjacent to the fusion line at about the same position as the natural cracks.

The basic technique used was to cycle a specimen at a constant amplitude load fluctuation. The crack length was measured as a function of the number of cumulative cycles. All tests were conducted under room temperature and air conditioning. Testing was carried out in the Amsler High Frequency Vibrophore. Tests were conducted under tension-to-tension, sinusoidal loading, at a frequency of approximately 100 Hertz. Previous studies[7,8] on steel have shown that FCP is not affected by the frequency or form of the cyclic stress-intensity-factor fluctuation when conducted

at room temperature in air. Fatigue crack extension was measured optically with a 50X Garret hairline microscope which had a calibrated micrometer. The complete test setup is shown in Fig. 17. One complete revolution of the micrometer moves the hairline a distance of 0.005 in. The micrometer has 100 dimensions per revolution, allowing an accuracy of measurement of the crack of 0.00005 in. The accuracy of defining the crack tip location by this optical technique is estimated to be 0.0005 in. An automatic digital counter was utilized on the Amsler Vibrophore to record the number of cycles for each crack length measurement.

4.2 Testing Methodology

(a) Crack Propagation Studies

Relatively high stress intensity factor ranges ($\Delta K = 22$ ksi $\sqrt{\text{in.}}$) were required to initiate a crack from the EDM notch. The stress intensity factor range ΔK was calculated using the following expression for the four-point bending condition[9].

$$\Delta K = \sqrt{a}\,\frac{3\Delta PL}{BW^2}\,f\,(a/w) \qquad (2)$$

where a = crack length

ΔP = load range

L = moment arm

B = thickness

w = width

and $f(a/w) = 1.99 - 2.47\,(a/w) + 12.97\,(a/w)^2 - 23.17\,(a/w)^3 + 24.8\,(a/w)^4$

Cracking was enhanced by loading the EDM notch tip in compression (reverse loading). The notch tip experiences a residual tension field when the load is released. This residual tensile stress enhances crack initiation when a cyclic load is applied. The load ratio, R, which is equal to P_{min}/P_{max}, was kept at 0.5 and has been shown to have negligible effect on the rate of crack propagation in Region B [10].

After crack initiation, the load was decreased in steps by approximately 10% until the stress intensity factor range (ΔK) was about 4 ksi $\sqrt{in}$. The load was then kept constant, and crack length and cycles were measured periodically. Testing was stopped when the crack length - width ratio, a/w, was about 0.65 to 0.70.

In the case of naturally cracked specimens, the testing and recording of data were more complicated, especially in the case of specimens which had more than a single growing crack. In all such cases, only the dominating crack was measured, as it was assumed to control the crack growth behavior. The crack length was estimated to be the length of the projection of the crack onto a section perpendicular to the direction of the applied bending stress.

(b) Crack Growth Threshold Studies

Tests were conducted on both EDM notched and natural crack specimens. In the testing of EDM notched specimens, the same methodology as in the crack propagation studies was used. The test was started at a high stress intensity factor range, and the load was reduced in steps of 10% untill at some level, the crack showed no further growth. This defined the

threshold level. Then the load was increased in steps until the crack exhibited growth once again. In this way, for each specimen, an upper and lower bound for the threshold value was established. At the "no-growth" load levels, the test was run for 20 x 10^6 cycles or more to ensure that a true threshold had been established. The load ratio, R, was kept at about 0.75, except in the first test where a load ratio of 0.5 was used. Previous studies [11-16] have indicated that the R ratio has a significant effect on the threshold ΔK value. In general, an increase in R ratio decreases the crack growth threshold value. A high R ratio was used to simulate the residual stresses from welding and the dead load. A maximum ratio of 0.75 was used based on the limitations of the testing apparatus. Three EDM notched specimens were tested, two at an R ratio of 0.75 and one at an R ratio of 0.5.

The main objective of the threshold studies of the natural-crack specimens was to evaluate and compare the natural crack behavior with the EDM notched specimens. The testing was started at low load levels with the natural cracks. Had the same procedure been adopted that was used for the EDM notched specimens, the crack would grow and no longer be a natural crack. After fatigue crack growth, the threshold behavior should be no different from that of the notched samples. The testing was started at low ΔK levels for the natural cracks and the load increased in increments until the crack showed growth. In this manner, a threshold value was established for the natural-crack specimens. A total of seven natural crack specimens were tested. Generally, about 20 to 30 million cycles were applied at each load increment.

4.3 Test Results and Discussion

(a) Crack Propagation Studies

The most commonly used means of evaluating FCP data is a log-log plot of the rate of fatitue crack growth (da/dN) versus the stress intensity factor range, ΔK. In this study, the growth rate was determined by the two point secant method. This consists of taking the slope of the line connecting two points on a "a" versus "N" plot and using that as the slope of the mean point between the two test points. It is expressed as:

$$\left(\frac{da}{dN}\right)_{\bar{a}_i} = \frac{a_{i+1} - a_i}{N_{i+1} - N_i} \tag{3}$$

where $\bar{a}_i = (a_i + a_i + 1)/2$

The ΔK values were also calculated at these mean values of crack size.

A straight line least squares fit to the test data was made using the Paris Power Law. The equation of the line has the form:

$$\log \frac{da}{dN} = \log A + n \, (\log \Delta K) \tag{4}$$

where A and n are regression constants

A computer program was used to evaluate and plot the data. Barsom's upper bound crack growth equation for ferrite pearlite steels[17] is also shown on each test plot and compared with the data and the mean regression line. The upper bound crack growth equation is given as:

$$\frac{da}{dN} = 3.6 \times 10^{-10} \Delta K^{3.0} \quad (5)$$

where a is in inches and ΔK in ksi $\sqrt{in}$.

The least square fit for the individual specimens tested are tabulated in Table 5. Typical computer plots of the crack growth rate versus ΔK test data are summarized in Figs. 18 to 22 for indivdual specimens. The remaining plots are presented in Appendix A. Figures 23 and 24 show all data points for naturally cracked and the EDM notched specimens, respectively. The upper bound crack growth relationship defined in Eq. 5 is plotted on Figs. 18 to 24 and provides a reference with which to compare the fatigue crack growth behavior of the electroslag weldments.

The summary plots shown in Figs. 23 and 24 indicate a wide scatter in the test data. This is particularly true for the natural crack specimens shown in Fig. 23. The irregular crack front caused significant interference with crack growth at the lower levels of crack growth rate. They indicated a higher level of crack growth threshold. Only after significant fatigue crack growth occurred did the crack growth rates start to approach the bound provided by Eq. 5.

The EDM notched specimens summarized in Fig. 24 had much less scatter and were in better agreement with Eq. 5. Most of the test data fell below the crack growth upper bound defined by Eq. 5. However, several specimens exhibited higher rates of growth. This upper bound was defined by the relationship

$$\frac{da}{dN} = 8.4 \times 10^{-10} \Delta K^{3} \quad (6)$$

and is also shown in Figs. 23 and 24. The electroslag welds in the Meadville Bridge appear to provide the same crack growth characteristics as ferrite-pearlite steels. The upper bound crack growth relationship suggested by Barsom (Eq. 5) is in good agreement with most of the test data. A higher rate of crack growth is occasionally possible and can exceed the rate provided by Eq. 5 by 233% (see Eq. 6).

Results from a weld centerline cracked specimen showed that there was no significant difference between the growth rates in other zones of the electroslag weldments.

The variations in the microstructure of the weld metal caused marked differences in the topographic features of the fatigue crack surfaces, as illustrated in Figs. 25 and 26. However, these variations did not influence the crack growth rates markedly, as can be seen by comparing the test data in Figs. 20 and 21.

The natural crack specimens showed more scatter in the test points than the notched specimens, mainly due to the presence of multiple cracks which did not always propagate perpendicular to the bending stress field. The natural crack specimens also showed significantly lower crack growth rates at low ΔK values (less than 10 ksi $\sqrt{\text{in.}}$). At higher ΔK values, the crack growth behavior was similar to that of the notched specimens, because by then, the crack had grown and was similar to the crack in the EDM notched specimens.

(b) Crack Growth Threshold Studies

The lower bound threshold data obtained from the EDM notched specimens and the natural crack specimens is summarized in Fig. 27 and compared with

data published by various investigators[11-16]. All of the natural crack data and most EDM data falls above the ΔK_{Th} value predicted by the equation: $\Delta K_{Th} = 6.4\ (1 - 0.85\ R)$.

Of the seven natural crack specimens tested, only four tests gave a definite value for a lower bound ΔK_{Th}. On two of the other three specimens, crack growth was observed at the lowest load applied level, because the natural crack was larger than estimated. The ΔK value determined from the mean surface crack length was lower than its ΔK based on the mean crack length in the section. However, it was found that the growth rates for these two specimens were consistant with the other natural crack specimens at the same ΔK levels. The other specimen which did not yield any ΔK_{Th} value was loaded in a fashion similar to the EDM notched specimens, starting with a high load and reducing the load until no growth was observed. It was found that the crack exhibited growth at lower ΔK levels than determined in the other natural crack specimens. This appeared to result because the crack had grown enough to be comparable to the cracks in the EDM notched specimens. After the crack surfaces were exposed, it was found that the natural cracks had an irregular profile. All ΔK_{Th} values were recalculated based on the estimated mean natural crack length. These dimensions and threshold values are the ΔK_{Th} values given in Fig. 27.

Figures 28 and 29 show the edge views of two of the natural crack specimens that were tested. The presence of multiple cracks is clearly visible in both figures. Figures 30 and 31 show the branching that developed with these cracks. The crack growth threshold was estimated based on the load level at which none of these cracks which were visible on the specimen surface showed any growth. Figures 32, 33, and 34 show

several of the natural crack profiles that were observed in the specimens. The initial crack length was estimated from the irregular crack profile on the test section.

The crack growth threshold studies showed that the natural crack specimens had a significantly higher threshold value (lower bound ΔK_{Th} of 5 ksi $\sqrt{in.}$) compared to the notched specimens ($\Delta K_{Th} \approx 2.5$ to 3 ksi $\sqrt{in.}$). The higher apparent ΔK values required for crack growth in the natural crack specimens do not appear to reflect a higher threshold value in terms of the material property; they rather indicate the difficulty of modeling the complex crack condition used to calculate ΔK and interpret the test results. All natural cracks showed an initial pattern of growth which was not perpendicular to the stress field. The cracks appeared to follow the grain boundaries of the electroslag welds. The results indicate that the edge crack model can be used to give a conservative prediction of threshold load levels for cracks already existing in the electroslag welds in the Meadville Bridges.

5. FRACTURE TOUGHNESS

Historically, CVN tests have been used in assessing the notch toughness of welds. However, the CVN specimen is small for use on electro-slag welds in that the area tested is the same order of magnitude as the grain size. Efforts have been made during the last two decades to develop alternatives to the impact test for assessment of brittle fracture risk which take into account the applied stress level, material thickness, temperature and defect size. This has resulted in the development of the fracture mechanics approach and the introduction of K_{IC} test for plane strain conditions, and the use of J-integral for elastic-plastic behavior[19].

Unbroken specimens used to obtain FCP data were further utilized in obtaining fracture toughness estimates. Plane strain fracture toughness (K_{IC}) tests which are described in ASTM E399 and which use the concepts of linear elastic fracture mechanics (LEFM) could not be carried out, as specimens did not meet the size requirement for plane strain $B \geq 2.5 \ K_{IC}{}^2/\sigma_{y.s}{}^2$) (where B is thickness, K_{IC} plane strain fracture toughness and $\sigma_{y.s}$, yield strength). Alternately, the J-integral approach was used. The J-integral was originally proposed by Rice and can be defined as a function of the work done in loading per unit of uncracked area[20]. This technique was further developed by Landes and Begley[21]. For a plate containing a deep notch and subjected to pure bending, Rice found that

$$J = \frac{2}{b} \int_{\delta}^{\delta_c} P d\delta_c \qquad (7)$$

where P = load/unit thickness

b = remaining unbroken ligament

δ_c = load line displacement of sample containing a crack

For the case of a three point bend specimen with a span to width ratio of four and with a deep crack ($a/W = 0.6$), the above equation reduces to $J = 2A/Bb$, where A is the area under the load-load point displacement curve up to the maximum load. B is the specimen thickness.

Both Charpy V-notch tests and three point bend test specimens were tested to evaluate the fracture toughness characteristics of the electroslag weldments.

5.1 Charpy V-Notch Tests

Three series of CVN impact tests were conducted on the electroslag weldment. The first series involved the evaluation of the impact properties at -17.8° C (0° F) and 4.4° C (40° F) for specimens notched at the centerline and fusion line, respectively. Standard impact specimens were taken from 1/4 thickness position. The notches were located by etching the weld prior to any cutting. Testing was performed according to ASTM specification E 23[23].

The second series of CVN tests involved determining the nature of the transition temperature range by performing tests over a range of service temperatures of the steel, namely between -40° C (40° F) and 100° C (212° F). The third series of tests involved testing the impact properties of unnotched Charpy specimens which had natural cracks serving as notches.

The CVN impact test results are presented in Table 6. Twelve centerline specimens from eight weldments were tested at -17.8° C (0° F), and the average impact energy absorbed was 21.2 J (15.6 ft-lb.). Two high and two low values were eliminated in the calculation. There is a significant variation in CVN energy absorbed values depending on the location of the specimens. The weld centerline exhibited the lowest impact properties. The CVN energy absorbed values increased when the specimens were located at the weld fusion line. Other references confirm this result[22-26]. This is to be expected when consideration is given to the orientation of the grains with respect to the direction of crack propagation in the Charpy specimen. At the centerline, the crack propagates through the fine grain area (zone I) parallel to the columnar grains. The fracture surface showed a fine columnar structure and energy absorbed values as low as 6.8 J (5 ft-lb.) have resulted. Even when the weld centerline contained coarse grains of zone II, properties were inferior, and the fracture appearance was a coarse columnar structure.

Tests conducted near the fusion line resulted in higher energy absorbed values, since fracture occurred by crack propagation transverse to the length of the columnar grains resulting in a coarse equiaxed fracture appearance, as shown in Fig. 35. The fracture appearance of some fusion line specimens do exhibit a mixed fine and coarse equiaxed grain structure at -40° C, resulting in lower CVN energy values.

Impact tests were also performed over a service temperature range of -40° C to 100° C (212° F). The results of these tests are plotted as energy-transition temperature curves shown in Fig. 36. Smooth curves

were drawn through the average values at each temperature for both fusion line and centerline specimens. The wide scatter in energy absorbed values at each temperature depicts the anisotropy of the weldment. Such directional variation is expected, since the columnar grains can have different orientations from the direction of crack propagation.

The three unnotched specimens which had natural cracks serving as notches at the fusion line showed high toughness values, because the natural cracks were not perpendicular to the CVN specimen length.

5.2 Fracture Toughness Tests

In this study an Instron Testing Machine was used to obtain the fracture toughness data. The load-displacement curve was recorded on an X-Y recorder built into the instrument. A three point bend fixture was utilized with a span to width ratio of four. The displacement gauge was seated on the specimen to which knife edges were adhesively bonded on either side of the crack. The apparatus is shown in Figs. 37a and 37b. Specimens were tested at temperatures ranging from -40° C to 100° C (40° F to 212° F). After the load-displacement curve was recorded, the specimens were cooled in liquid nitrogen and broken open. The uncracked ligament "b" measured from the end of the fatigue crack extension, and "B", the specimen thickness was measured. The area under the curve is calculated up to the point where the load drops suddenly indicating unstable crack extension. Figure 38 shows a typical load-displacement curve and how the area was measured. The J-integral calculated can be related to the linear elastic fracture toughness K_j by the equation 8.

$$K_j = (JE)^{1/2} \quad (8)$$

The results are tabulated in Table 7. The average stress intensity factor K_J, as calculated from the J-integral value was 140 ksi $\sqrt{in.}$ at -17.8° C (0° F).

Figure 39 summarizes the results of the fracture toughness tests. A lower bound to the fracture toughness data is provided by the solid line. The minimum fracture toughness of the Meadville Bridge electroslag weldments is about 110 ksi $\sqrt{in.}$ This appears to be a reasonable lower bound for use in estimating the critical crack size in the Meadville Bridges.

The wide scatter in values of K_J obtained can be attributed to the orientation and size of the coarse columnar crystals of zone II. The weld centerline showed the lowest toughness value. This is because the crack propagates through zone I parallel to the columnar grains

6. METALLOGRAPHY OF ELECTROSLAG WELDS

The high heat input, the slow solidification and cooling rates experienced because of the welding method results in an outer coarse columnar grain structure (zone II) in the weldment. The interior zone consists of thin elongated columnar crystals (zone I). Paton[23] describes four different types of grain structure arrangements that can be produced in electroslag weldments, as shown in Fig. 40. All weldments studied were either of Type I with coarse and fine columnar crystal zones or Type III with only a coarse columnar zone. The relative amounts of coarse and fine columnar crystal structures vary from specimen to specimen. Figures 41 and 42 show the macrostructure in the transverse plane of Type III and Type I weldments, respectively. The Zone II crystals start to solidify at the fusion line, grow inwards and in the direction of the welding, as seen in Figs. 6 to 10, which shows a longitudinal section of the weld. The equiaxed central zone is zone I, which is a fine columnar grain structure oriented parallel to the welding direction.

Between the fusion line and the base metal, two heat-affected zones (HAZ) occur and are illustrated in Figs. 43 and 44. HAZ I is a zone of grain coarsening that occurs because of overheating experienced during welding. The grain size decreases steadily away from the fusion line, as HAZ II approaches, which appears light in the macrostructure shown in Fig. 41 and is a region of grain refinement.

In the microstructure of zone II shown in Fig. 45, the prior austenite grain boundaries are seen as a network of ferrite bands. In

some regions the ferrite is seen as long acicular plates. The size and distribution of ferrite and pearlite within the primary crystal boundaries is known as the secondary structure, and Figs. 45 and 46 show pearlite (dark) surrounded by ferrite (light) distributed in a Widmanstatten pattern and by grain boundary ferrite. This Widmanstatten ferrite is characterized by its acicular appearance and is a nonequilibrium phase. The secondary structure appearing in zone I weld metal as illustrated in Fig. 47 is usually considerably coarser than that of zone II weld metal. This is because of the formation of larger deposits of ferrite in zone I as a result of the slower cooling rate that it experiences during the austenite transformation. Figures 6, 7, 8, 48, 49, and 50 show the cracks and branching that was observed.

In seven naturally cracked specimens, copper was found. Figure 51 shows a scanning electron micrograph of copper along the crack. An energy dispersive spectrum (EDS) shown in Fig. 52 confirms the presence of copper. Copper globules were occasionally observed near the surface of the weld, and cracks were observed to have emanated from every one of them, as illustrated in Fig. 53 and verified by an EDS shown in Fig. 54. Obviously, the solid copper shoes used to contain the molten slag and weld pool got heated to high enough temperatures to cause incipient melting of the shoes and contamination of the weld pool. Consequently, during solidification of the weld, cracks occurred along the ferrite bands and were filled with the molten copper, as shown in Fig. 55. The melting of the copper shoe was probably due to insufficient slag depth during welding.

7. FRACTOGRAPHIC STUDIES

The fractured surfaces of the fatigue crack propagation specimens were exposed after the fracture toughness tests. The specimens were ultrasonically cleaned in a bath of acetone. Replicas were sequentially stripped from the crack surfaces to remove as much of the corrosion products as possible. The fracture surfaces were viewed on a scanning electron microscope to observe the general morphology of the fracture and to characterize the nature of the natural cracks.

Transmission electron microscope studies were carried out on replicas stripped from regions near the natural crack tips. The replicas were shadowed with chromium before being carbon-coated to enhance the contrast. The main aim of the study was to examine the possibility of fatigue crack propagation at the crack tips.

Examination of the fractured surfaces in the scanning electron miscroscope (SEM) showed that the natural cracks were severly corroded, and any fine detail of the fracturing processes was obliterated. Figure 56 shows the intergranular crack along the long columnar grains. Corrosion products mask most of the microscopic dtails. Figure 57 is a SEM fractograph of the end of a natural crack in Core N. The bottom left region of the fractograph shows a cleavage fracture that resulted when the specimen was broken open at liquid nitrogen temperature. Figure 58 shows a dendritic structure of a copper deposit detected on the grain boundary of the columnar grains near the weld surface. The copper was apparently introduced when the solid copper shoes melted. An energy dispersive spectrum

of the dendritic region, Fig. 59 confirms the presence of copper. Fatigue striations in the weld metal obtained during the fatigue crack propagation test are shown in Figs. 60 and 61 for Cores D and E. The striation spacing was 4×10^{-6} in./cycle. The fatigue crack propagation surface is unusually uneven, and this may partly be attributed to the anisotropic nature of the microstructure. TEM examination of the replicas taken from the natural crack surfaces indicated mainly corrosion products. There were, however, isolated regions near the crack tip where fatigue striations were detected. Figures 62 and 63 show fractographs from Core N. The measured striation spacings in the two specimens were 3.5×10^{-6} in. and 2.76×10^{-6} in.

The striation spacings can be used to estimate the corresponding ΔK values at the crack tip using the Hertzberg and VonEuw relationship[27]

$$\Delta S = 24 \left(\frac{\Delta K_e}{E} \right)^2 \qquad (9)$$

where ΔS = spacing in/cycle

ΔK_e = effective stress intensity range, ksi $\sqrt{\text{in.}}$

= $(0.5 + 0.4\ R)\ \Delta K$

Since the dead-live load ratio in the bridge is about 0.5, $\Delta K_e = 0.7\Delta K$. This yielded ΔK values between 7 and 8 ksi $\sqrt{\text{in.}}$ when equated to the striation spacing.

If the striation spacing is equated to Eq. 5, a stress intensity range of about 20 ksi $\sqrt{\text{in.}}$ results. Equation 6 would yield 15 ksi $\sqrt{\text{in.}}$

The large stress intensity ranges suggested by the striation spacing is caused by the fact that only the high stress range cycles create visible striations. Smaller stress cycles which advance the crack tip and increase the spacing between the large visible striations do not create detectable striations.

The crack depth in Core N, where the striations shown in Figs. 62 and 63 were observed, was about 0.25 in. deep. Using an edge crack model for the irregular surface crack and equating the stress intensity factor range obtained by Eqs. 5, 6, and 9 would suggest maximum stress ranges equal to the numerical value to ΔK. It is possible that a maximum stress range of 7 or 8 ksi would occur, but higher stress ranges are not likely. This further confirms the overestimate of the striation spacing which results from random variable loading.

The surface condition of much of the natural cracks was obscured by a layer of general corrosion products. This corrosion layer could be removed by mechanical stripping of the surface with cellulose acetate tape, the final result being that all loose surface oxide was removed. In this operation, the tape is moistened with acetone and pressed onto the opened natural crack surface. After the acetone has evaporated, the tape is pulled from the surface, taking the adhering oxide with it. Successive repetitions of this process result in cleaning, after which removing surface features are seen. If corrosion is extensive, however, the original surface features may no longer be observable.

Figures 64 through 67 show SEM fractographs of such areas. Figures 64 and 65 show crack surfaces covered by heavy corrosion product (without stripping). The true surface features are completely obscured. Figures

66 and 67 show two cleaned areas, with most of the corrosion products removed. The true surface features are still obscured by corrosion pits and oxidation attack. Such conditions are typical of old fracture surfaces, especially when they have been exposed to the atmosphere. The regions at the crack tip, especially if the crack is tight, are most likely to retain true surface features.

8. ANALYSIS OF CRACKS IN THE STRUCTURE

The cracks in the girder flanges of the Meadville Bridges mainly occur near the fusion line at the weld transition in thickness, as was illustrated in Figs. 2, 3, 4, and 5. These cracks were irregular and branched along the grain boundaries which can be seen in Figs. 6, 7, and 8. The crack shape indicates that the cracks can be conservatively modeled as edge cracks. Hence, the stress intensity factor will be estimated as:

$$K = 1.12\ \sigma\sqrt{\pi a}\ \sqrt{\sec\frac{\pi a}{2t}} \qquad (10)$$

where a = depth of crack

t = flange thickness

The cracks seen in Figures 2, 3, 4, and 5 indicate that the front and back free surface corrections used in Eq. 10 are reasonable factors. Their use is consistent with observations and previous estimates of the stress intensity factor for this type of crack condition. A greater degree of accuracy is not needed in estimating the stress intensity factor.

The ΔK values calculated from the striation spacing indicated that the 0.25 in. deep cracks in Core N were subjected to a stress range of 7 to 8 ksi. This seems a reasonable level of maximum stress range. Measurements on similar bridge structures have demonstrated that the maximum stress range in service is seldom equal to the design stress range[28]. Since only the largest striations are visible on the crack surface, the measured spacing is larger than it should be. It is probable that the actual stress range is smaller than 7 or 8 ksi.

Table 8 summarizes the crack conditions that were observed in several of the cores. The correlation of the crack size and ultrasonic Db response

is not very good. The apparent reason for the wide variation is because of the irregular nature of the natural cracks and the fact that most exhibited significant branching.

If Eq. 10 is equated to the lower bound fracture resistance of 110 ksi $\sqrt{in.}$, nearly full thickness fatigue cracks can develop before crack instability is predicted.

Figure 68 shows the average daily truck traffic observed between 1970 and 1977. This indicates that the truck traffic has stabilized at about 800 vehicles per day. Two extrapolated conditions are also plotted in Fig. 68. One assumes a static condition with no increases in traffic. The second condition provides for modest growth of 3% per year. At 800 trucks per day, 292,000 cycles will accumulate each year.

The traffic conditions and the fatigue and fracture characteristics of the electroslag weld joints indicate that none of the remaining cracks in the Meadville Bridges pose a serious threat for the next ten years. The amount of crack propagation is likely to be negligible, as the remaining cracks are small (see Table 1b). Indeed, it is possible that little significant growth will occur in the twenty year period to 2000 A.D.

It is not anticipated that repair or reinforcement of the remaining joints will be required before that time. A precedent procedure would be for a thorough review of the condition of the bridge to be undertaken in 1990 and 2000. Visual and ultrasonic examination of blast cleaned joints should provide information on the condition of the cracked joints and permit development of a strategy for repair should such be necessary. For intermediate periods (i.e. during biyearly inspections) it is advisable to make a visual observation of the joints listed in Table 1b as is convenient.

9. SUMMARY AND RECOMMENDATIONS

The examination, tests and analysis of the results of the electroslag weldments and discontinuities in the I79 bridges at Meadville has provided the following observations and recommendations.

a. Summary of Observations

1. Most of the cracks in the electroslag groove welds appear to have resulted from copper melting from the shoes and contaminating the weld pool. This caused solidification cracking along or near the fusion line at the time of welding.

2. Some evidence of fatigue crack growth was detected in a few of the weld core samples. However, most of the crack surfaces were so severely corroded that the details of the cracking process were obliterated. The fact that the cracks were introduced at the time of fabrication meant that the crack surfaces were exposed and susceptible to corrosion for a significant length of time.

3. The fatigue crack growth rate of the electroslag weldments was found to be reasonably represented by the upper bound growth rate of ferrite-pearlite steels. Only one or two samples provided a higher rate of crack propagation. The evidence suggests that the fatigue crack propagation behavior of the electroslag welds is directly comparable to structural steels and other weld processes.

4. The apparent crack growth threshold of the natural cracks in the electroslag weld metal is higher than a notched specimen with a single fatigue crack front. Crack branching and inclination increase the apparent threshold, since the complex crack cannot be accurately modeled.

5. The minimum fracture toughness of the electroslag welds at Meadville is about 110 ksi $\sqrt{in.}$ for the minimum anticipated service temperature.

6. The test results indicate that nearly full flange thickness cracks would need to develop before brittle fracture could occur.

b. Recommendations

1. The defects and cracks that remain in the electroslag weld joints of the Meadville Bridge structures do not pose a threat to the fatigue and fracture resistance of these joints for the next twenty years at the current level of truck traffic. Hence, there is no need to splice the remaining joints until the end of this century.

2. It is recommended that a detailed examination of these joints be carried out in 1990 and 2000. This should include ultrasonic examination of the unspliced joints and visual examination of the blast cleaned groove weld .

3. The usual periodic biyearly bridge inspections should include a visual check of the joints tabulated in Table 1b.

Table 1: SUMMARY OF JOINTS IN CRAWFORD COUNTY BRIDGE AT MEADVILLE WITH DEFECTS

a) Joints With Large Defects

Southbound Bridges		Northbound Bridges	
Joint**	UT Rating*	Joint	UT Rating*
G1W4	+6	G3W2	R, + 2
G2W1	R, + 6	G3W4	R
G3W1	R, + 6	G5W1	R
G3W2	R, + 2	G5W2	R, + 9
G3W4	R, - 2	G5W3	R, - 1
G5W1	No defect in 9/24/80 PTL	G5W4	R
G5W4	R, 0	G6W1	R
G6W1	R	G6W4	R
G6W3	R, 0	G7W3	-4
G6W4	R, + 4	G11W4	R, + 2
G7W2	R, + 10	G13W3	R, + 16
G7W3	R + 36		

b) Joints With Small Defects

G1W1	+8	G1W3	+8	G10W1	+12
G1W3	R, + 12	G1W4	R	G10W3	+8
G2W2	+16	G2W2	R	G11W1	+10
G2W3	+8	G3W1	+6	G11W2	+4
G2W4	+8	G3W3	+10	G13W1	+8
G3W3	+16	G4W1	+10	G13W2	+12
G4W1	R, + 10	G4W3	+14	G13W4	+8
G4W2	+2	G4W4	R	G14W2	+16
G4W4	+4	G6W2	+5	G14W3	+16
G5W2	R, + 8	G8W1	+12	G14W4	+12
G5W3	+6	G8W2	+15		
G6W2	+10	G9W1	+8		
G7W1	+2	G9W2	+6		
G7W4	+6	G9W4	+12		

*R indicates radiographic defect
** shop drawing designation

TABLE 2: LOCATION OF SAMPLE CORES
REMOVED FROM THE MEADVILLE BRIDGE

Shop Dwgs. Designation	Lab. Designation	4 in. Core Location*		Flange Thickness at Joint
SB G5W4B	A	Center on thin FL	5 in. from tip	1 7/16 - 1 3/4
SB G1W3B	B	Center on existing crack	8 in. from tip	1 7/16 - 1 3/4
SB G6W1A	C	Center on thin FL	5 in. from tip	1 1/16 - 1 7/1
NB G5W3B	D	Center on thick FL	2 in. from tip	1 7/16 - 1 3/4
SB G3W1A	E	Center on thin FL	5 in. from tip	1 1/16 - 1 7/1
SB G2W1A	F	Center on weld	6 in. from tip	1 1/16 - 1 7/1
NB G11W4A	G	Center on thin FL	1-3/4 in. from tip	1 - 1 1/2
NB G6W4A	H	Center on thin FL	1-3/4 in. from tip	1 1/16 - 1 7/1
NB G3W2A	I	Center on thin FL	4 in. from tip	1 7/16 - 1 3/4
NB G13W3B	J	Center on weld	3 in. from tip	1 1/2 - 1 3/4
NB G5W2A	K	Center on thick FL	2 in. from tip	1 7/16 - 1 3/4
NB G6W1A	L	Center on thin FL	1-3/4 in. from tip	1 1/16 - 1 7/1
SB G3W2B	M	Center on thin FL	2-1/2 in. from tip	1 7/16 - 1 3/4
SB G6W3A	N	Center on thin Fl	3 in. from tip	1 7/16 - 1 3/4
SB G7W2B	O	Center on thin plate FL	4* in. from tip	1 7/16 - 1 3/4

*Center of core

FL = Fusion Line

TABLE 3

CHEMICAL ANALYSIS OF THE WELDMENT AND BASE PLATE

Sample Element	Base Plate	Weld Zone II	Weld Zone II	Weld Zone I	A-36 Plate
Mn	0.830	1.160	1.100	1.350	1.2 max.
Ni	0.044	0.038	0.024	0.026	-
Cr	0.010	0.033	0.021	0.010	-
Cu	0.240	0.170	0.120	0.110	-
Mo	0.005	0.005	0.005	0.005	-
V	0.010	0.010	0.010	0.010	-
Al	0.010	0.010	0.010	0.010	-
C	0.170	0.660	0.170	0.160	.12 max.
P	0.009	0.010	0.020	0.009	.04 max.
S	0.035	0.038	0.024	0.022	.05 max.
Si	0.280	0.160	0.190	0.190	-

TABLE 4

TENSILE PROPERTIES OF THE WELDMENT AT ROOM TEMPERATURE

Specimen	Yield Strength		Ultimate Strength		Percentage Elongation	Percentage Reduction in Area
	MPa	KSI	MPA	KSI		
G21	329	47.7	499	72.4	22.5	47.6
H21	380	55.1	576	83.5	*	64.0
I41	334	48.4	490	71.0	20.0	51.4
I42	348	50.5	531	76.9	24.0	59.1
I51	347	50.3	501	72.7	24.5	52.8
I52	314	45.5	489	70.9	22.9	62.9
K42	357	51.7	529	76.8	23.1	51.0
K41	340	49.3	499	72.3	25.5	54.1
051	312	45.2	477	69.2	26.7	62.1
052	348	50.5	520	75.4	26.6	64.0
G1	303	43.9	446	64.7	25.7	64.5
H1	344	49.9	516	74.8	*	64.0
A36	248 min	36 min	400 to 552	58 to 80	20 min.	-

* Specimens failed outside the gauge length.

TABLE 5. LEAST SQUARES FIT TO THE
FATIGUE CRACK PROPAGATION RATES OF ELECTROSLAG WELDMENTS

Specimen	Nature of Crack	Location	FCP Rate* (in/cycles)
A2	Natural	Fusion Line	$3.28 \times 10^{-10} \Delta K^{2.68}$
A3	Natural	Fusion Line	$4.98 \times 10^{-13} \Delta K^{5.16}$
B2	Natural	Fusion Line	$2.09 \times 10^{-9} \Delta K^{0.91}$
C6	Natural	Fusion Line	$2.31 \times 10^{-14} \Delta K^{5.63}$
F3	Natural	Fusion Line	$3.79 \times 10^{-11} \Delta K^{2.49}$
E3	Notched	Fusion Line	$7.81 \times 10^{-10} \Delta K^{2.44}$
E5	Notched	Fusion Line	$6.06 \times 10^{-11} \Delta K^{3.4}$
J2	Notched	Fusion Line	$2.71 \times 10^{-8} \Delta K^{1.29}$
J4	Notched	Center Line	$2.03 \times 10^{-10} \Delta K^{3.06}$
M2	Notched	Fusion Line	$4.03 \times 10^{-10} \Delta K^{2.89}$
M3	Notched	Fusion Line	$2.57 \times 10^{-11} \Delta K^{3.91}$
M4	Notched	Fusion Line	$7.48 \times 10^{-11} \Delta K^{3.21}$
N3	Notched	Fusion Line	$6.19 \times 10^{-13} \Delta K^{4.81}$
O3	Notched	Fusion Line	$1.03 \times 10^{-9} \Delta K^{2.04}$

*ΔK in Ksi$\sqrt{in}$

TABLE 6

CHARPY IMPACT TESTS OF THE WELDMENT

Specimen	Position	Types of Grains	Temperature °C	Energy Absorbed J (ft.lbs.)
A3	Centerline	Zone I	-40	11.5 (8.5)
E3	"	"	"	12.2 (9.0)
D4	"	"	"	9.5 (7.0)
K7	"	Zone II	"	27.1 (20.0)
Average	"	-	"	15.1 (11.1)
03	Fushionline	Zone II	"	30.5 (22.5)
J2	"	"	"	8.1 (6.0)
B3	"	"	"	19.0 (14.0)
N4	"	"	"	29.2 (21.5)
Average	"	"	"	21.7 (16.0)
A6	Centerline	Zone I	-17.8	19.7 (14.5)
E3	"	"	"	23.7 (17.5)
N3	"	Zone II	"	16.3 (12.0)
D4	"	Zone I	"	17.6 (13.0)
I7	"	"	"	27.8 (20.5)
I7	"	"	"	19.7 (14.5)
J6	"	"	"	26.4 (19.5)
J6	"	"	"	6.8 (5.0)
N6	"	Zone II	"	9.5 (7.5)
N6	"	"	"	54.2 (40.0)
07	"	Zone II	"	43.4 (32.0)
07	"	"	"	18.3 (13.5)
Average	"	-	"	23.6 (17.5)
03	Fushionline	Zone II	-17.8	34.6 (25.5)
J2	"	"	"	31.2 (23.0)
B3	"	"	"	71.9 (53.0)

TABLE 6 - Continued

Specimen	Position	Types of Grains	Temperature °C	Energy Absorbed J (ft.lbs.
NA	"	"	"	42.0 (31.0)
Average	"	"	"	42.2 (33.1)
A3	Centerline	Zone I	4.4	35.9 (26.5)
E3	"	"	"	31.2 (23.0)
02	"	Zone II	"	35.9 (26.5)
N3	"	"	"	54.9 (40.5)
Average	"	-	"	39.5 (29.)
K5	Fusionline	Zone II	"	42.1 (31.0)
K6	"	"	"	23.0 (17.0)
A7	"	"	"	64.4 (47.5)
E5	"	"	"	70.5 (52.0)
D5	"	"	"	27.1 (20.0)
D5	"	"	"	131.5 (97.0)
D7	"	"	"	88.1 (65.0)
D7	"	"	"	37.3 (27.5)
M5	"	"	"	122.0 (90.0)
M5	"	"	"	98.9 (73.0)
M7	"	"	"	73.9 (54.5)
M7	"	"	"	64.4 (47.5)
H	"	"	"	48.8 (36.0)
H	"	"	"	52.2 (38.5)
H	"	"	"	33.9 (25.0)
G	Fusionline	Zone II	4.4	87.5 (64.5)
G	"	"	"	55.6 (41.0)
G	"	"	"	46.8 (34.5)
G	"	"	"	82.0 (60.5)
Average	"	"	"	65.8 (48.5)
A6	Centerline	Zone I	26.7	57.0 (42.0)

TABLE 6 - Continued

Specimen	Position	Types of Grains	Temperature °C	Energy Absorbed J (ft.lbs.)
E4	"	"	"	43.4 (32.0)
K7	"	"	"	54.0 (40.0)
03	"	Zone II	"	81.4 (60.0)
N21	"	"	"	82.7 (61.0)
N71	"	"	"	58.3 (43.0)
J71	"	Zone I	"	14.9 (11.0)
061	"	Zone II	"	62.4 (46.0)
Average	"	-	"	56.8 (41.9)
E5	Fushionline	Zone II	"	81.4 (60.0)
K5	"	"	"	58.3 (43.0)
K6	"	"	"	88.1 (65.0)
I21	"	"	"	93.6 (69.0)
D61	"	"	"	82.0 (60.5)
K21	"	"	"	63.7 (47.0)
M61	"	"	"	90.2 (66.5)
Average	"	"	"	79.6 (58.7)
N22	Centerline	Zone II	49	69.8 (51.5)
J72	"	Zone I	"	31.2 (23.0)
J52	"	"	"	62.4 (46.0)
042	"	Zone II	"	74.6 (55.0)
Average	"	-	"	59.5 (43.9)
I31	Fushionline	Zone II	"	105.8 (78.0)
K31	"	"	"	103.1 (76.0)
D62	"	"	"	123.4 (91.0)
M62	"	"	"	131.5 (97.0)
Average	"	"	100	115.9 (85.0)
N72	Centerline	Zone I	"	97.6 (72.0)

TABLE 6 - Continued

Specimen	Position	Types of Grains	Temperature °C	Energy Absorbed J (ft.lbs.)
J51	"	"	"	81.4 (60.0)
062	"	Zone II	"	99.7 (73.5)
041	"	"	"	103.7 (76.5)
Average	"	-	"	95.6 (70.5)
I32	Fushioline	Zone II	"	104.4 (77.0)
K32	"	"	"	99.0 (73.0)
I22	"	"	"	122.0 (90.0)
K22	"	"	"	100.3 (74.0)
Average	"	"	"	106.4 (78.5)
A7	Natural crack	"	4.4	80.0 (59.0)
NA	"	"	"	183.0 (135.0)
N5	"	"	"	264.4(195.0)

TABLE 7

FRACTURE TOUGHNESS OF WELDMENTS*

Specimen	Temperature	J = 2A/Bb		$K_J = \sqrt{JE}$	
	°C	KN/M	(lb/in)	M Pa $\sqrt{m}$	Ksi $\sqrt{in}$
A2	-17.8	90.2	515	137	124.3
B2	"	7.13	407	121	110.5
B6	"	195.9	1119	201	183.3
C6	"	199.8	1141	203	185.0
D2	"	217.0	1239	212	192.8
D3	"	154.5	882	179	162.7
ES	"	195.8	1118	201	183.2
F3	"	99.1	566	143	130.3
K5	"	226.8	1295	217	197.1
K7	"	13.1	75	52	47.4
M2	"	163.7	935	184	167.5
M3	"	244.1	1394	225	204.5
M4	"	135.7	775	166	152.5
N3	"	80.6	460	129	117.5
O3	"	304.0	1736	251	228.2
Average	"	159.5	911	156	141.0
J4	"	29.8	170	79	71.4
A3	-40	71.8	410	122	111.0
A5	"	251.8	1438	228	207.7
D4	"	101.4	579	145	131.8
E3	"	50.4	288	102	93.0
I6	"	24.0	137	71	64.3
K6	"	149.6	854	176	160.1
O2	"	133.8	764	166	151.4
Average	"	111.9	639	144	131.0

TABLE 7 - continued

Specimen	Temperature	J = 2A/Bb		$K_J = \sqrt{JE}$	
	^oC	KN/M	(lb/in)	M.Pa $\sqrt{m}$	Ksi $\sqrt{in}$
E4	21.1	343.5	1956	266	(242.3)
J2	21.1	351.5	2007	270	(245.4)
Average	21.1	347.1	1982	268	(243.8)

*All specimens are notched at the fusion line except J4 which is notched at the centerline.

TABLE 8. CRACK SIZE IN CORE

Core	Location	Variation in Crack Depth, in.	Average Crack Depth, in.	NDT* UT Db Rating
A	SB G5W4	0.14 to 0.36	0.21	0
B	SB G7W3	0.24 to 0.45	0.35	+6
C	SB G6W1	0.12 to 0.28	0.20	+5
D	NB G5W3	0.10 to 0.70	0.15	-1
E	SB G3W1	0 to 0.15	0.12	+6
F	SB G2W1	0.18 to 0.35	0.27	+6
N	SB G6W3	0.10 to 0.25	0.15	0

*All cracks were apparent on the radiographs. The ultrasonic DB levels were obtained with 60 and 70° probes. The cores were not necessarily removed at the location of maximum response.

NOTE: No significant cracks were apparent in the other cores.

REFERENCES

1. ENR
   Cracked Girder Closes I-79 Bridge,
   Engineering News Record, February 10, 1977

2. Grata, J.
   Cracks Found in Unfinished Brady Street Bridge,
   Pittsburgh Press, May 25, 1977.

3. Lindberg, H.A.
   FHWA Notice N5040.23, Electroslag Welding,
   February 16, 1977.

4. Fisher, J.W.; Pense, A.W.; Wood, J.D.; and Somers, B.R., "An Evaluation of Electroslag Welds in Three Bridges," Fritz Engineering Laboratory Report 438-1(81), Lehigh University, Bethlehem, PA.

5. Harrison, J.D.
   "An Analysis of Data on Non-Propagating Fatigue Cracks on a Fracture Mechanics Basis", British Welding Journal, Vol. No. 3, pp. 94-98, March 1970.

6. Paris, P.C., and Erdogan, F., "A Critical Analysis of Crack Propagation Laws", Transactions of the ASME, Journal of Basic Engineering, Series D, 85, No. 3, pp 528-534, 1963.

7. Barsom, J.M., "Corrosion Fatigue Crack Propagation below K_{ISCC}", Journal of Engineering Fracture Mechanics, 3 No. 1 July 1971.

8. Barsom, J.M., "Effect of Cydic Stress Form on Corrosion Fatigue Crack Propagation Below K_{ISCC} in a High Yield Strength Steel", in Corrosion Fatigue: Chemistry, Mechanics and Microstructure, International Corrosion Conference Series, Volume NACE-2, National Association of Corrosion Engineers, Houston, 1972.

9. Tada, H.; Paris, P.C., Irwin, G.R., The Stress Analysis of Cracks Handbook, Del Research, Hellertown, PA (1973).

10. Barsom, J.M., "Fatigue Crack Growth Under Variable Amplitude Loading in ASTM A514 Grade B steel ASTM STP 536", American Society for Testing and Material, Philadelphia, PA (1973).

11. Bucci, R.J.; Clark, W.G., Jr.; and Paris, P.C., "Fatigue-Crack Propagation Growth Rates Under a Wide Variation of ΔK for an ASTM A517 Grade (T-1) Steel". Stress analysis and growth of cracks, ASTM STP 513, (1972).

12. Schmidt, R.A., "A Threshold in Metal Fatigue", Master of Scinece Thesis, Lehigh University (1970).

13. Paris, P.C., "Testing for Very Slow Growth of Fatigue Cracks," MTS Closed Loop Magazine, Vol. 2, No. 5 (1970).

14. Harrison, J.D., "An Analysis of Data on Non-Propagating Fatigue Cracks on a Fracture Mechanics Basis." Brit. Welding Journal, Vol. 2 No. 3 (March 1970).

15. Pook, L.P., "Fatigue Crack Growth Data for Various Materials Deduced From the Fatigue Lives of Pre-Cracked Plates." Stress Analysis and Growth of Cracks, Proc. 1971 National Symposium on Fracture Mechanics, Part I; ASTM STP 513 (1972).

16. Paris, P.C.; Bucci, R.J.; Wessel, E.T.; Clark, W.G., and Mager, T.R., "Extensive Study of Low Fatigue-Crack-Growth Rates in A533 and A508 Steels," Stress Analysis and Growth of Cracks, Proc. 1971 National Symposium on Fracture Mechanics Part I; ASTM STP 513 (1972).

17. Barsom, J.M., "Fatigue-Crack Propagation in Steels of Various Yield Strengths." J. Eng. Industry, Series B, Vol. 93, No. 4 (Nov. 1971), pp. 1190-1196.

18. ASTM A8, Tension Testing of Metallic Materials, ASTM Standards, Part 10, 1979.

19. Rice, J.R., Journal of Applied Mechanics, Transactions ASME, Vol. 35 pp. 379-386, June 1968.

20. Rice, J.R., Paris, P.C. and Merkle, J.G., "In Progress in Flaw Growth and Fracture Toughness Testing," ASTM, STP 536, pp. 231-245 ASTM 1973.

21. Landes, J.D. and Begley, J.A., "Test Results from J-Integral Studies, An Attempt to Establish a J_{IC} Testing Procedure," ASTM STP 530, pp. 170-186, ASTM 1975.

22. Campbell, H.C., "Electroslag, Electrogas and Related Welding Processes," WRC Bulletin, No. 154, pp. 14-16, Sept. 1970.

23. Paton, B.E., "Electroslag Welding of Very Thick Materials," Welding Journal, Vol. 41, pp. 115-122, Dec. 1962.

24. Woodley, C.C., Burkekin, F.M., and Wells, A.A., "Electroslag Welded Wide Plate Tests on 3" Thick Mild Steel," British Welding Journal, Vol. 45, pp. 165-193, March 1966.

25. Culp, J.D., "Electroslag Weldments - Performance and Needed Research," Welding Journal, Vol. 59 pp. 27-42, July 1979.

26. Benter, W.P., Schilling, G.C., "Acceptance Criteria for Electroslag Weldments in Bridges," National Cooperative Highway Research Program Report 201, May 1979.

27. Hertzberg, R.W. and VonEuir, E.F.J., "Crack Closure and Fatigue Striations in 2024-T3 Aluminum Alloy," Metallurgical Transactions, Vol. 4, March 1973, pp. 887-889.

28. Cudney, G.R., "The Effects of Loading on Bridge Life," Highway Research Record 253, Highway Research Board, 1968.

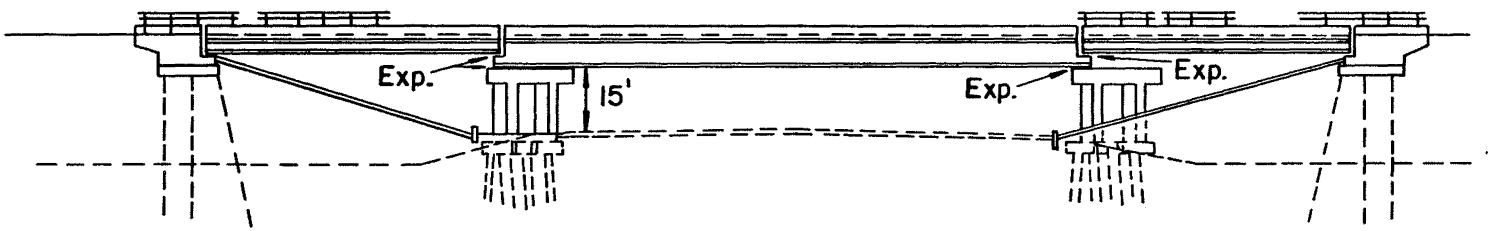

ELEVATION

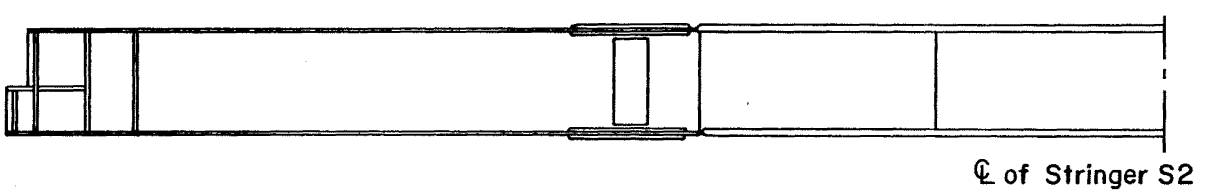

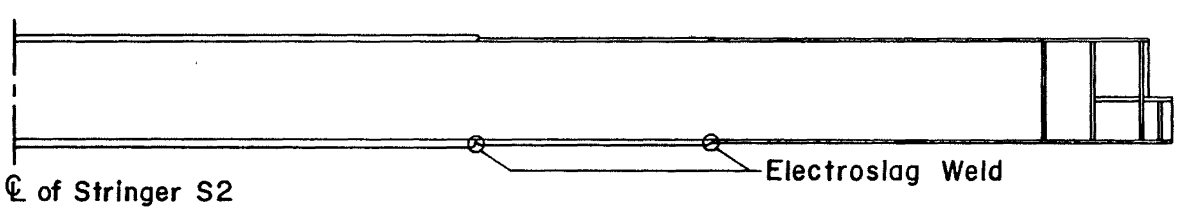

ELEVATION OF TYPICAL STRINGER

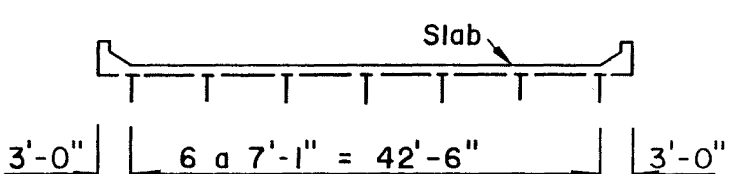

TYPICAL SECTION THROUGH DECK

Fig. 1a. Elevation and Gross section of Meadville Bridge.

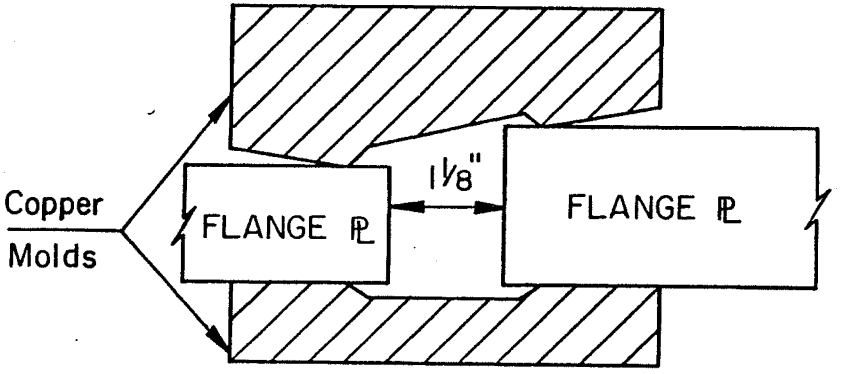

ELECTROSLAG WELD DETAIL

Note:

All flange butt welds are to be electroslag welding process. All flange splices subject to tensile stresses and the tension area of each web splice shall be smooth and radiographed by the fabricator.

Fig. 1b. Electroslag groove weld detail at Meadeville.

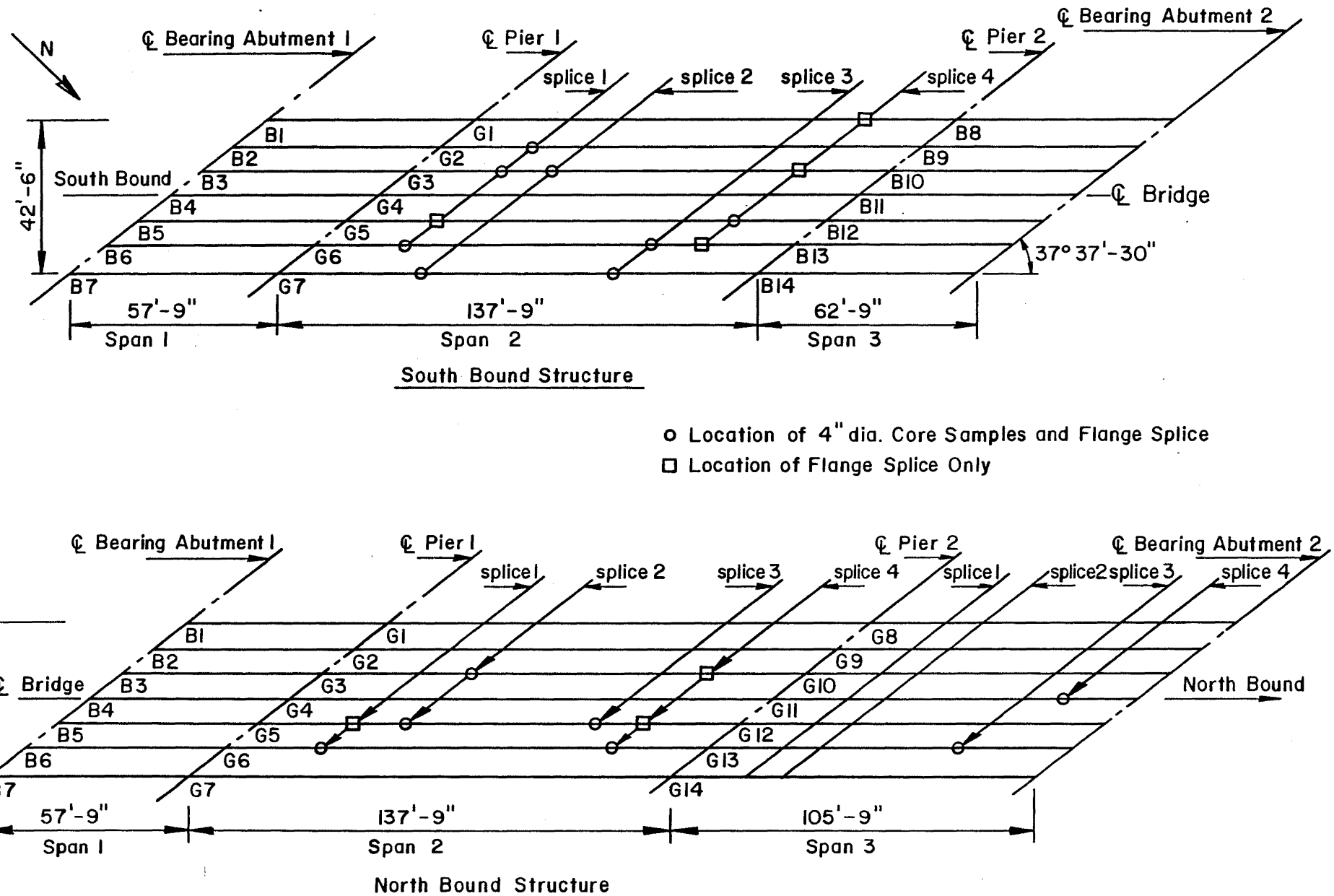

Fig. 1c. Framing Plan for Bridge Structure

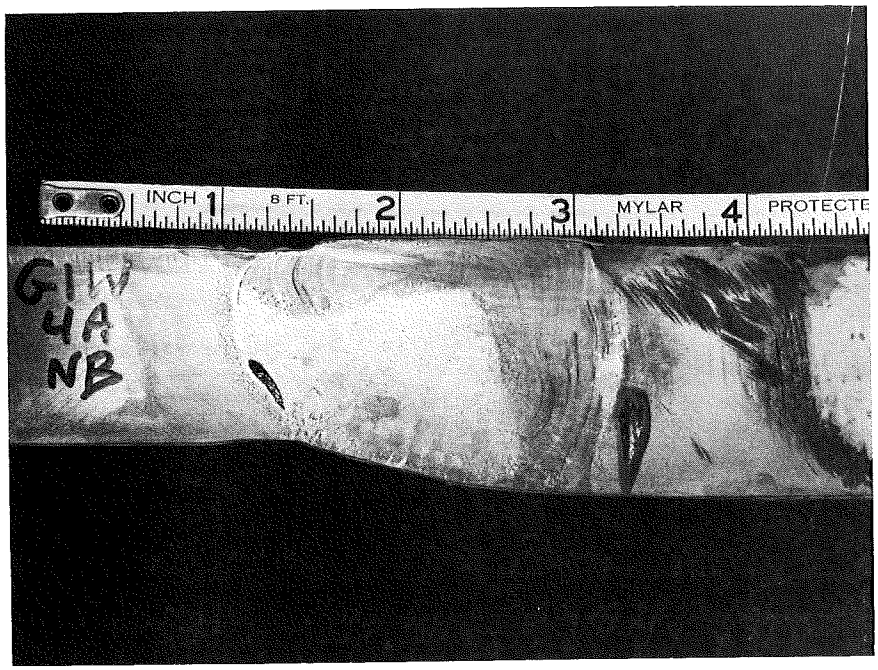

Fig. 2. Flange tip at northbound girder G1 W4A showing slag at fusion line.

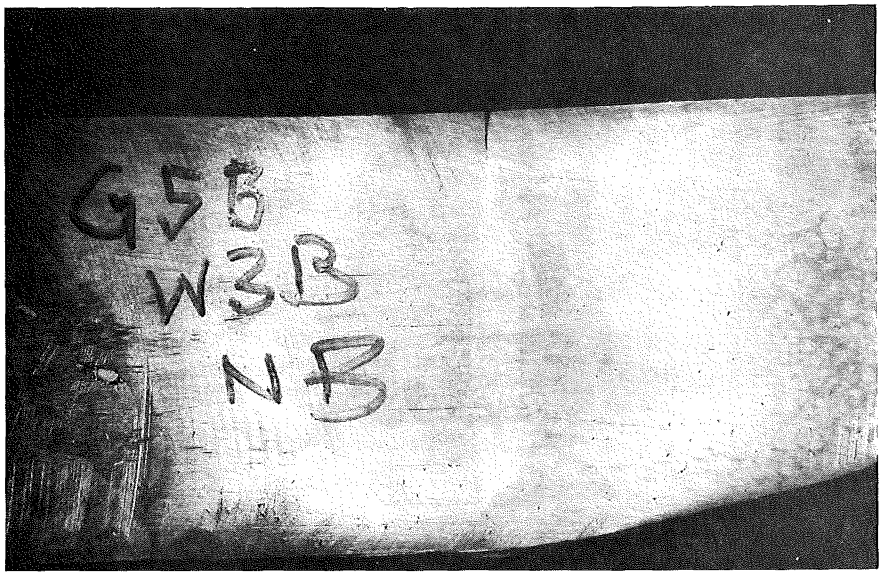

Fig. 3a. Flange tip at northbound girder G5 W3B showing lack of fusion.

Fig. 3b. Lack of fusion extending across northbound girder G5 W3B about 2 inches.

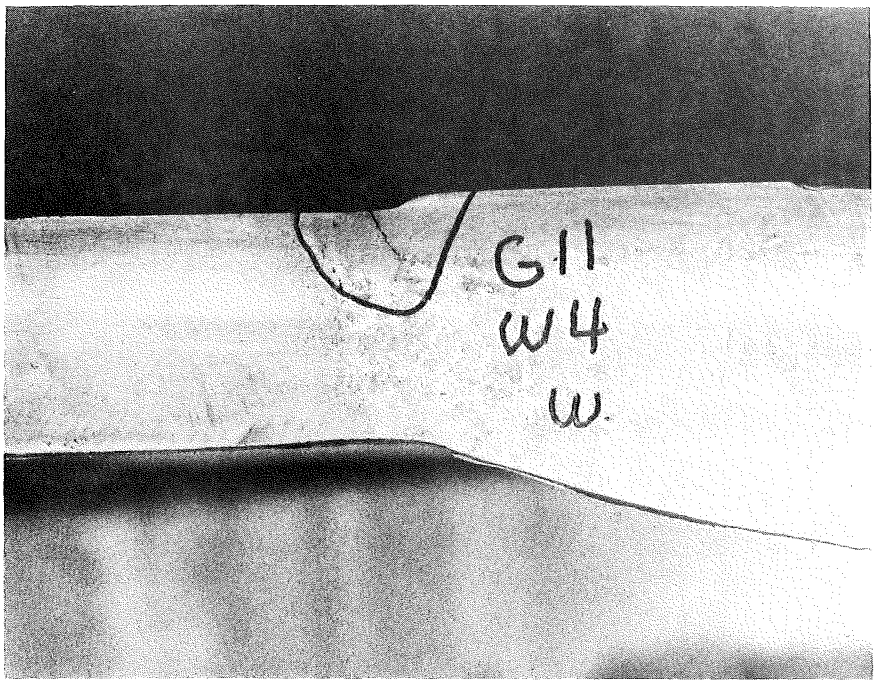

Fig. 4. Crack in flange tip of northbound girder G11 W4A . Crack in electroslag weld near reinforcement.

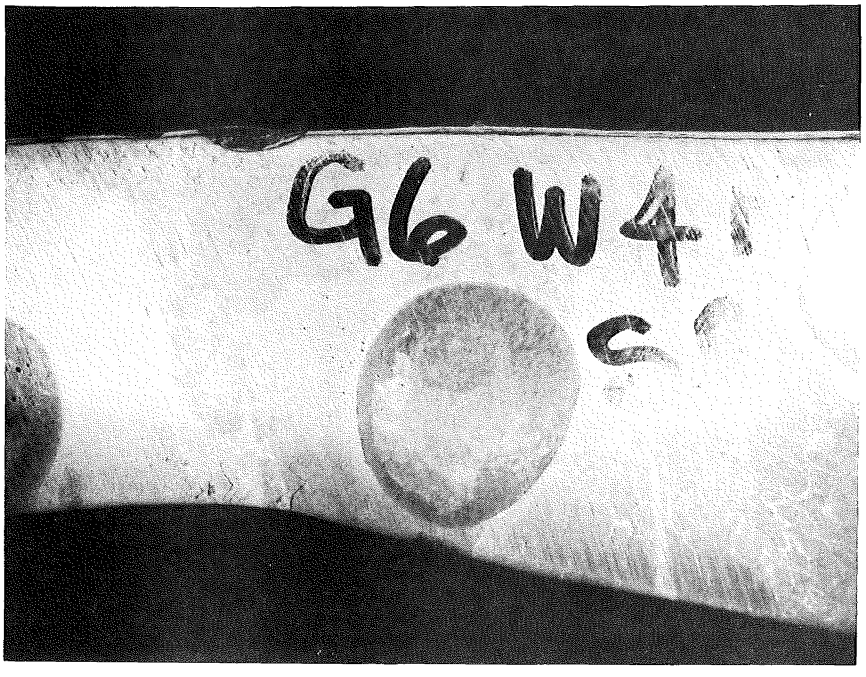

Fig. 5. Cracks in southbound girder G6 W4A at transition region. Irregular cracks follow grain boundaries, note that reinforcement has been removed from this weld joint.

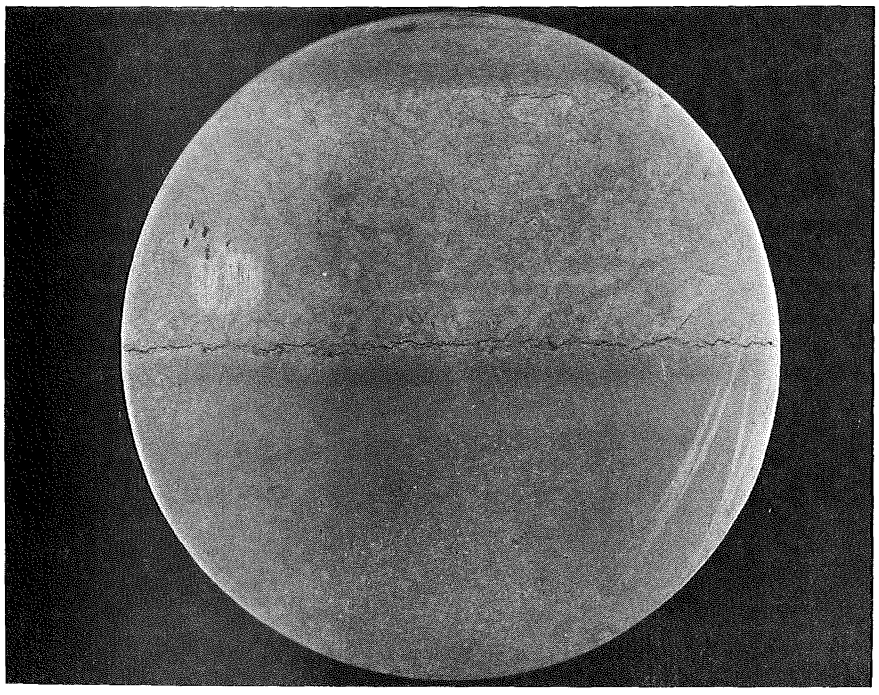

Core A

Fig. 6. Sample core removed from the southbound girder G5 W4B

Core B

Fig. 7. Sample core removed from the southbound girder G7 W3B.

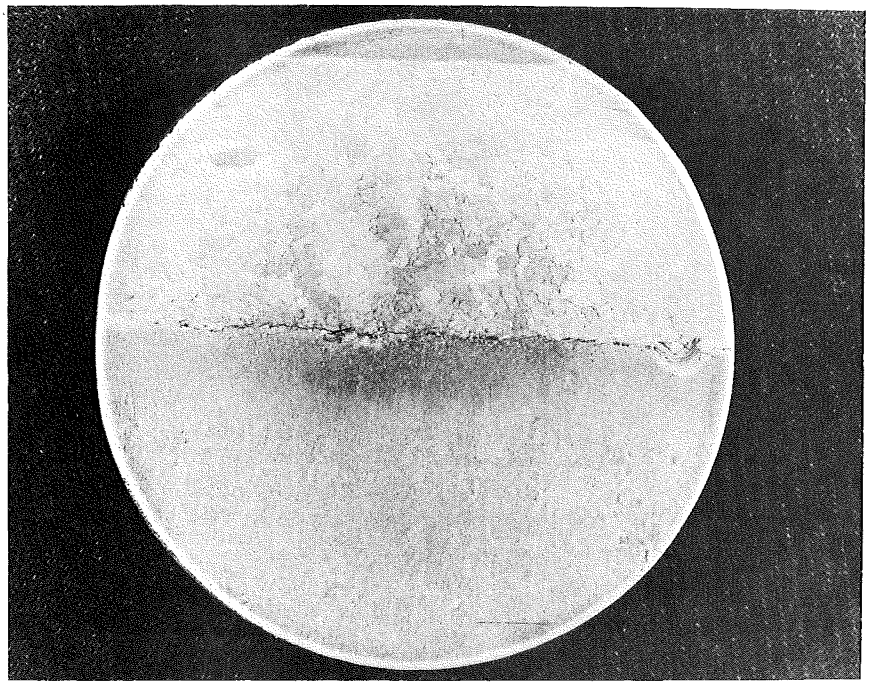

Core C

Fig. 8. Sample core removed from southbound girder G6 W1A (C).

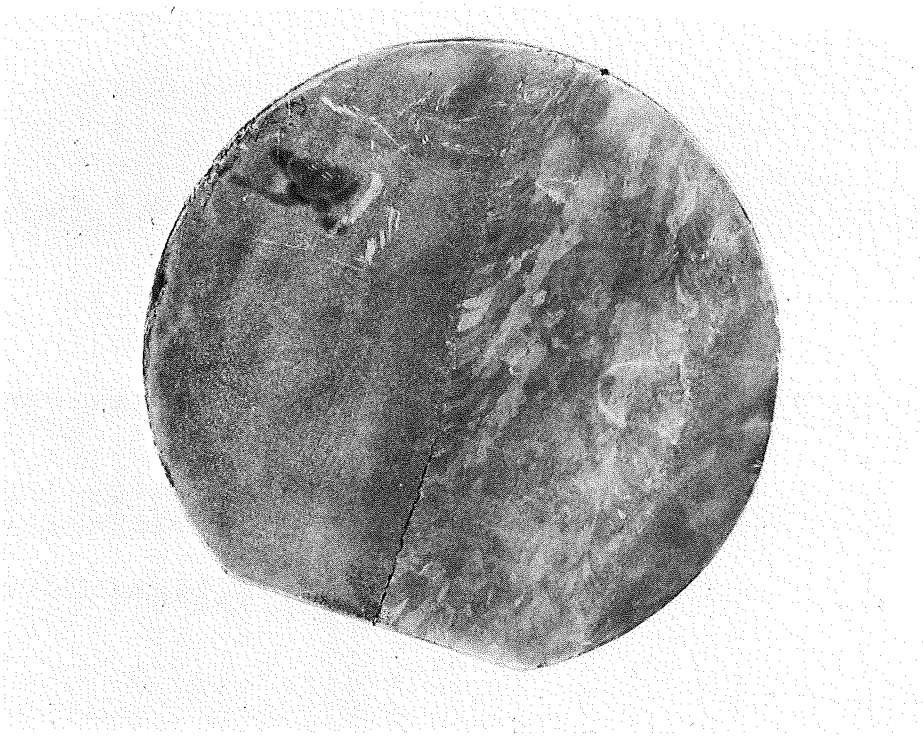

Core D

Fig. 9. Core removed from northbound girder G5 W3B, showing propagation of flange tip crack.

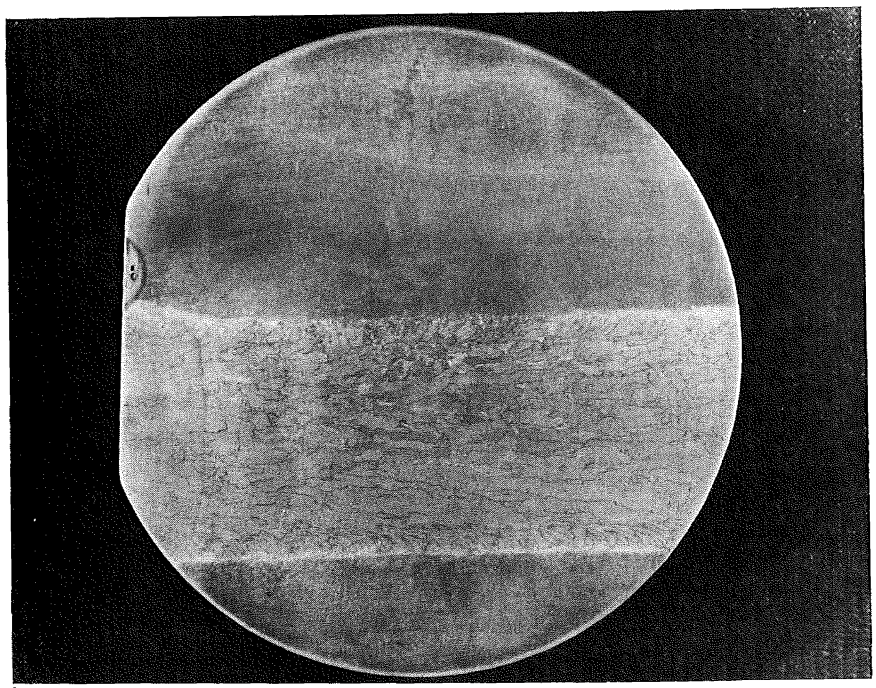

Fig. 10. Core removed from northbound girder G4 W2A showing repair weld on flange tip crack.

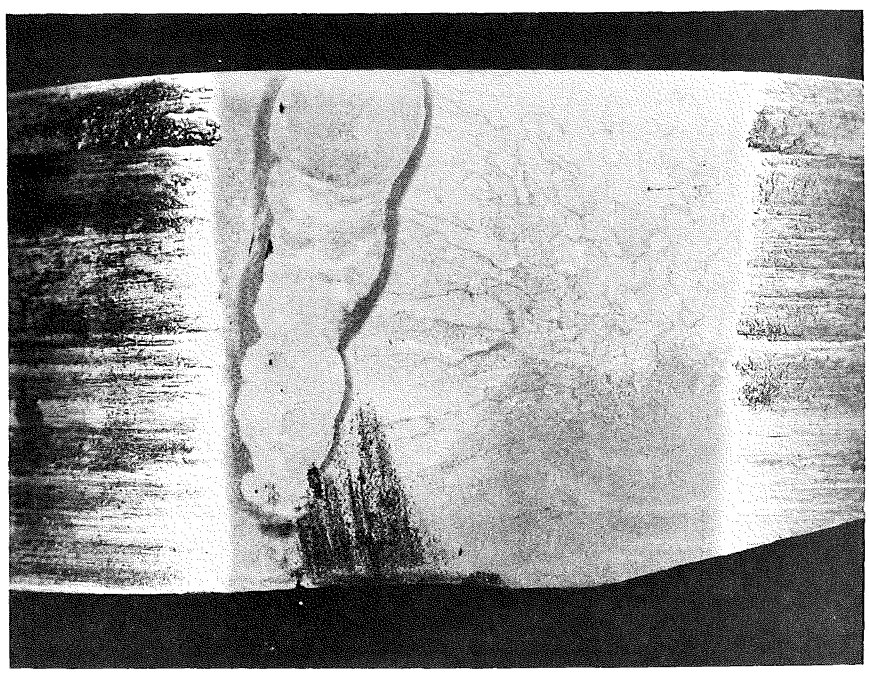

Fig. 11. Side view of core from northbound girder G4 W2A showing repair weld.

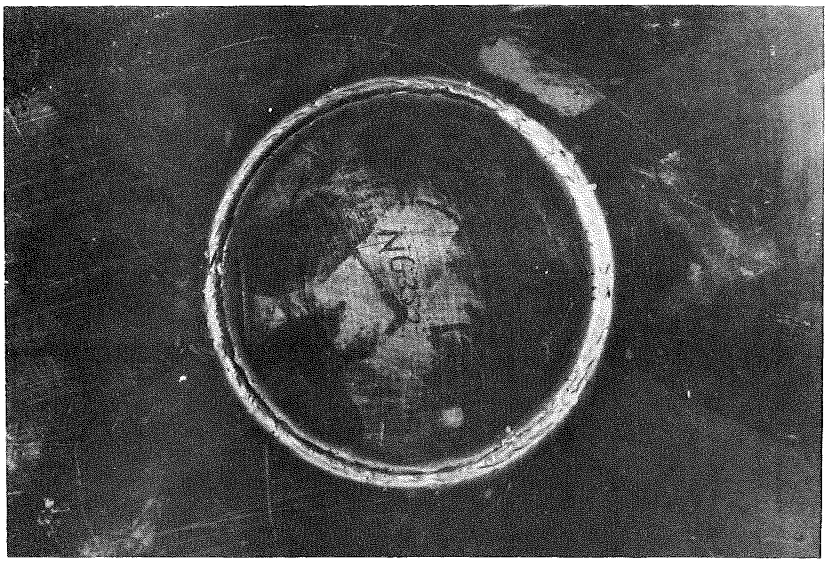

Fig. 12. A 4 inch sample core electron beam welded into a A-36 steel plate.

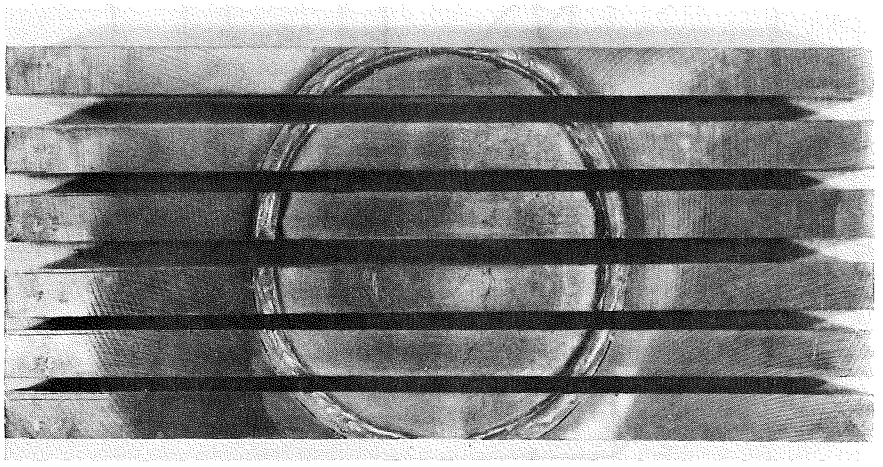

Fig. 13. Core sliced into bars.

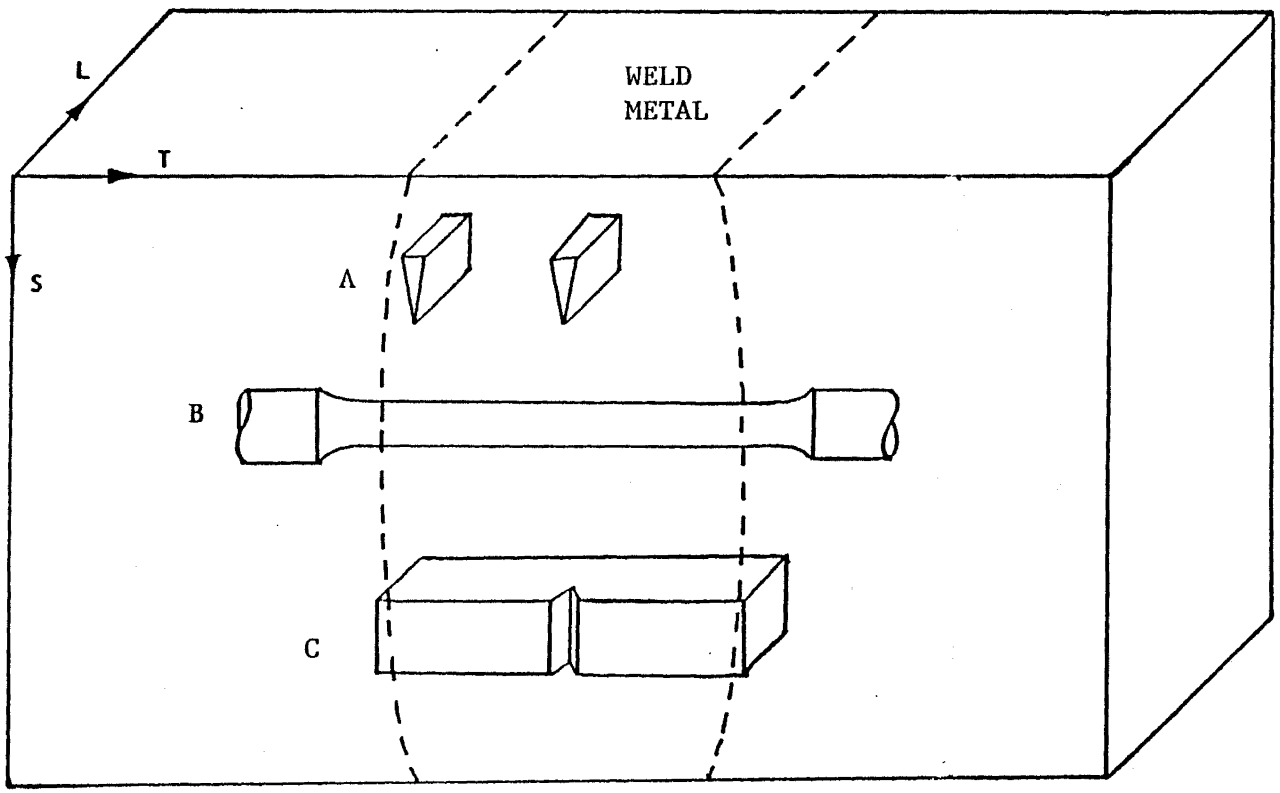

Figure 14. Orientation of A - Fatigue crack propagation direction
B - Tensile specimens
C - CVN specimens

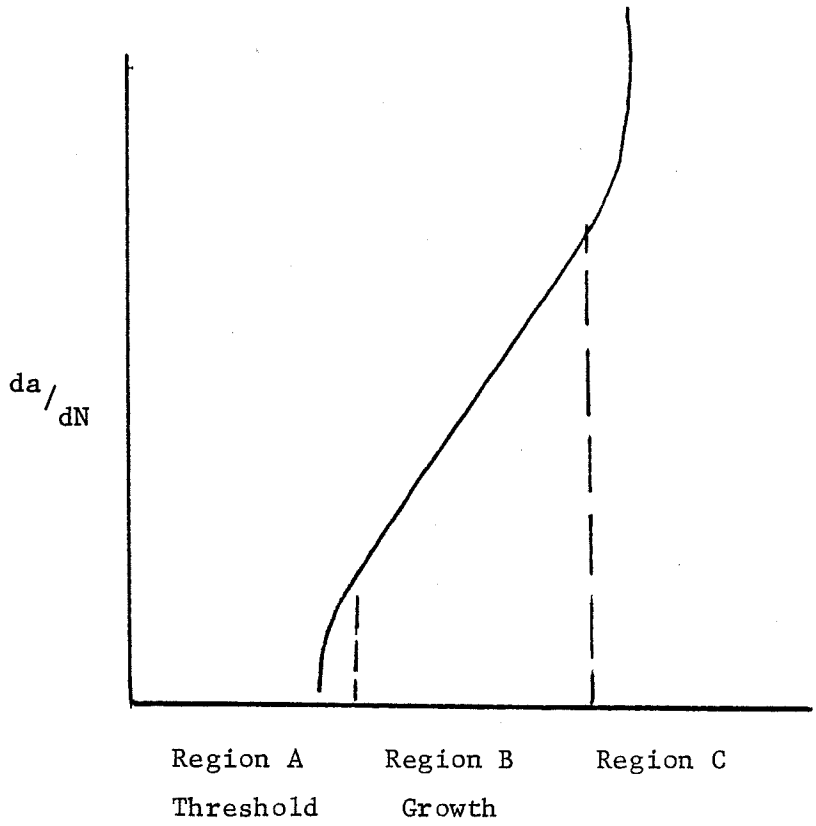

Fig. 15. Three regions of fatigue crack growth.

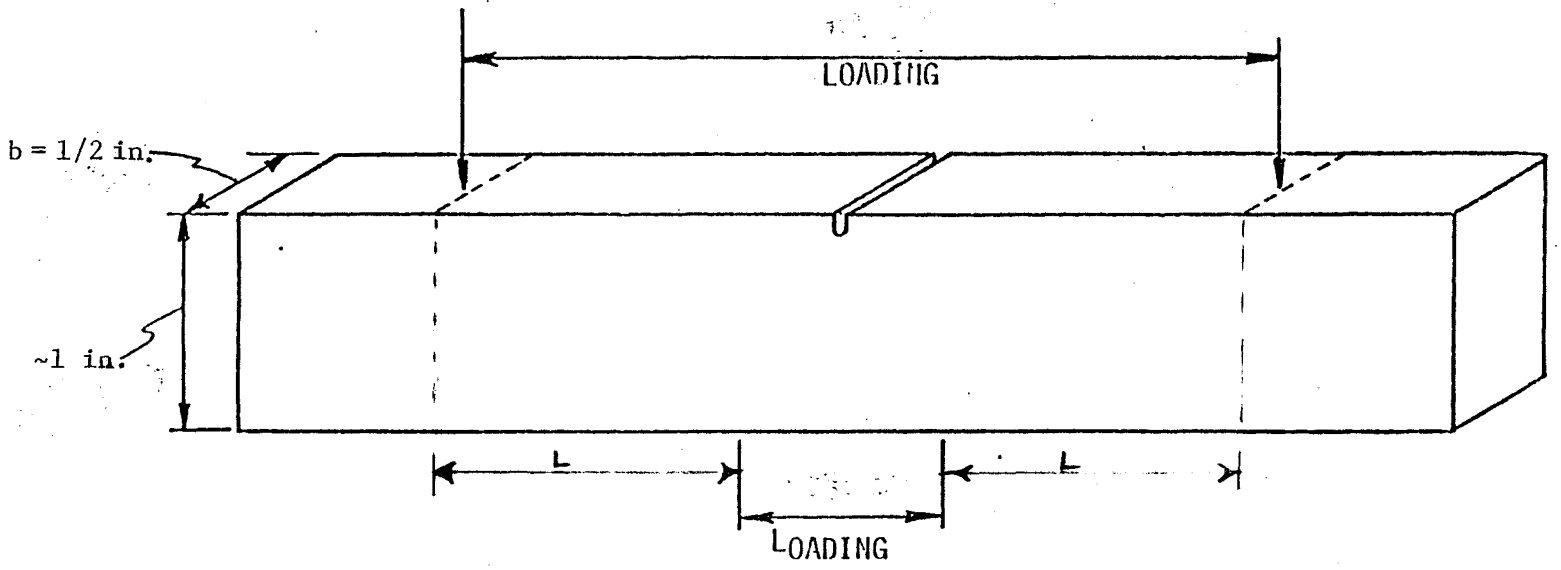

Fig. 16 Four-point-bend specimen.

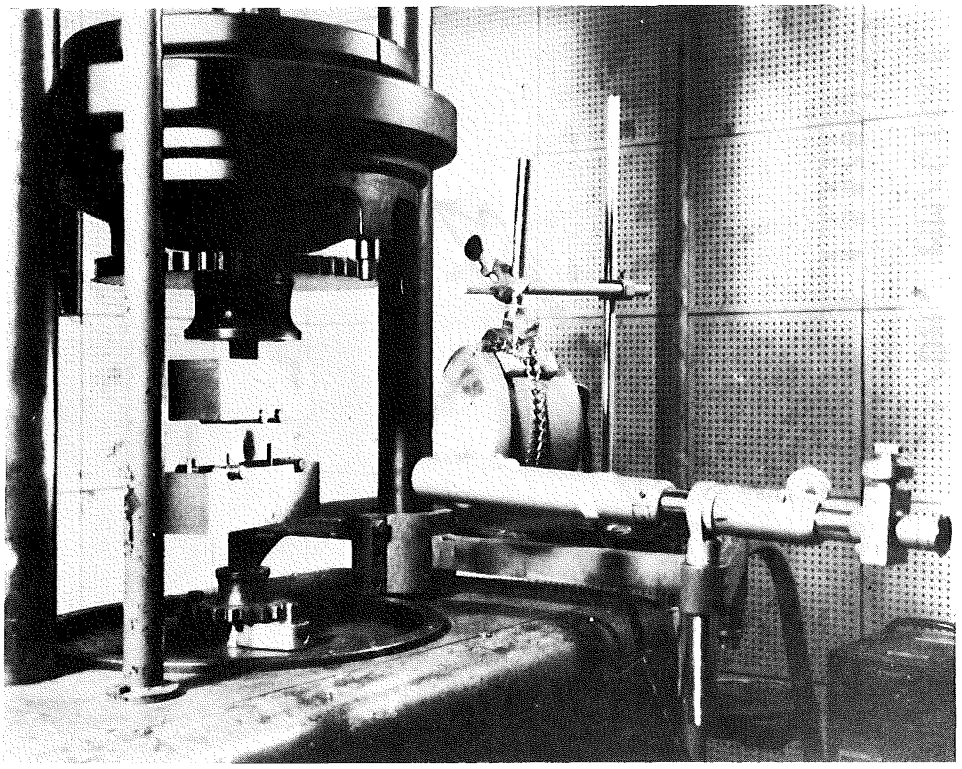

Fig. 17 Amsler Vibrophore and Garret microscope.

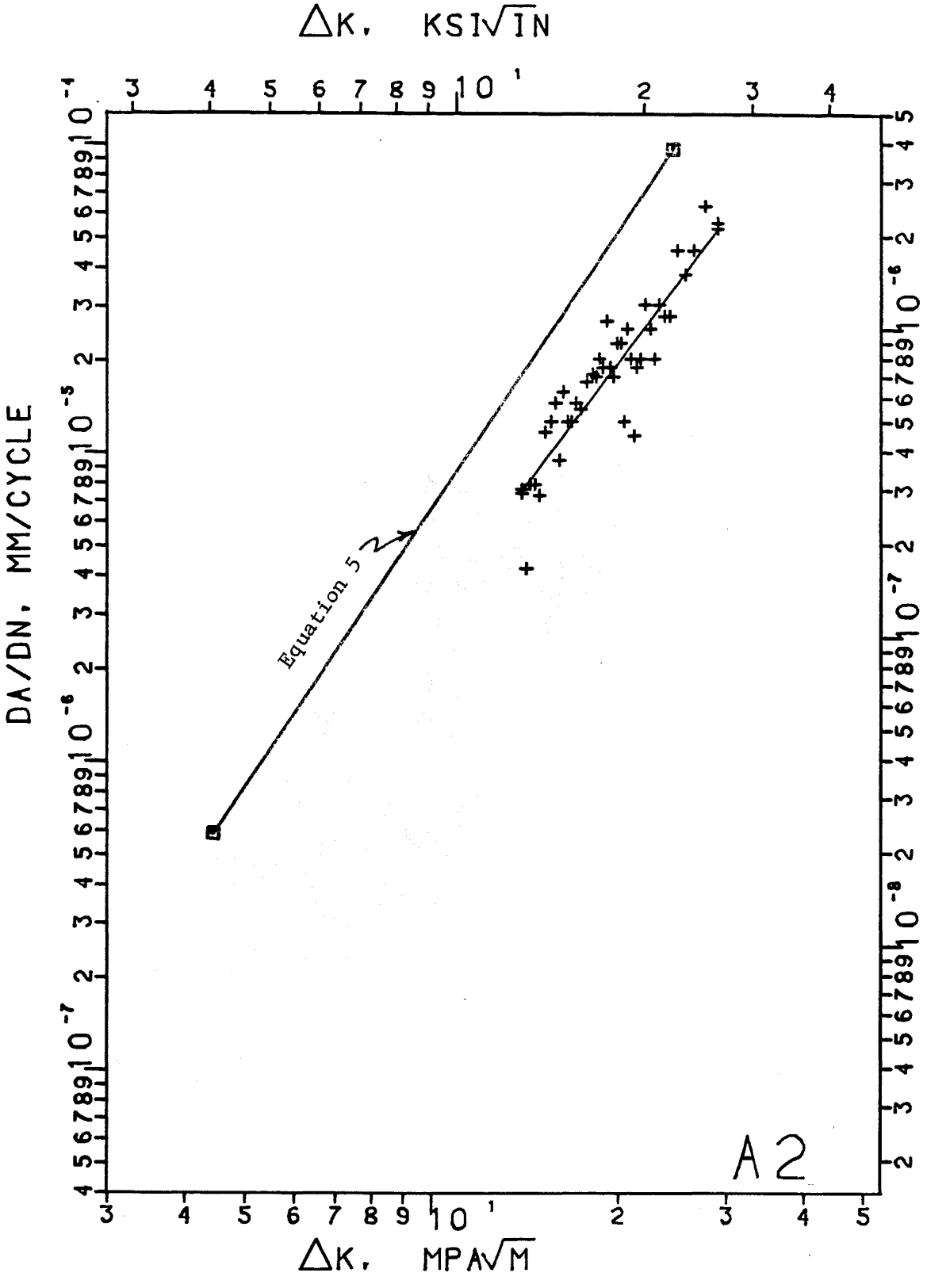

Fig. 18. Fatigue data of specimen A2 with natural cracks at the fusion line.

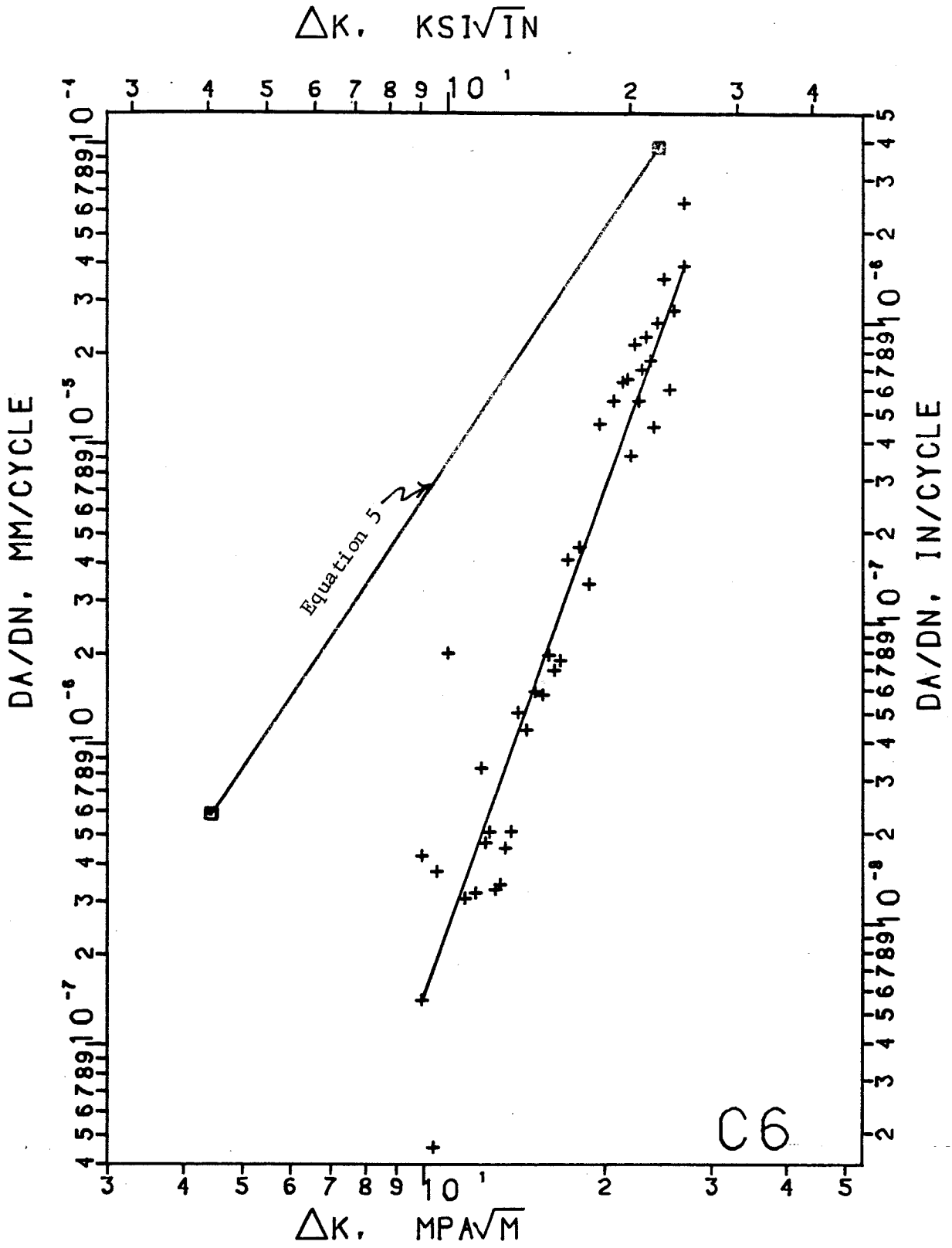

Fig. 19. Fatigue date of specimen C6 with natural cracks at the fusion line.

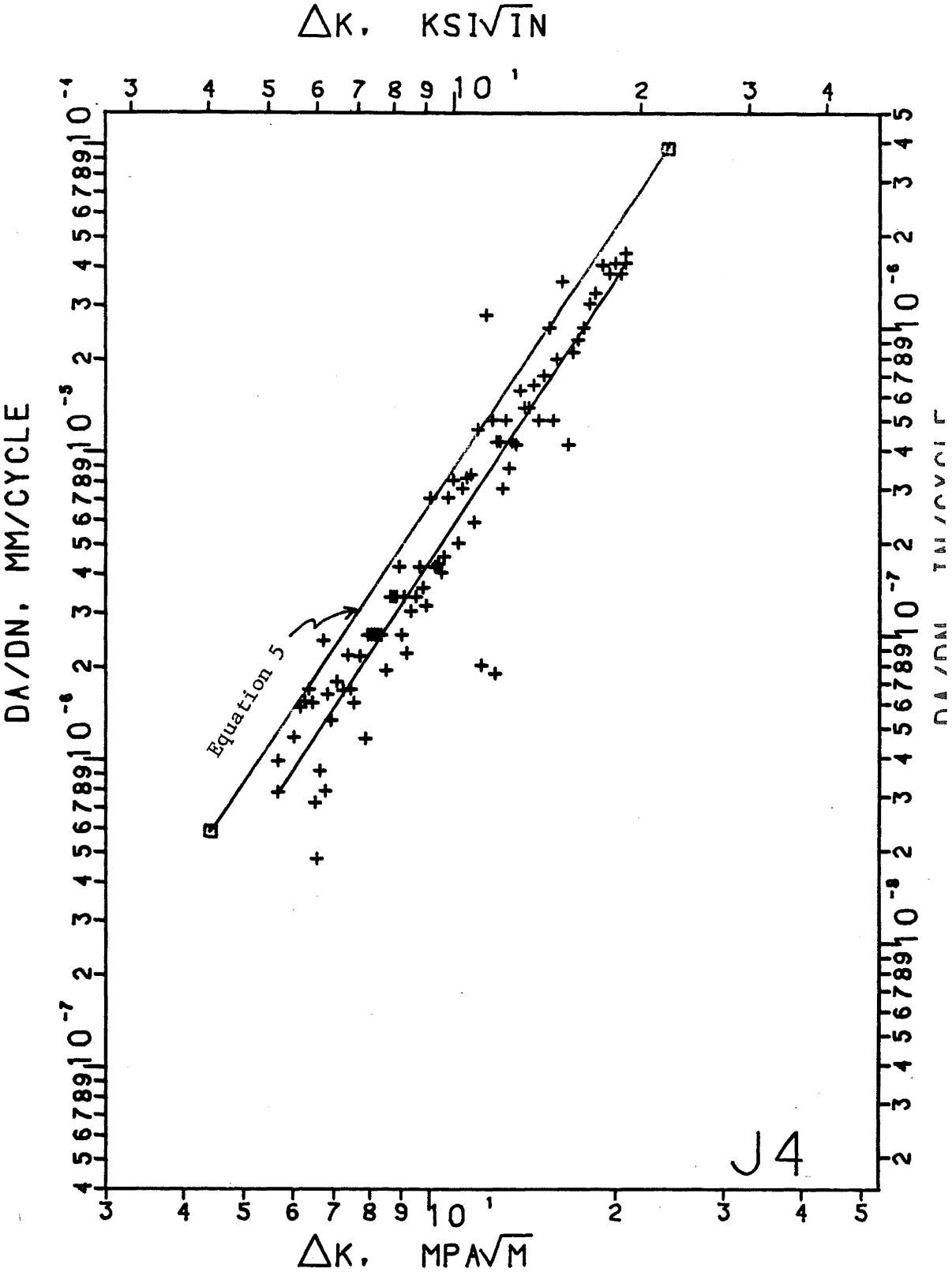

Fig. 20. Fatigue data of specimen J4 EDM notched at the center line.

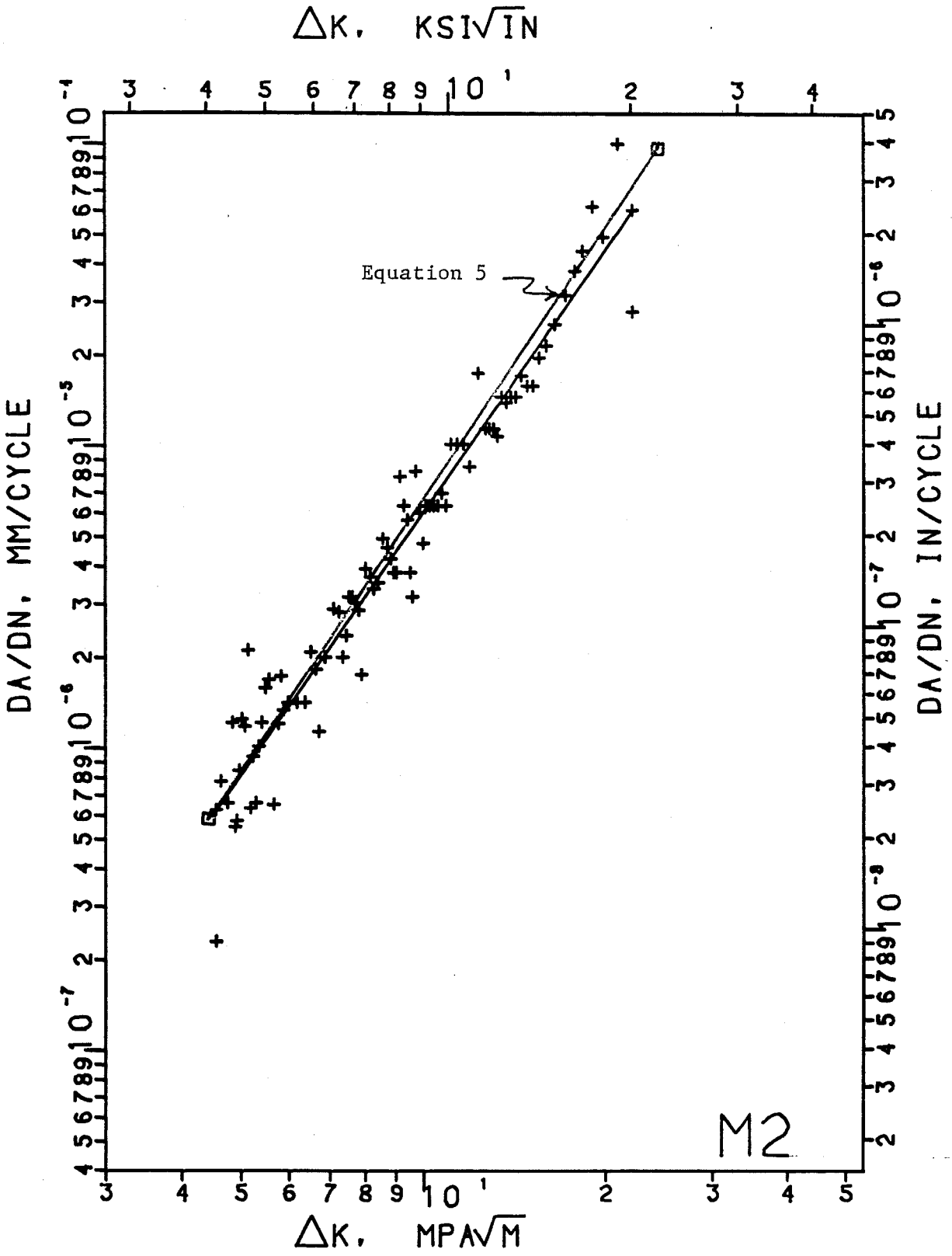

Fig. 21. Fatigue data of specimen M2 EDM notched at the fusion line.

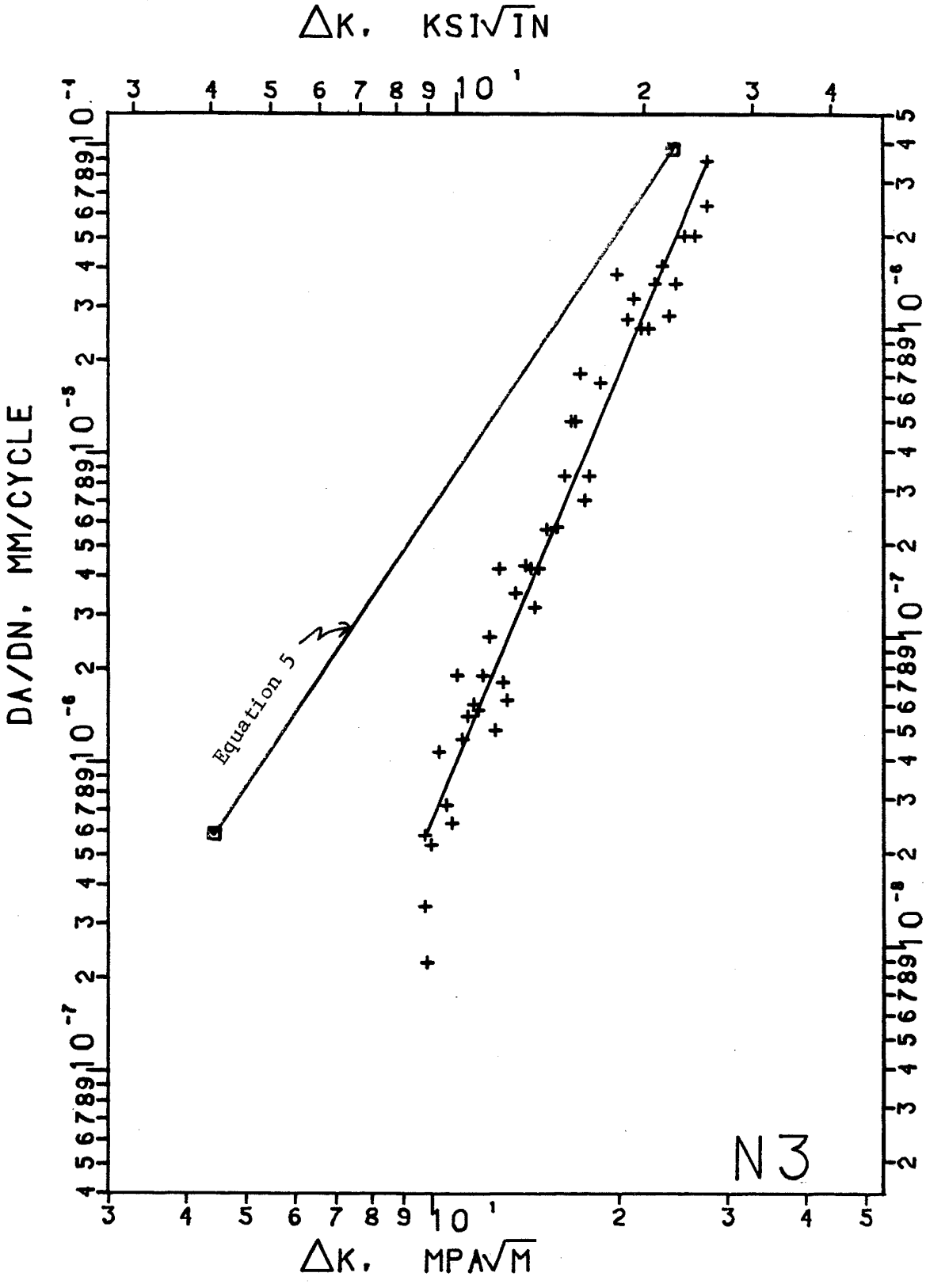

Fig. 22. Fatigue data of specimen N3, EDM notched at the fusion line.

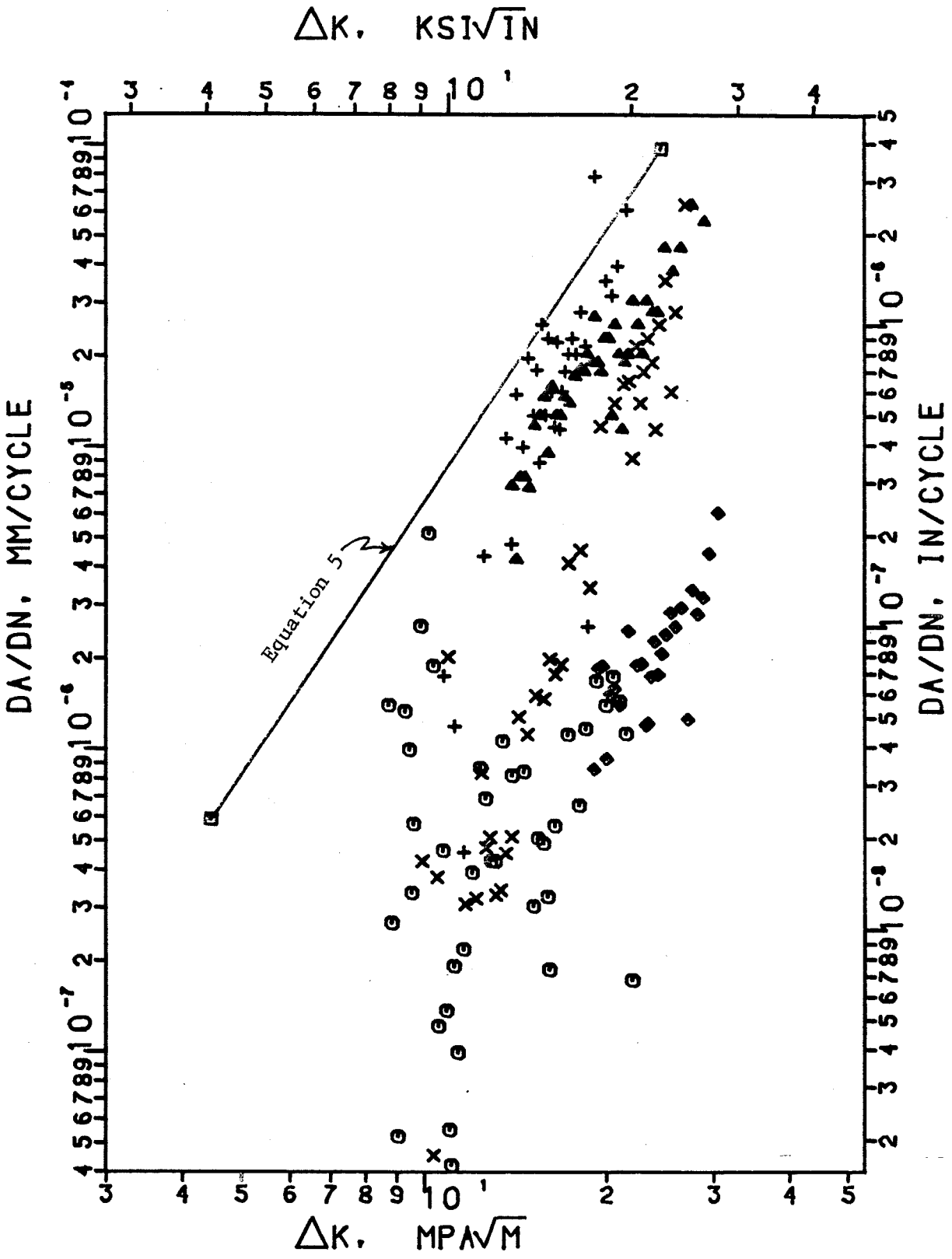

Fig. 23. Fatigue data of all naturally cracked specimens.

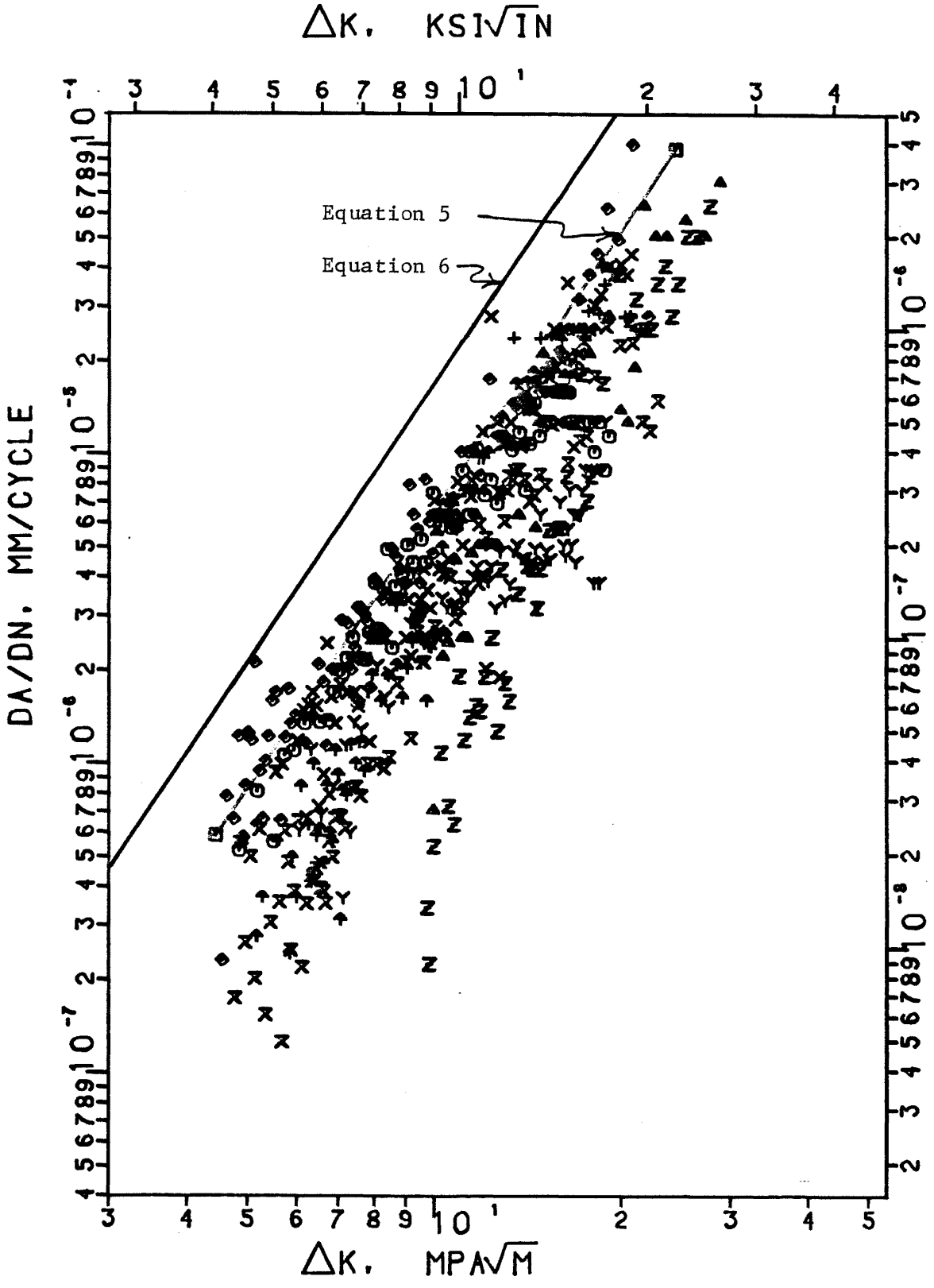

Figure 24. Fatigue data of all EDM notched specimens.

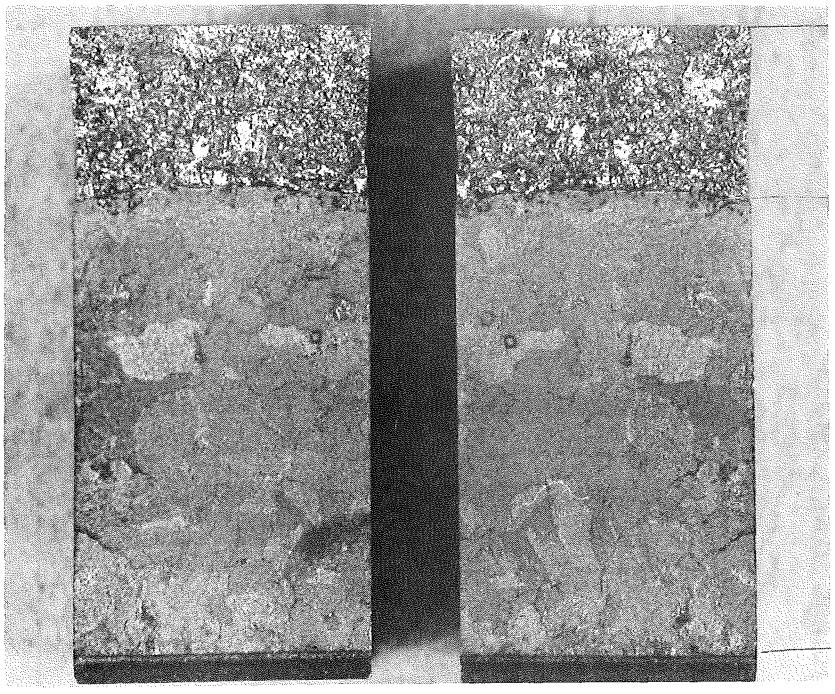

Fig. 25. Topographic features of a fatigue crack through zone II weldment.

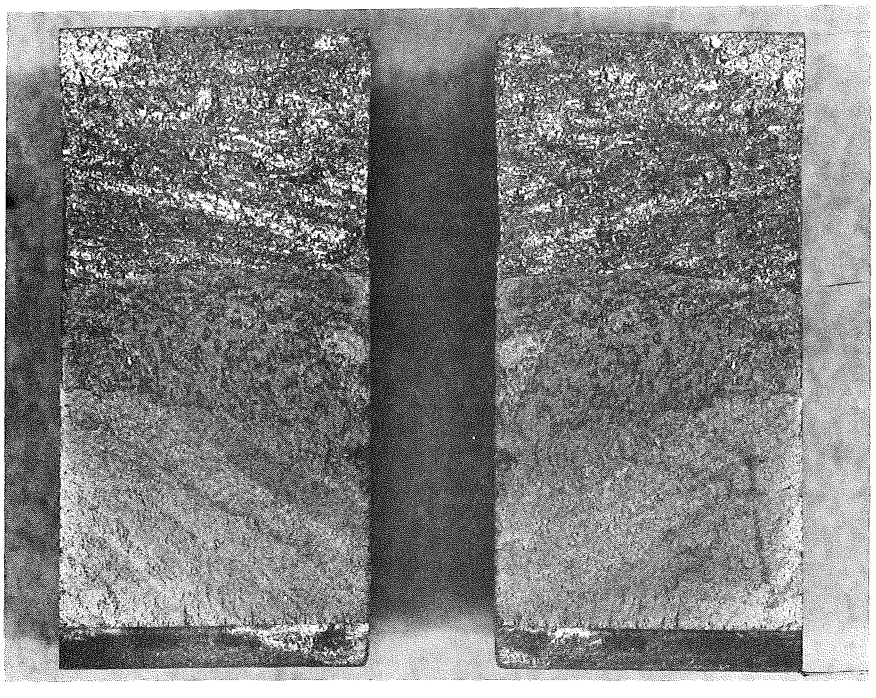

Fig. 26. Topographic features of a fatigue crack through zone I weldment.

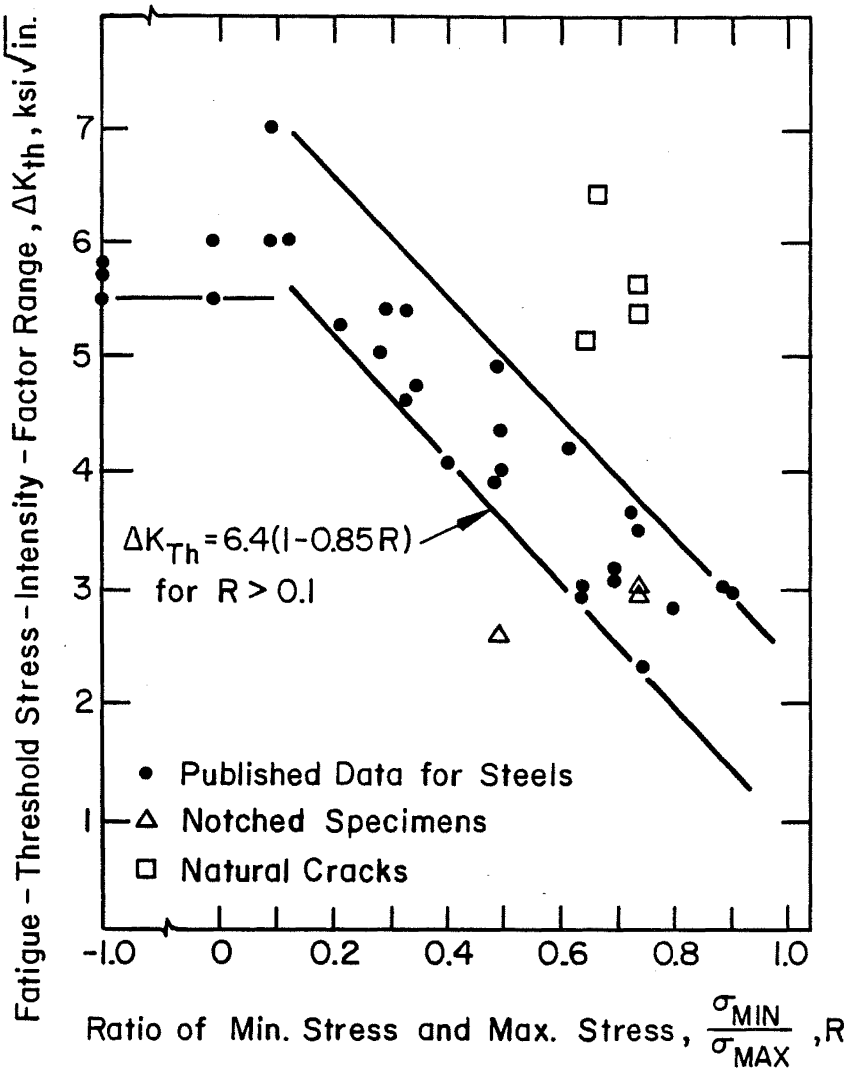

Fig. 27. Comparison of data from threshold studies with previous studies.

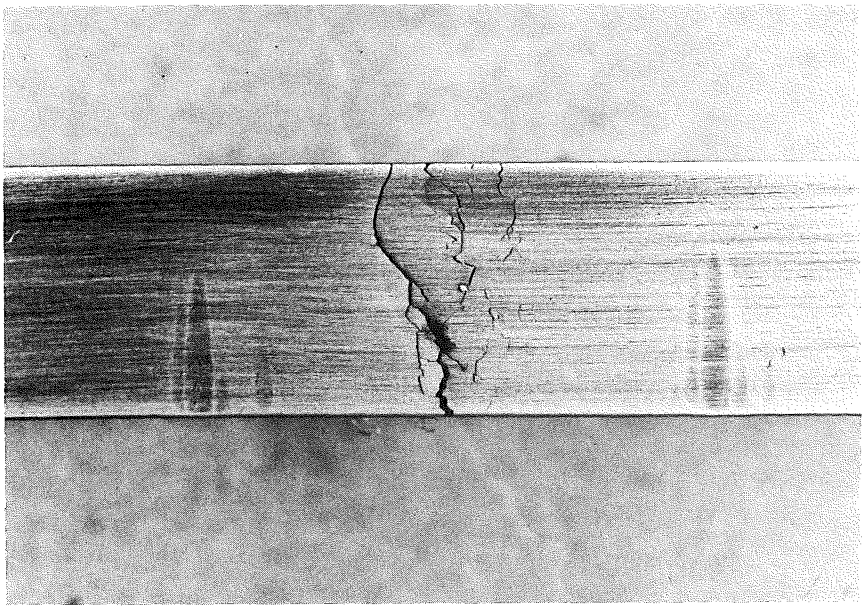

Fig. 28. Edge view of specimen A4 showing natural cracks at fusion line.

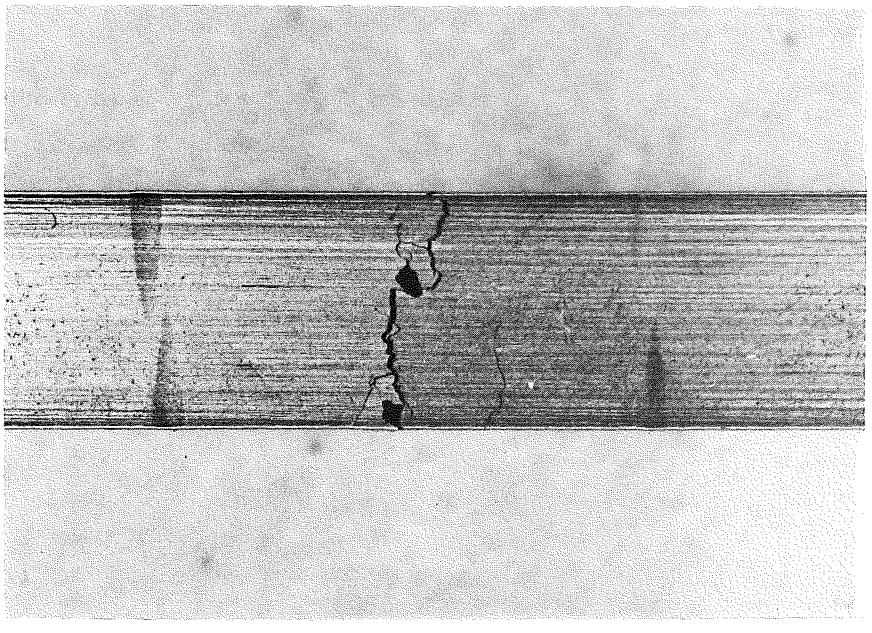

Fig. 29. Edge view of specimen F5 showing natural cracks at fusion line.

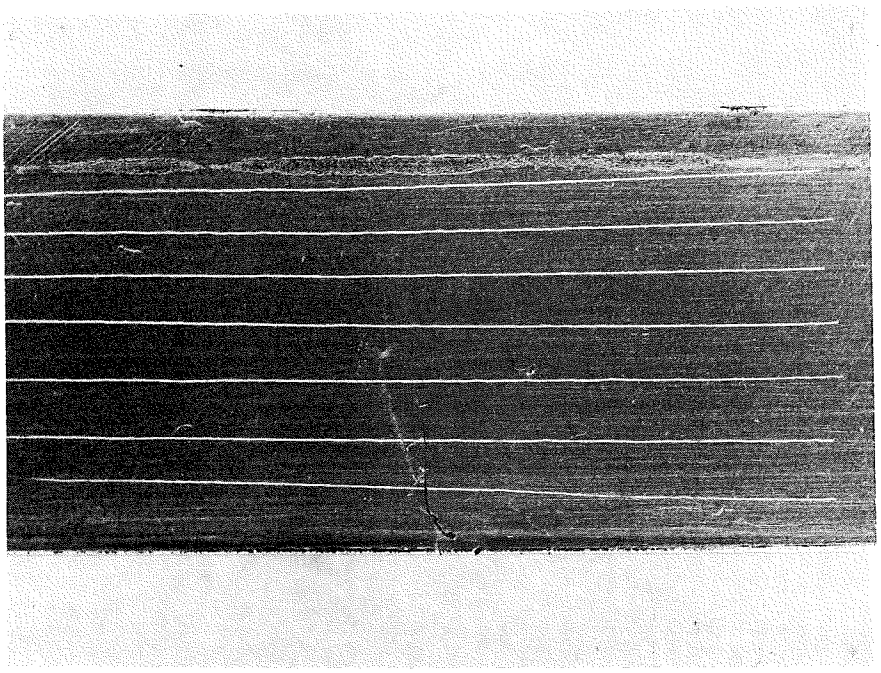

Fig. 30. Branching of the cracks in specimen A4.

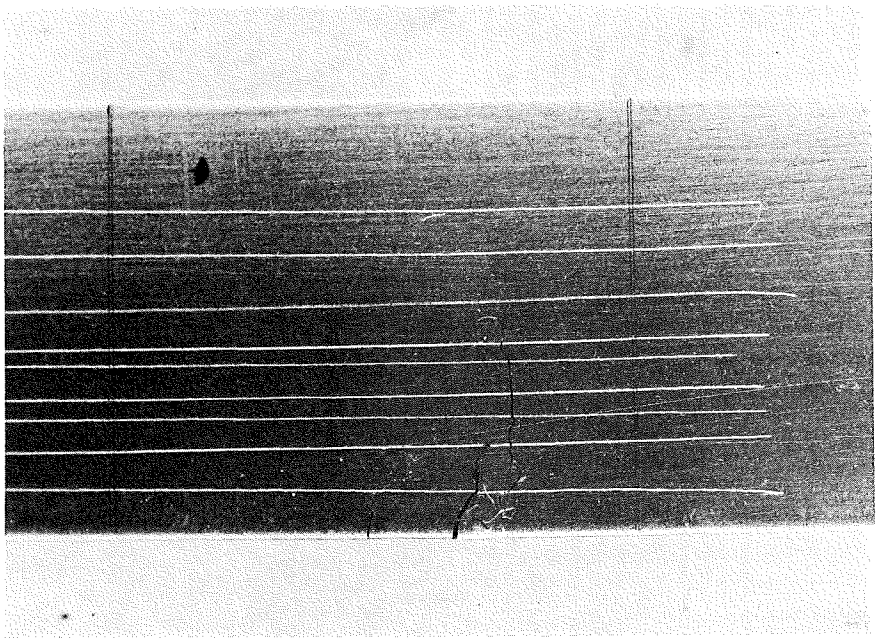

Fig. 31. Branching of the cracks in specimen F5.

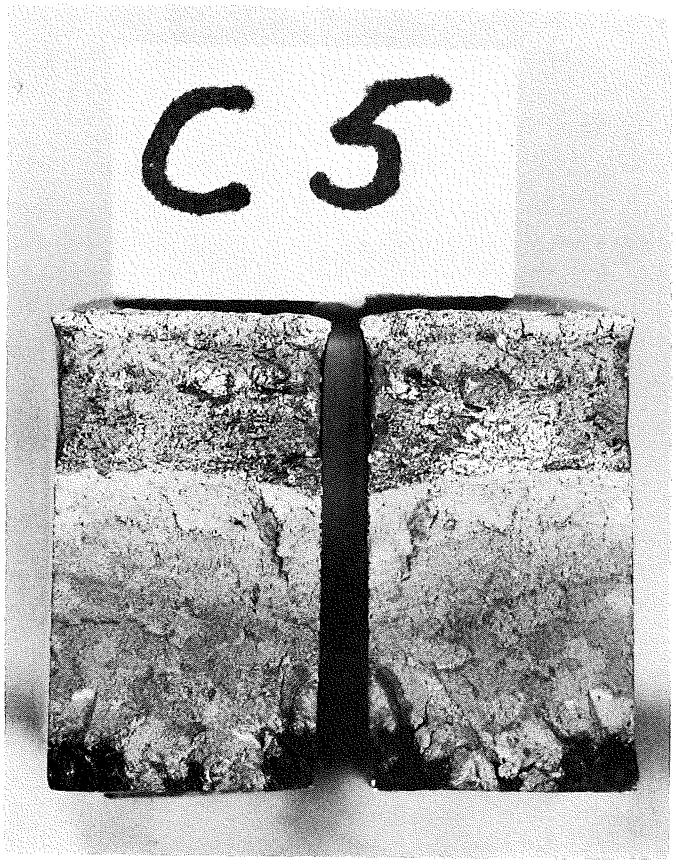

Fig. 32. Natural crack profile in specimen C5.

Fig. 33. Natural crack profile in specimen B4.

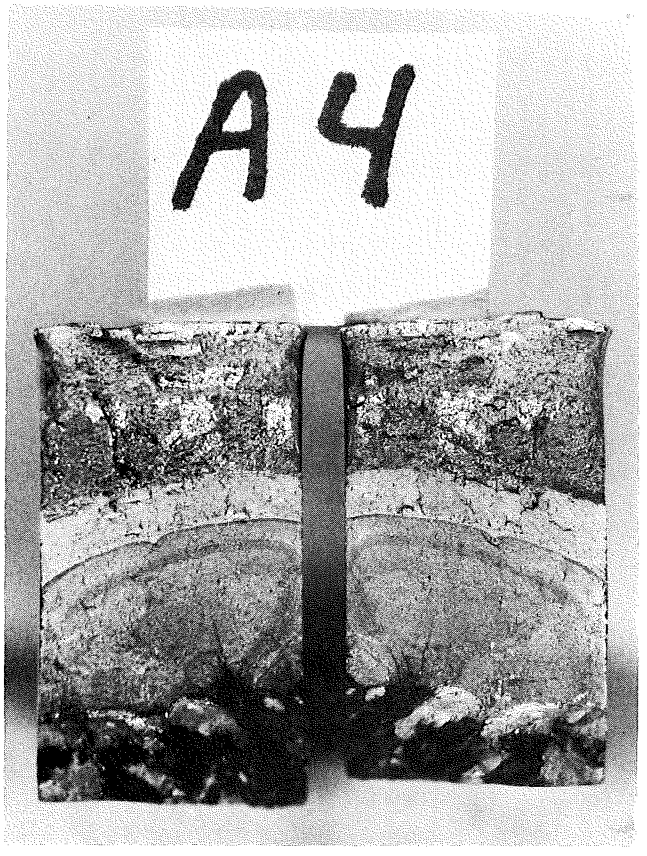

Fig. 34. Natural crack profile in specimen A4.

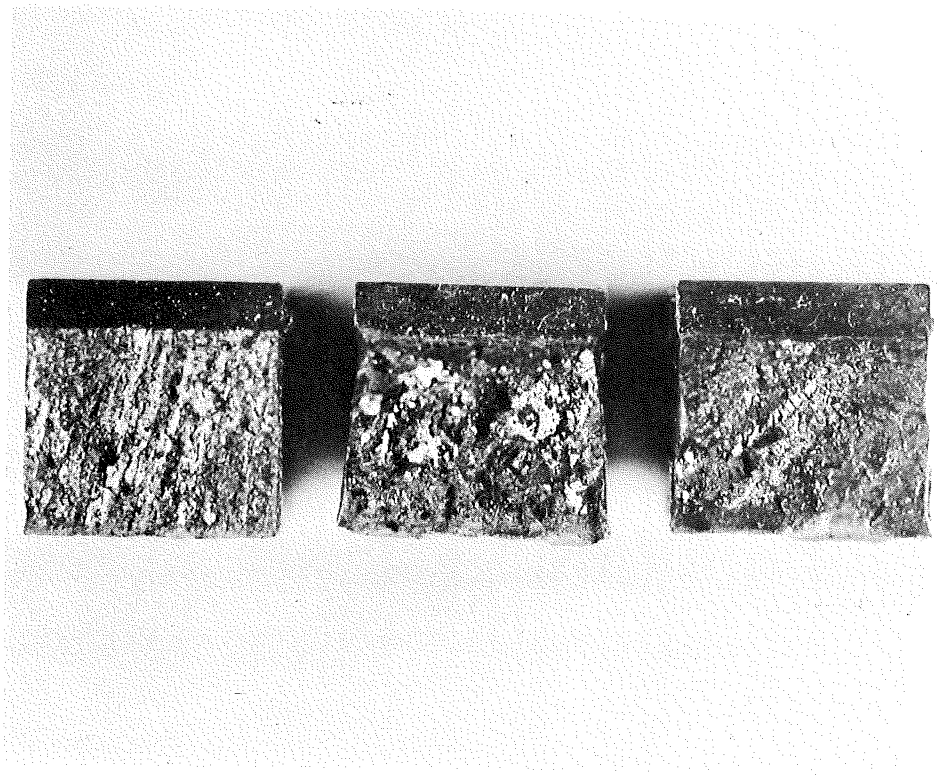

Fig. 35. Typical fractured CVN specimen.

A - Fine columnar structure

B - Coarse equiaxed structure.

C - Coarse columnar structure.

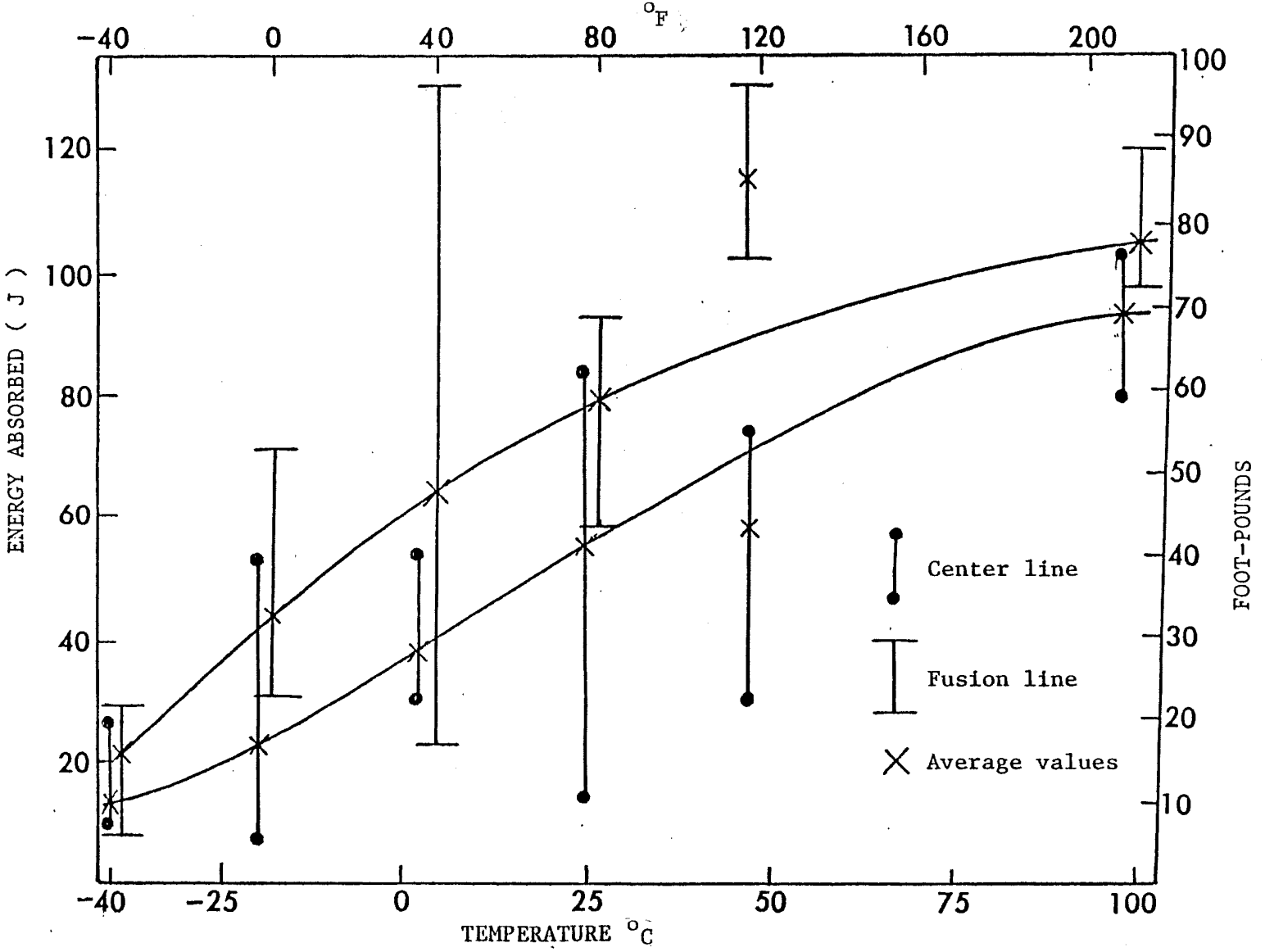

Figure 36 Charpy impact energy vs temperature.

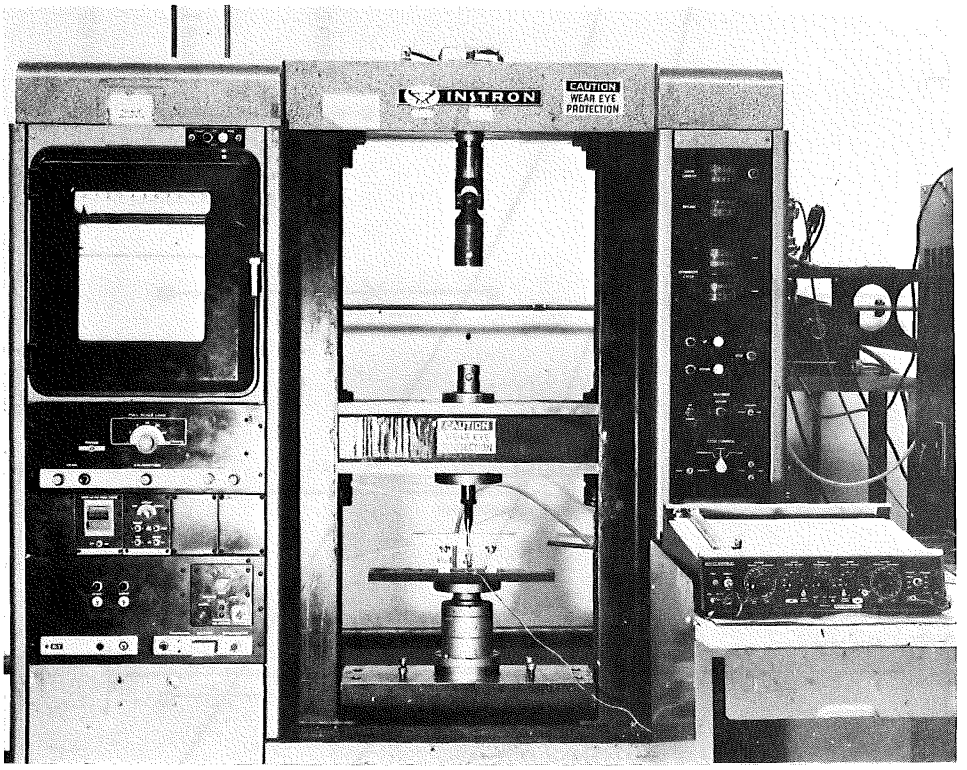

Fig. 37a. Set up to determine the fracture toughness using the J-integral technique.

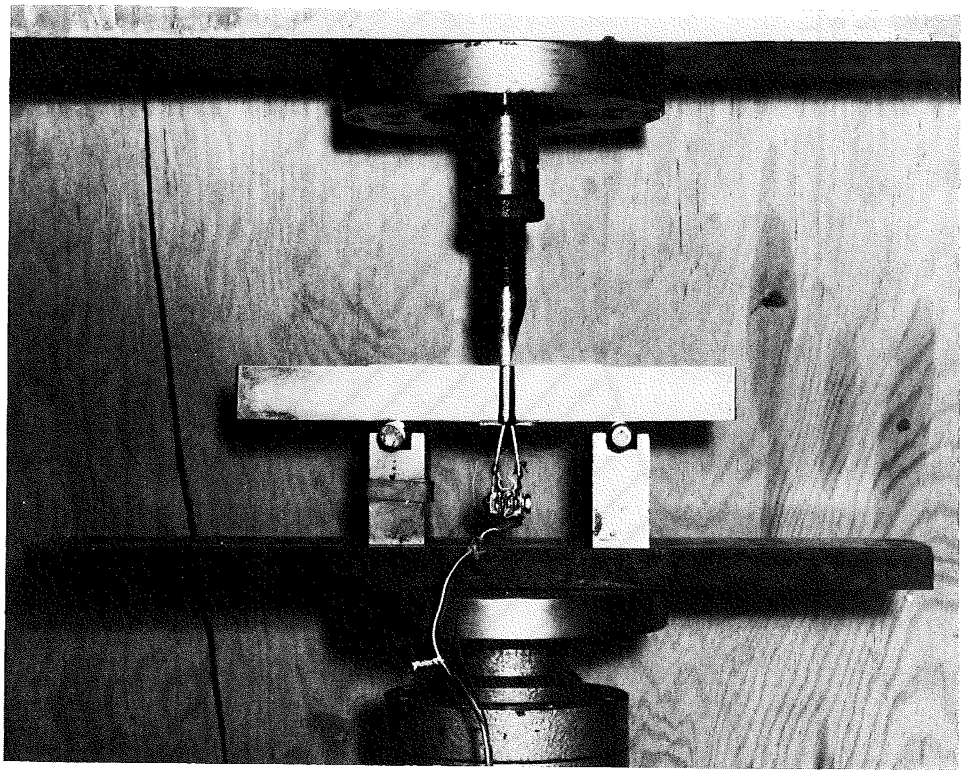

Fig. 37b. A close up of the 3 point bend specimen with the clip gauge attached to measure the displacement.

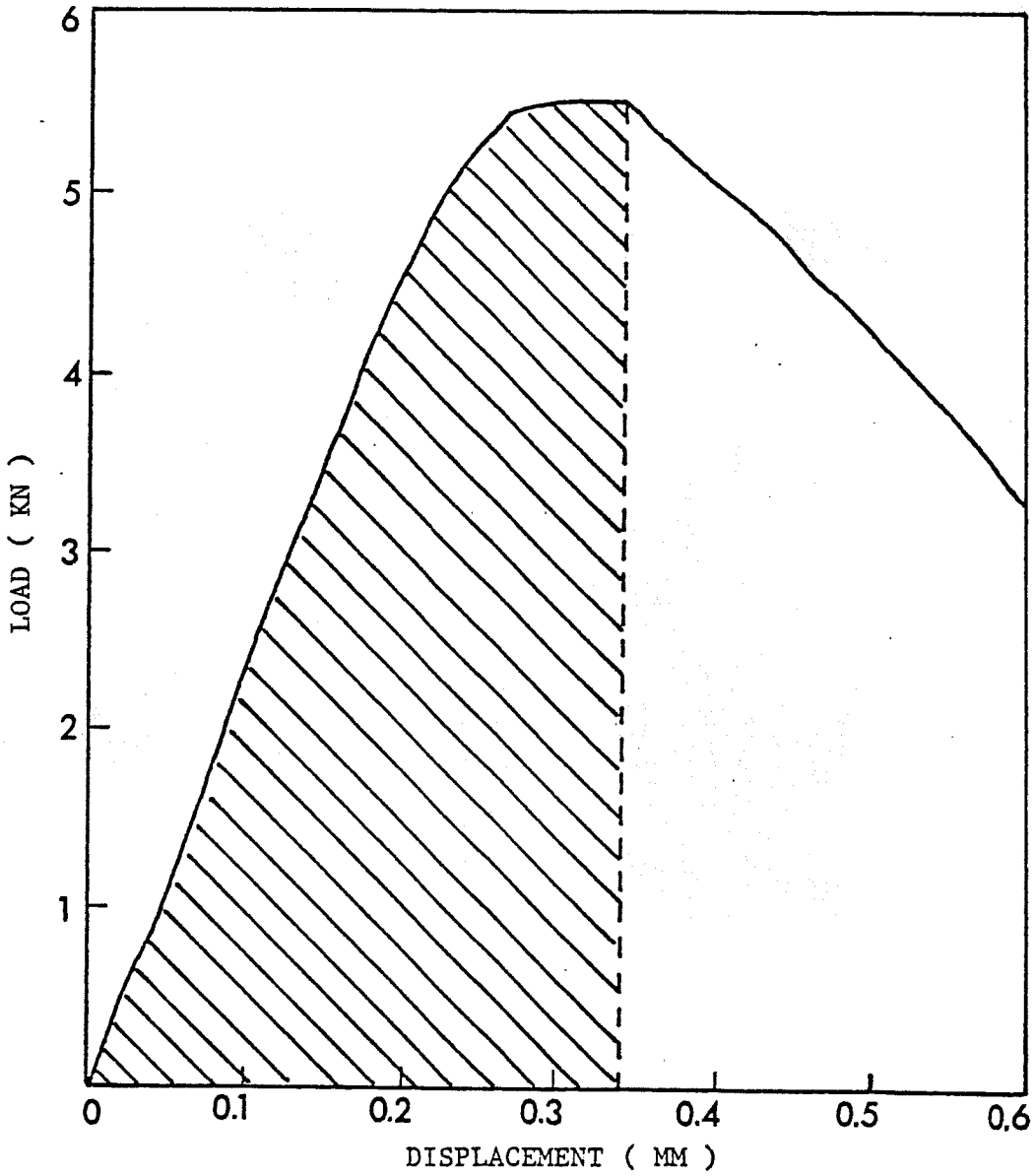

Figure 38. Load displacement curve.

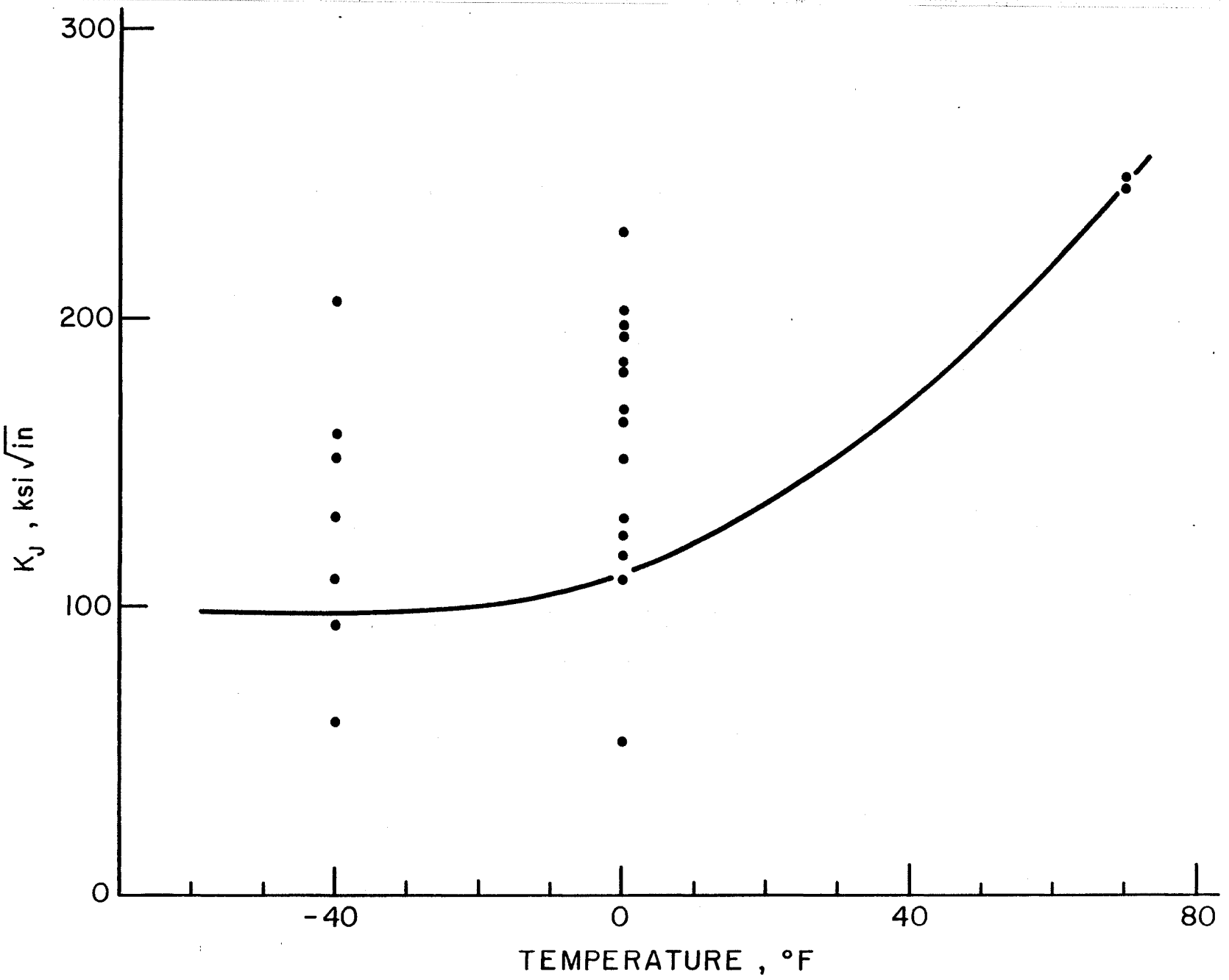

Fig. 39. K_J as a function of temperature.

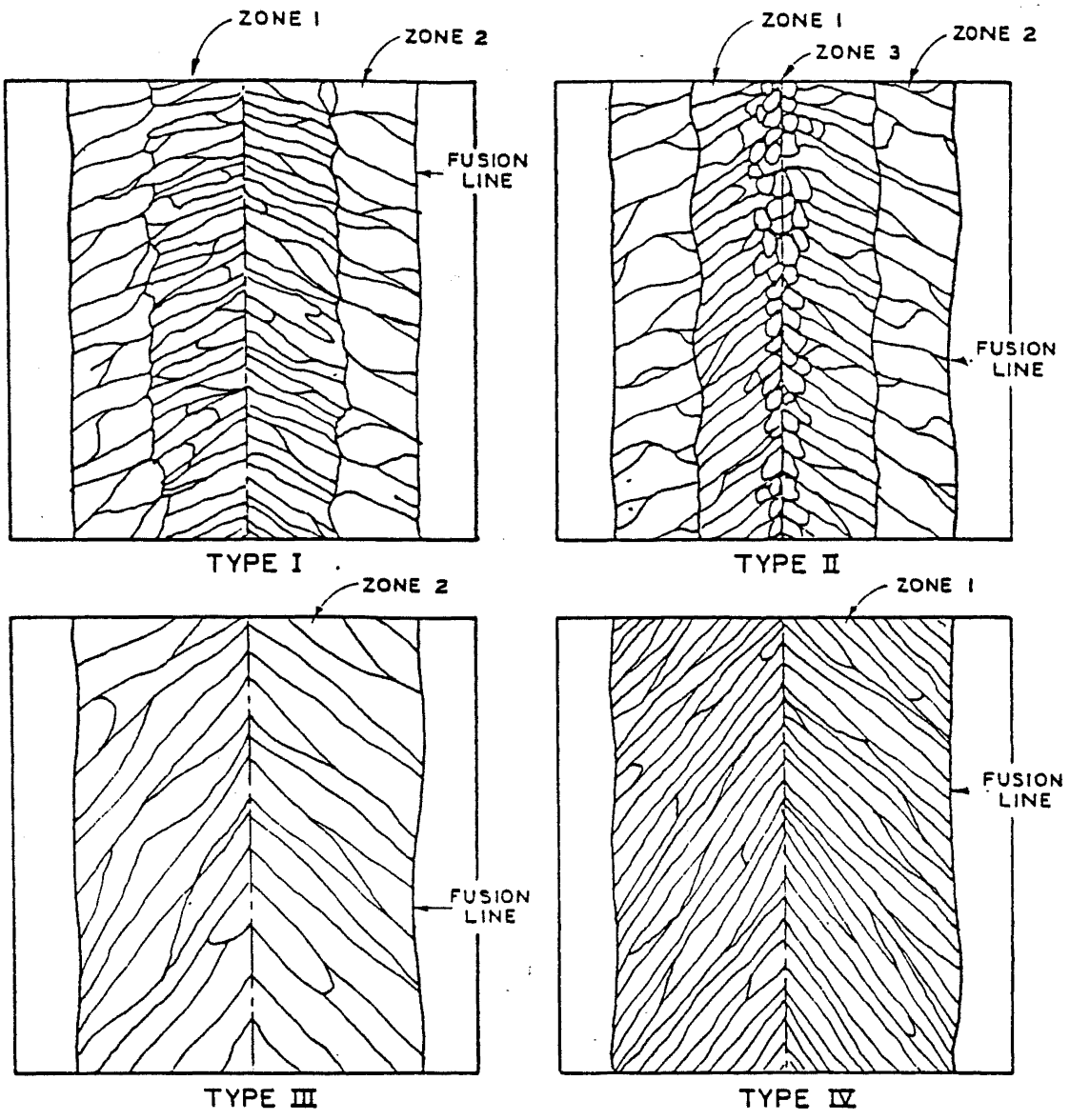

Fig. 40. Sketch of electroslag joint types, longitudinal section through the weld. Type I - coarse (Zone 2) and fine (Zone 1) columnar crystals. Type II - Zones 1 and 2 plus coarse, equiaxed crystals (Zone 3). Type III - all Zone 2 crystals. Type IV - all Zone I crystals (after Ref. 24).

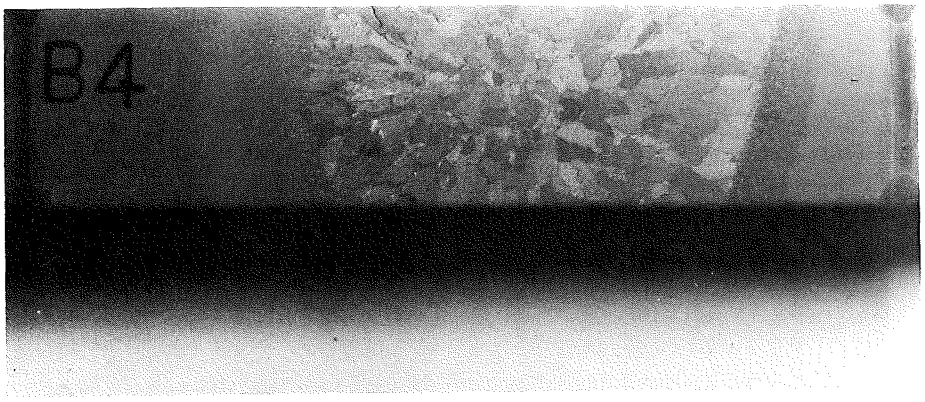

10% Nital etch.

Fig. 41. A transverse section of Type III weldment showing only coarse columnar grains.

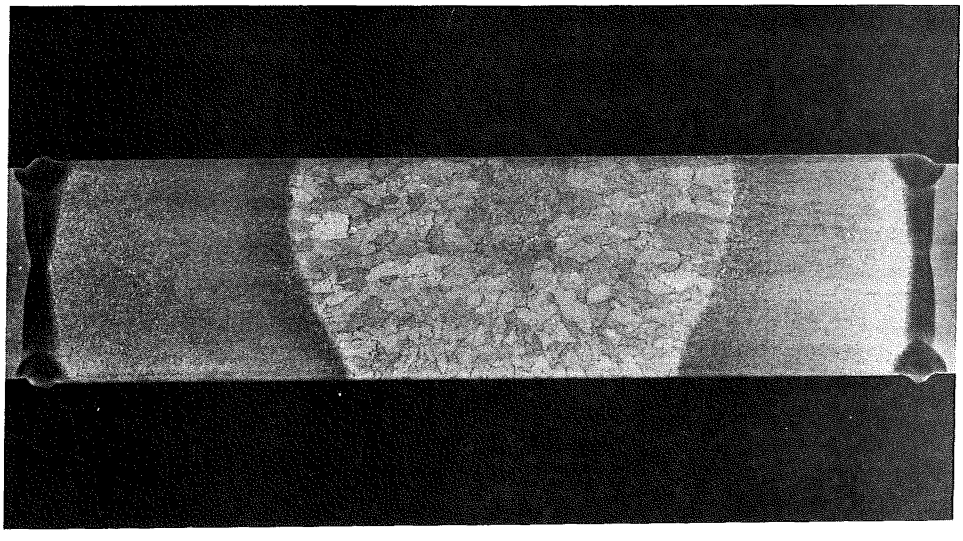

10% Nital etch.

Fig. 42. A transverse section of Type I weldment showing both coarse and fine columnar grains.

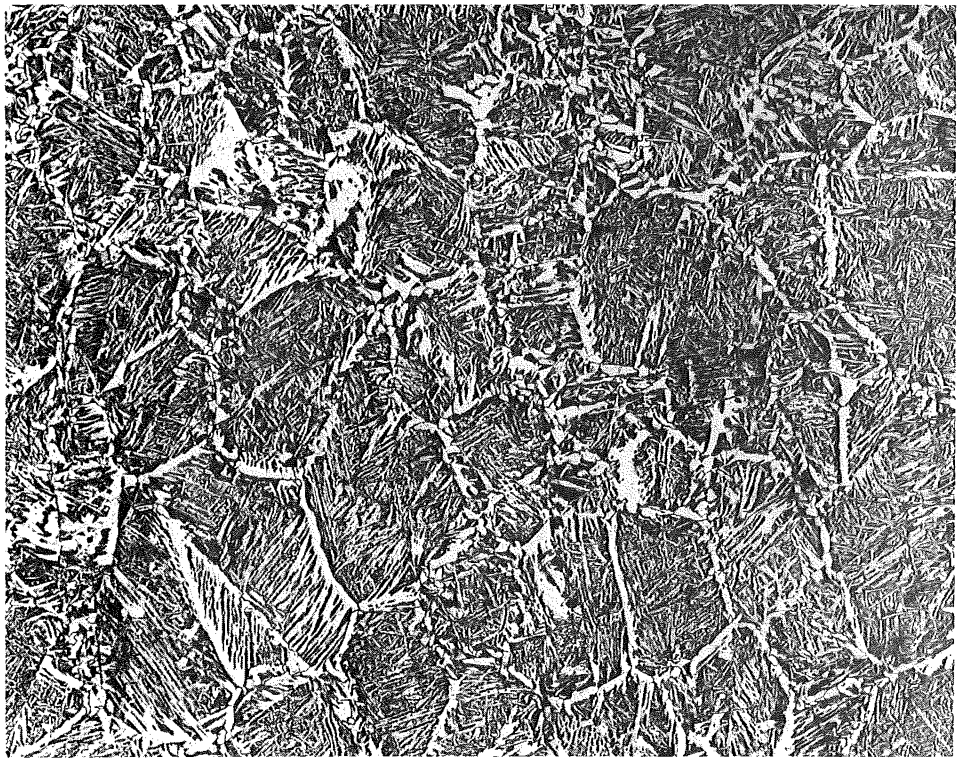

Fig. 43. Coarse grained heat affected Zone I. Mag. 40X 2% Nital etch.

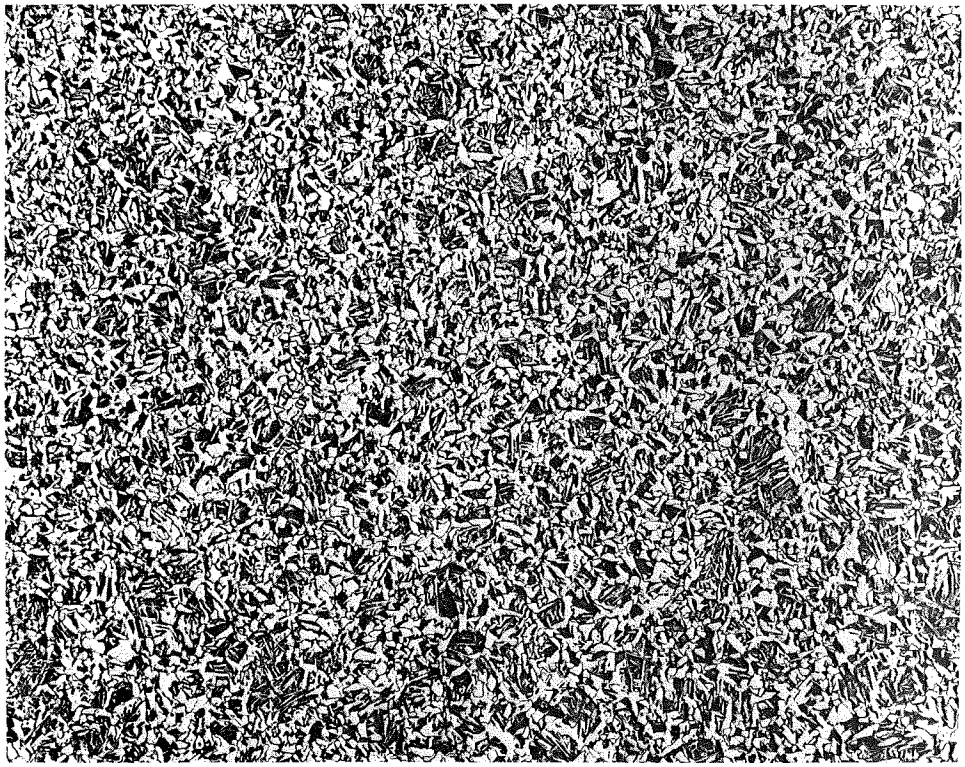

Fig. 44. Fine grained heat affectd Zone II. Mag. 40X 2% Nital etch.

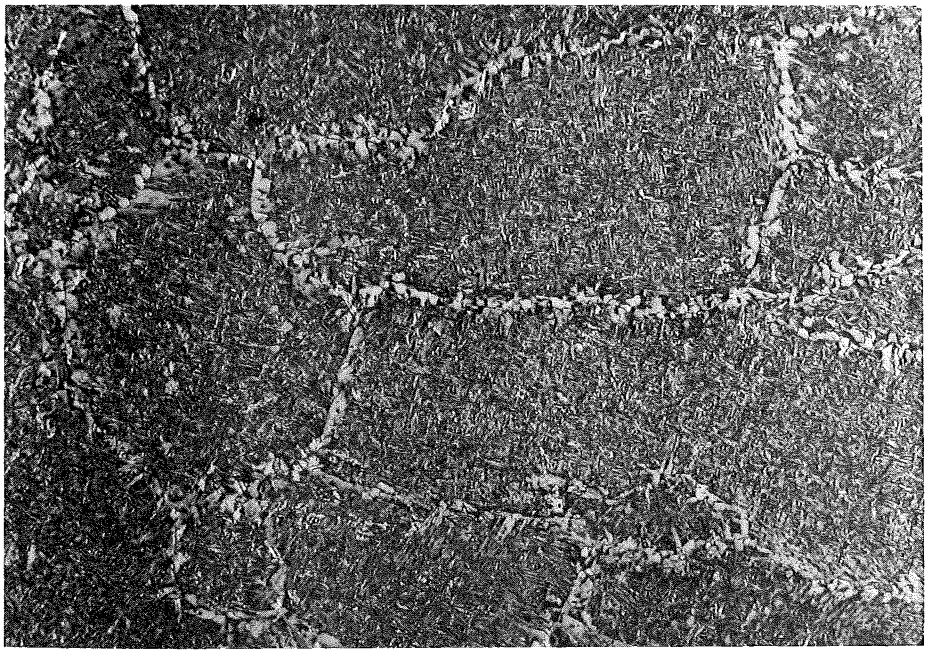

Mag. 40X
2% Nital etch.

Fig. 45. Coarse columnar grains near the weld center, (Zone II).

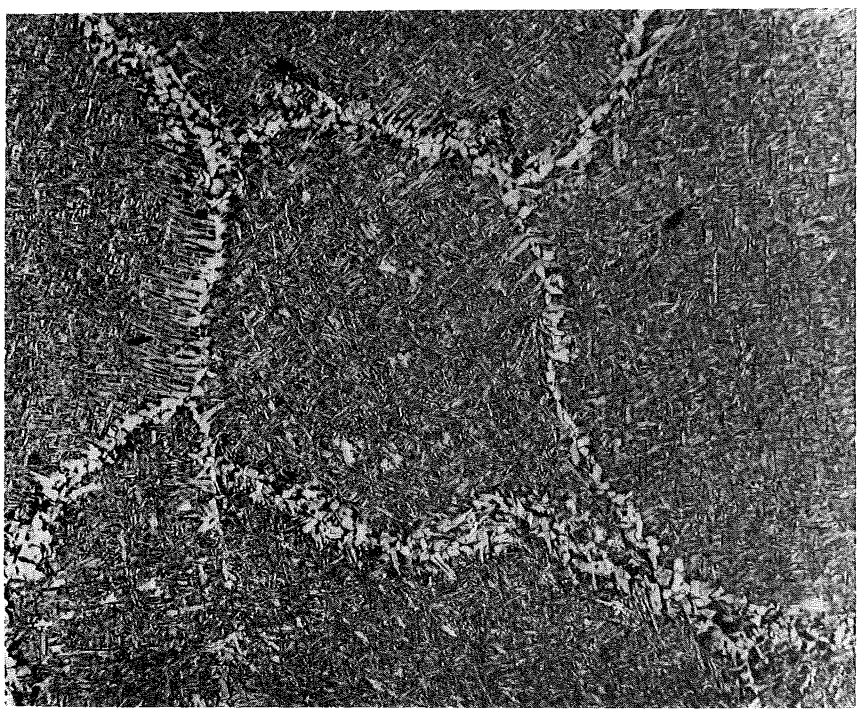

Mag. 40X
2% Nital etch.

Fig. 46. Coarse grains (Zone II) near the fusion line.

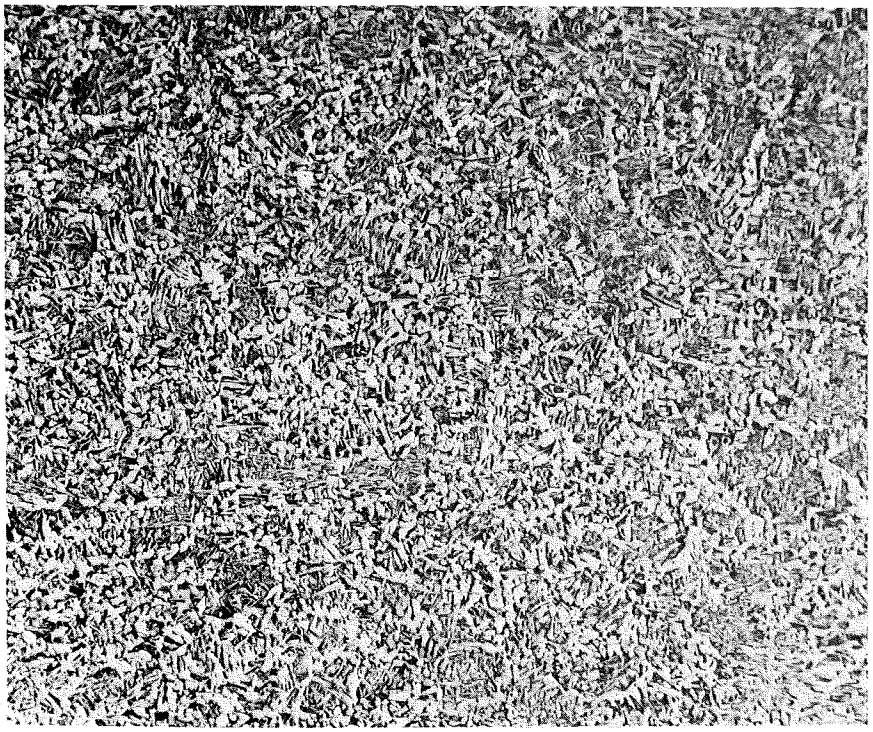

Mag. 40X
2% Nital etch.

Fig. 47. Fine grains (Zone I) near the center of the weld.

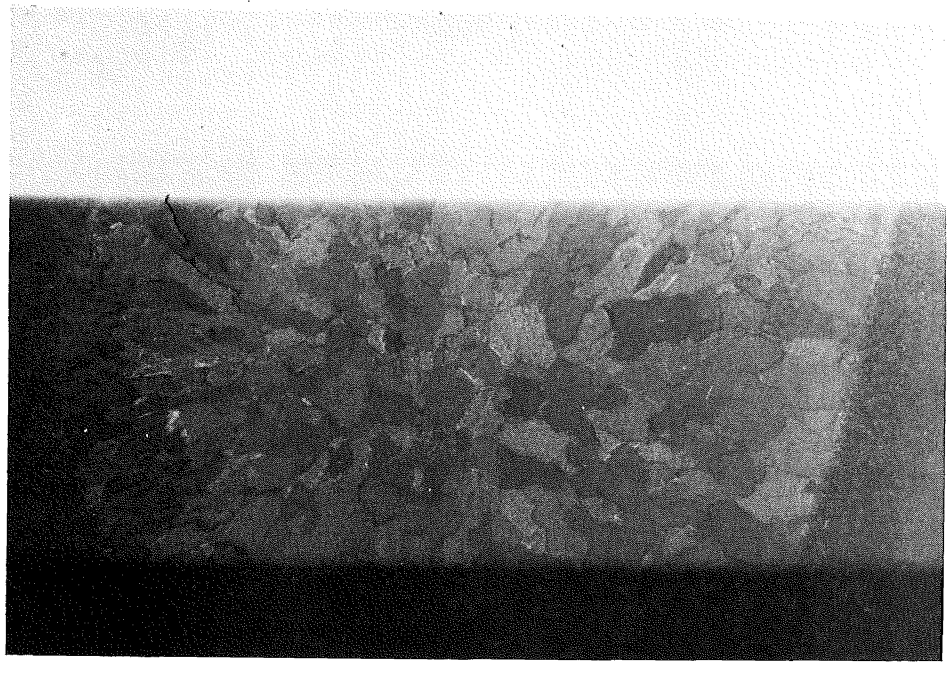

Mag. 2X
10% Nital etch.

Fig. 48. Transverse section of the weldment showing intergranular cracks near the fusion line.

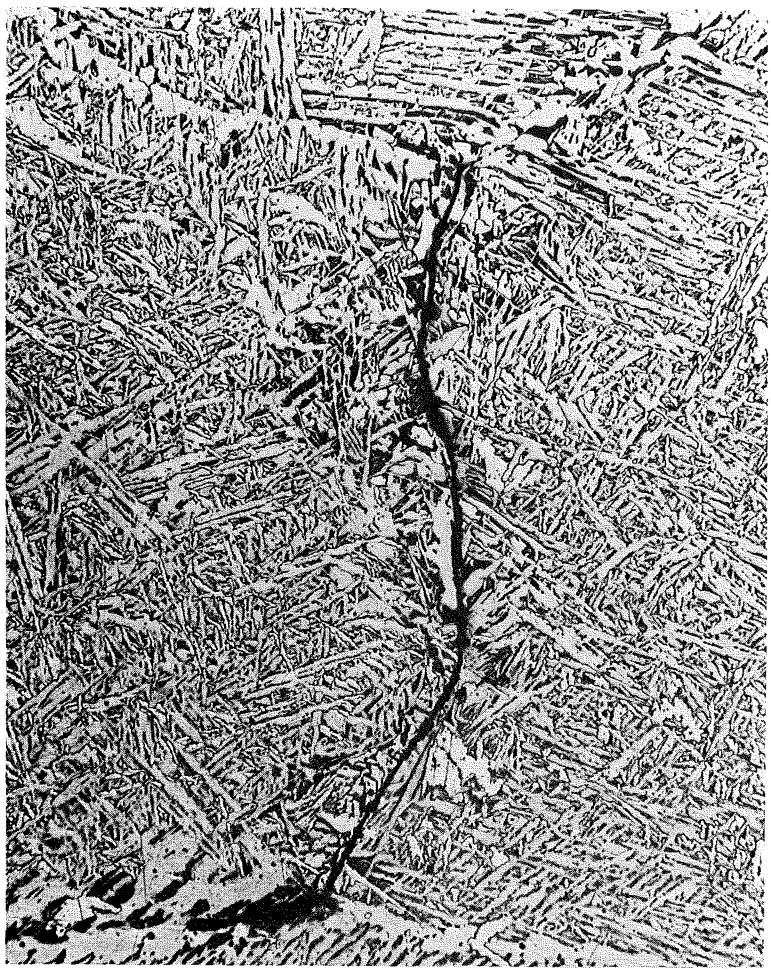

Mag. 125X
2% Nital etch.

Fig. 49. Crack propagation along the ferrite band.

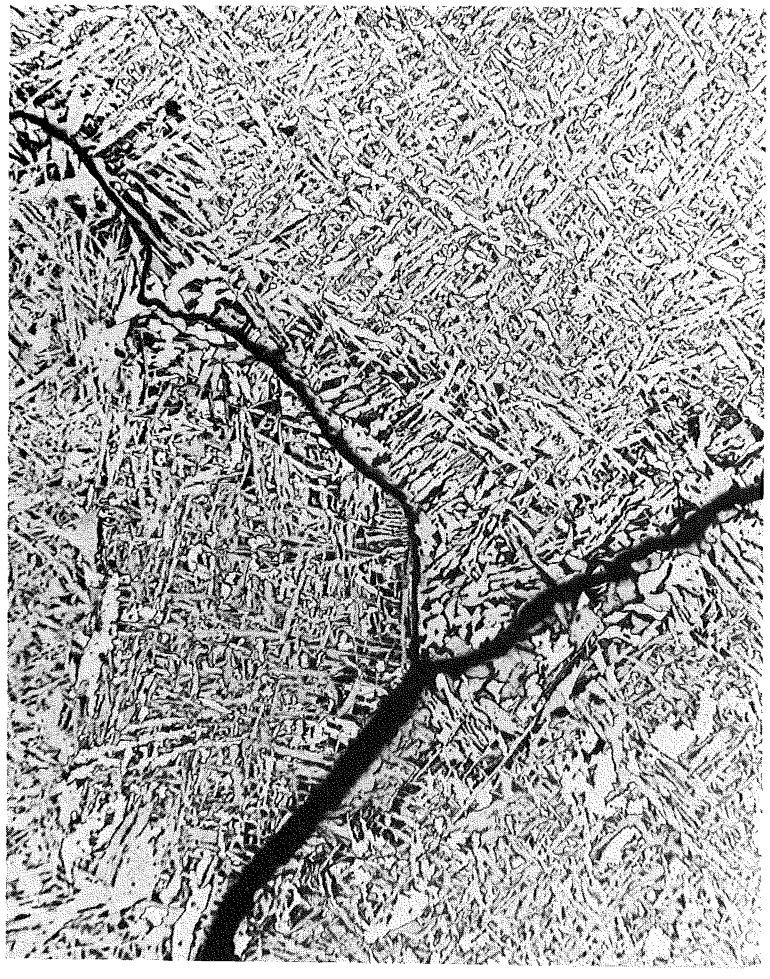

Mag. 125X
2% Nital etch.

Fig. 50. Crack branching along the ferrite network.

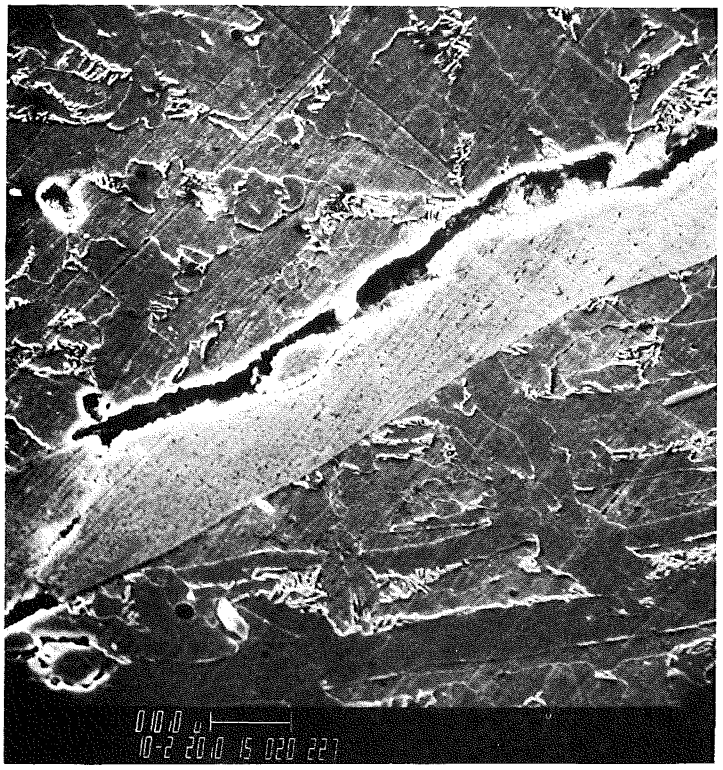

Mag. 1000X
2% Nital etch.

Fig. 51. SEM photograph of a crack filled with copper (Core F).

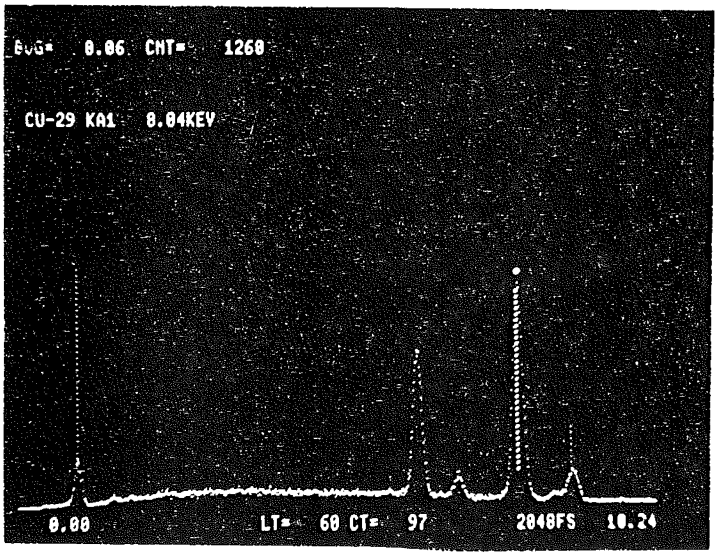

Fig. 52. EDS of the above region.

Mag. 120X
2% Nital etch.

Fig. 53. SEM photograph of a crack emanating from a copper globule.

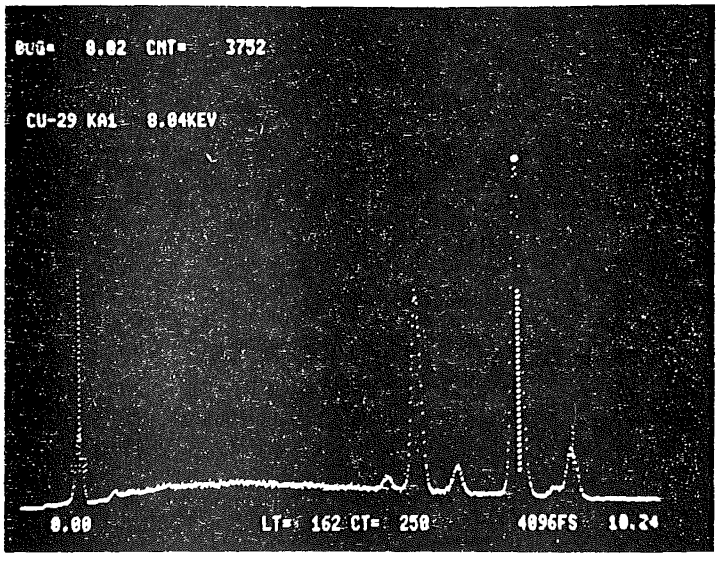

Fig. 54. EDS of the above copper particle.

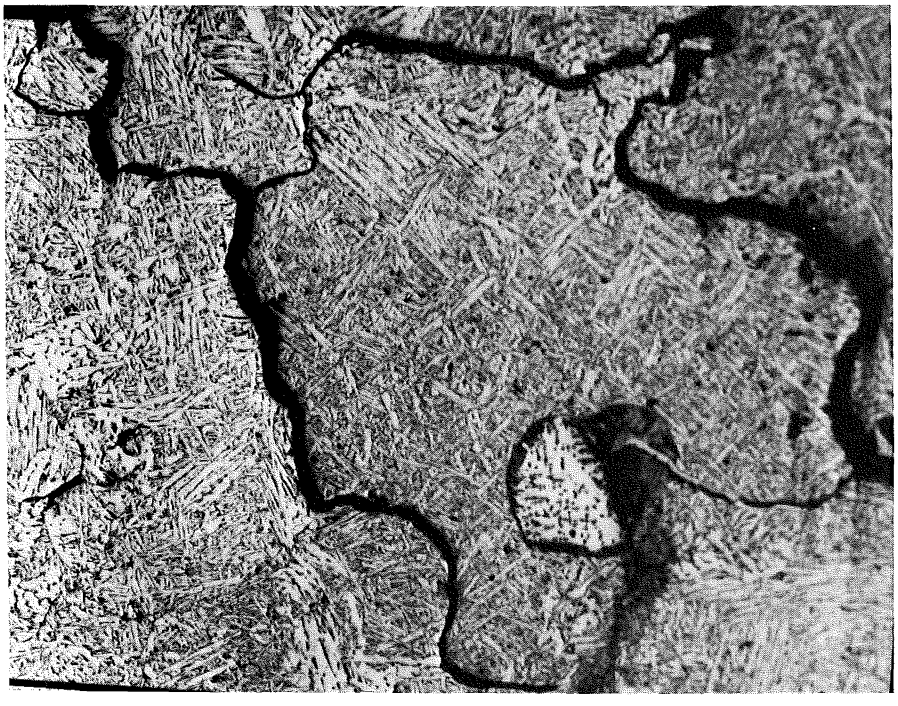

Mag. 40X
2% Nital etch.

Fig. 55. Intergranular cracks along the ferrite bands. Note the copper globule and the crack eminating from it.

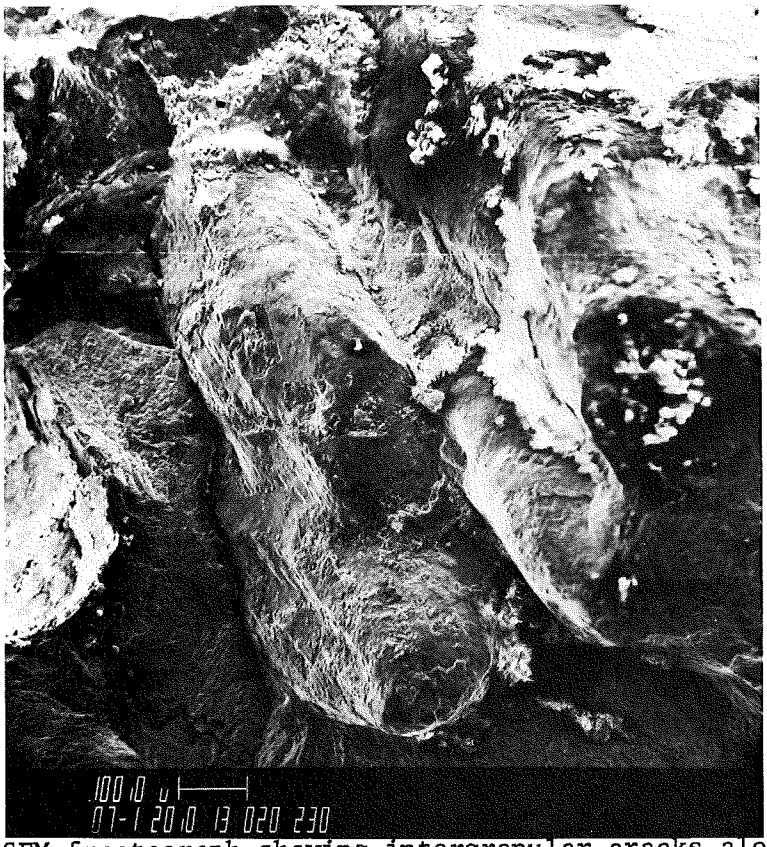

Fig. 56. SEM fractograph showing intergranular cracks along the large columnar grains.

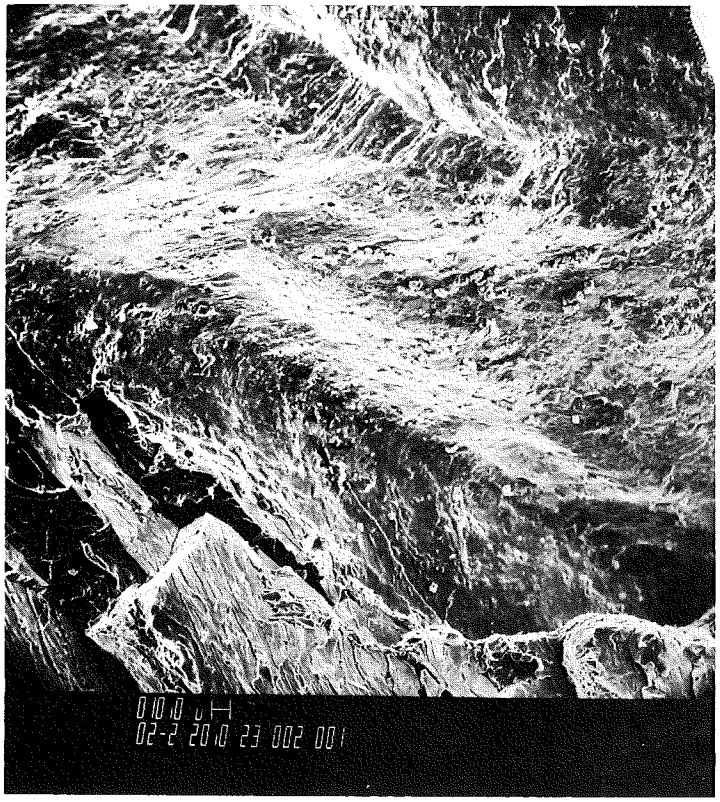

Fig. 57. SEM fractograph of the natural crack tip.

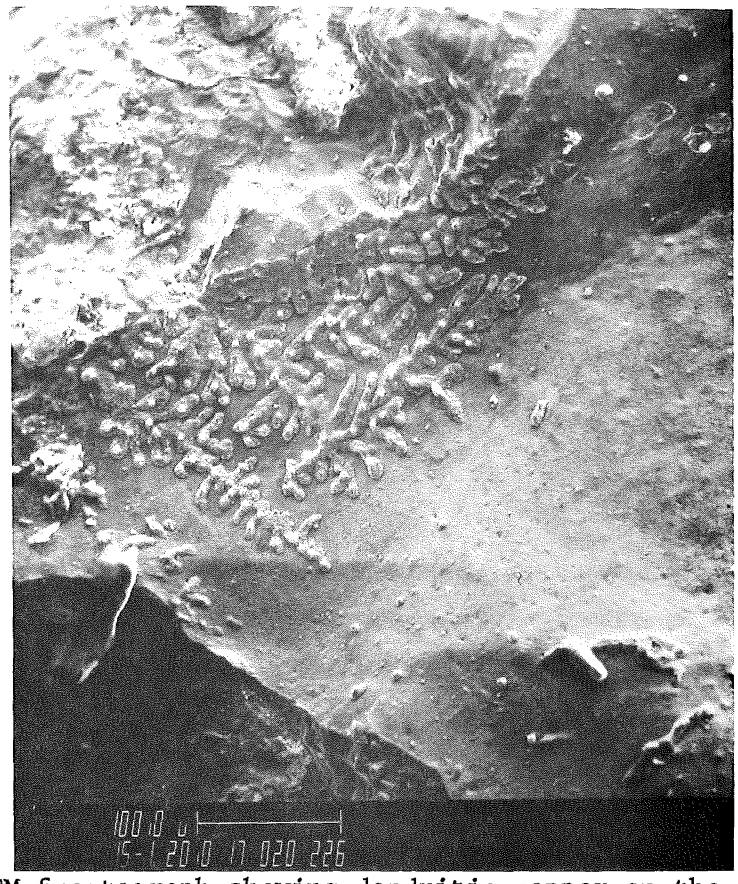

Fig. 58. SEM fractograph showing dendritic copper on the intergranular crack surface (Core F).

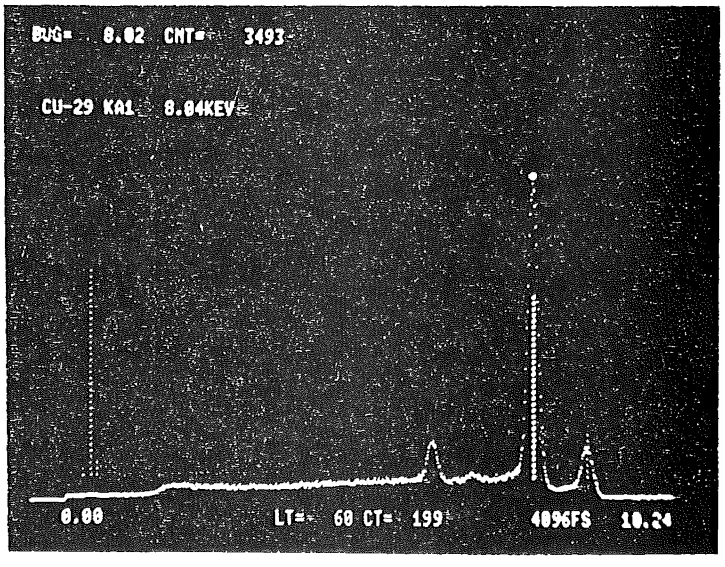

Fig. 59. An EDS of the dendritic region shown above.

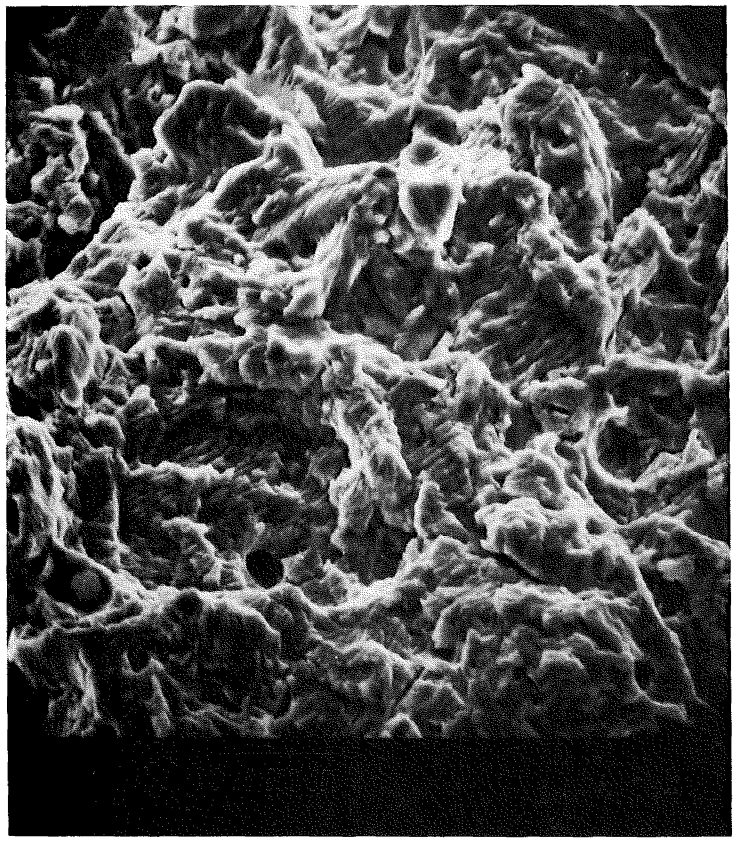

Fig. 60. SEM fractograph showing fatigue striations in the weldment created by laboratory test (Core D).

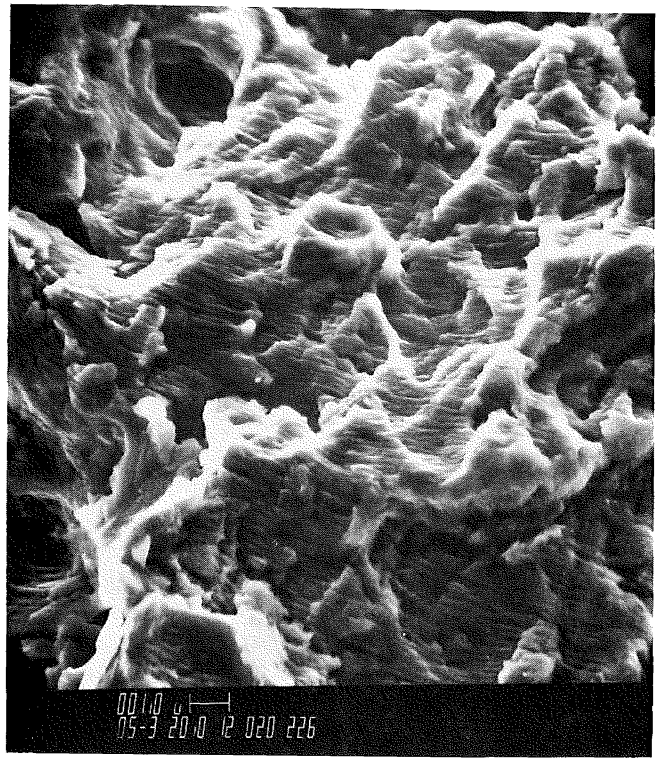

Fig. 61. SEM fractograph showing fatigue striations in the weldment created by laboratory tests (Core E).

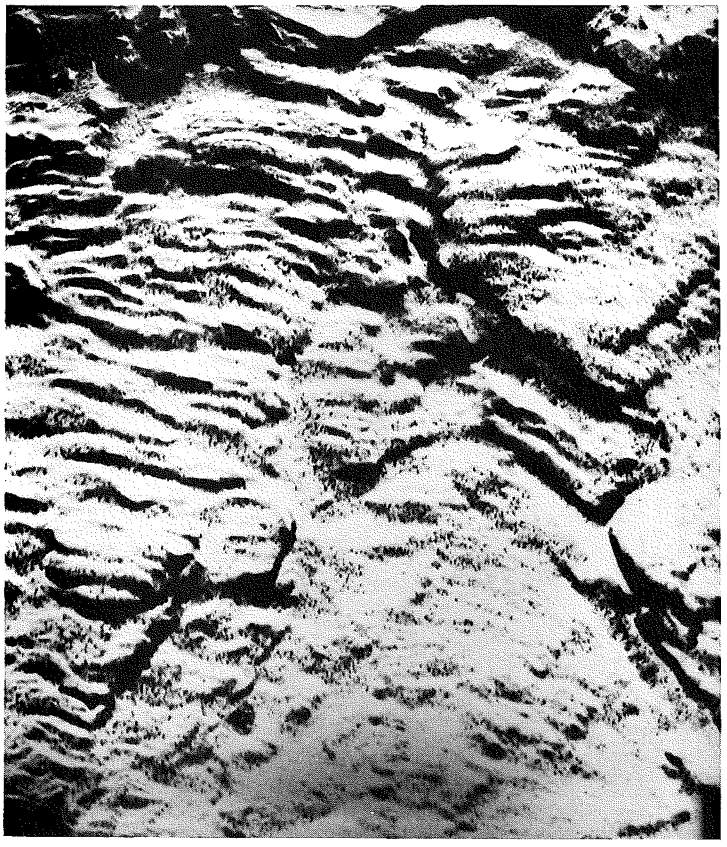

Mag. 34,000X

Fig. 62. TEM fractograph of a replica taken from the tip of the natural crack (Core N).

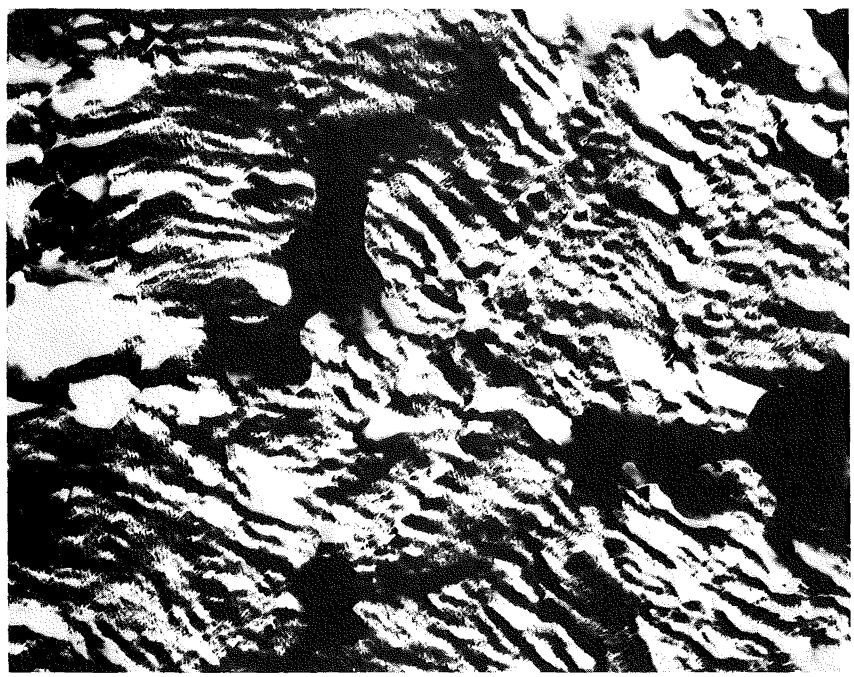

Mag. 29,000X

Fig. 63. TEM fractograph of a replica showing fatigue striations at the tip of the natural crack (Core N).

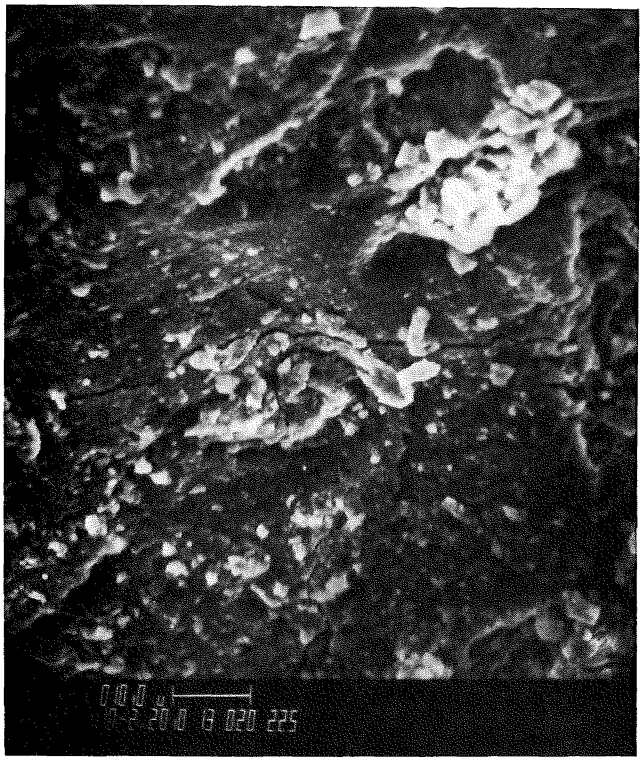

Mag. 1000X

Fig. 64. SEM fractograph of surface of Core N showing heavy corrosion product.

Mag. 100X

Fig. 65. SEM fractograph of surface of Core N showing heavy corrosion product.

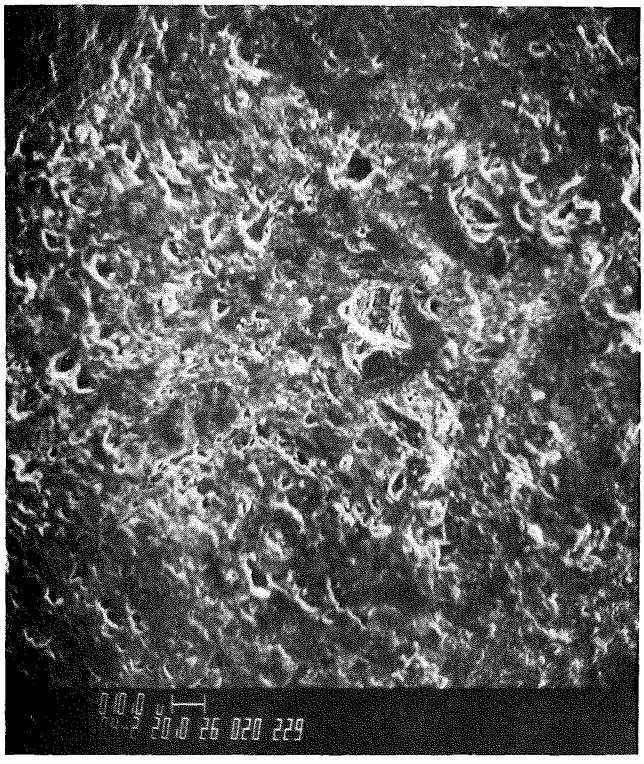

Mag. 4000X

Fig. 66. SEM fractograph of crack surface of Core N with oxide removed by stripping.

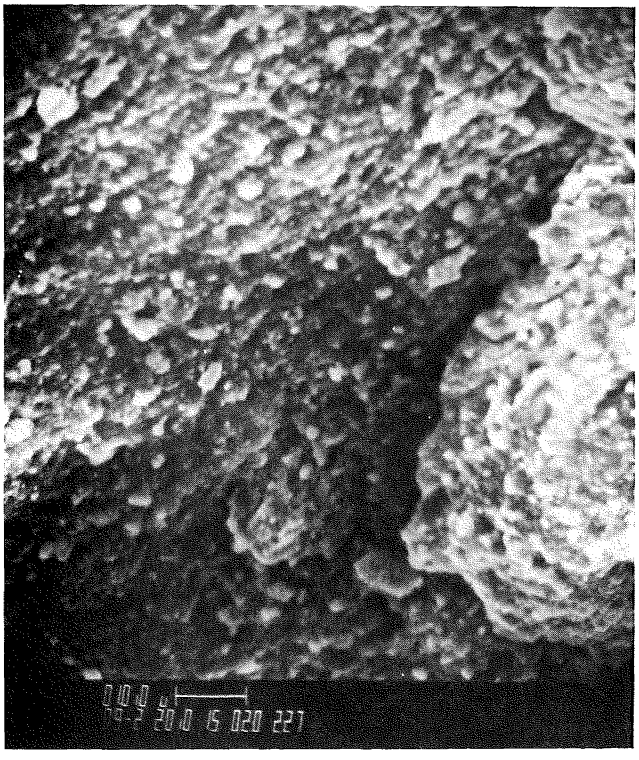

Mag. 9000X

Fig. 67. SEM fractograph of crack surface of Core N with oxide removed by stripping.

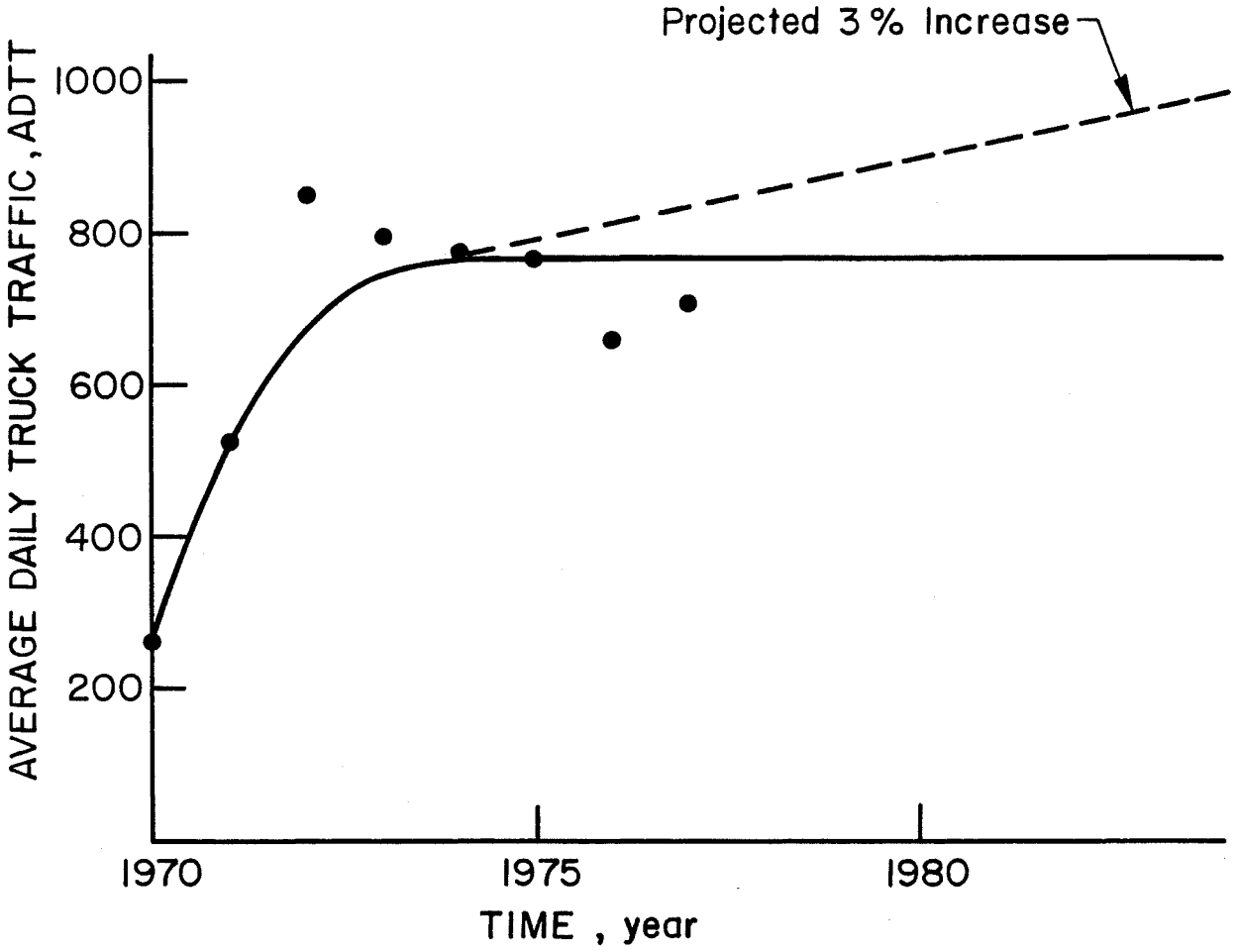

Fig. 68. Average daily truck traffic on I79 at Meadville Bridge.

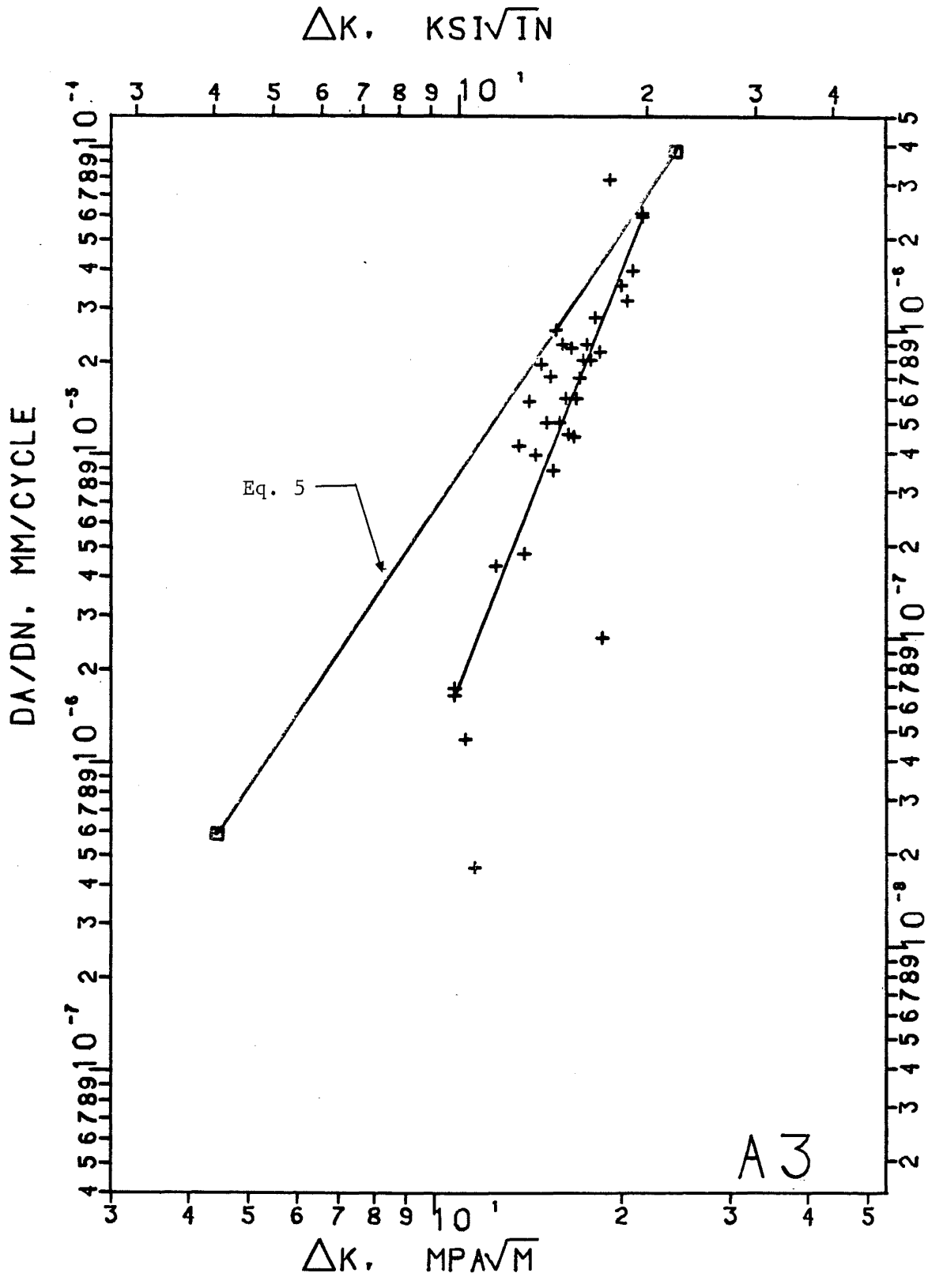

Fig. A1. Fatigue data for specimen A3 with natural cracks at fusion line.

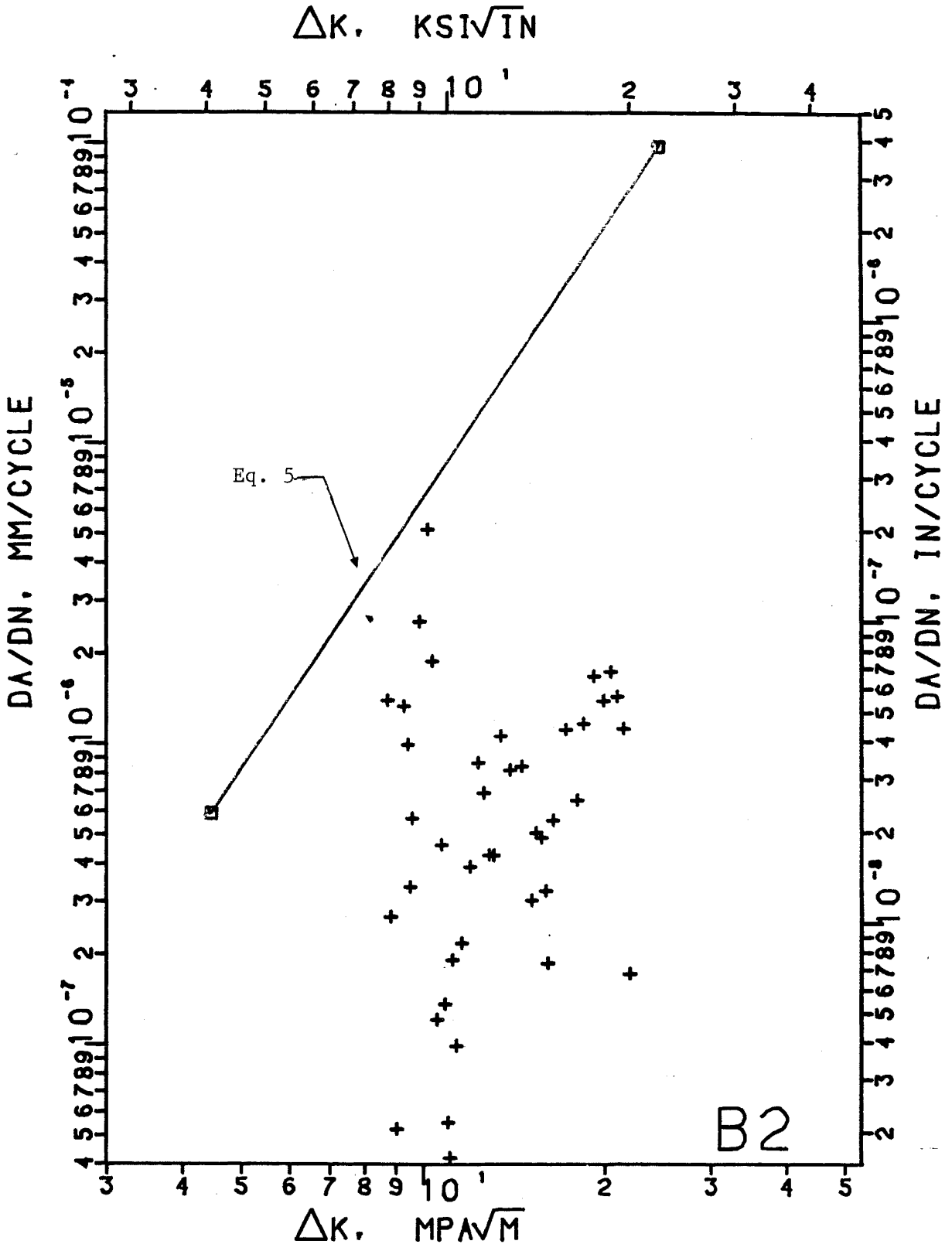

Fig. A2. Fatigue data for specimen B2 with natural cracks at the fusion line.

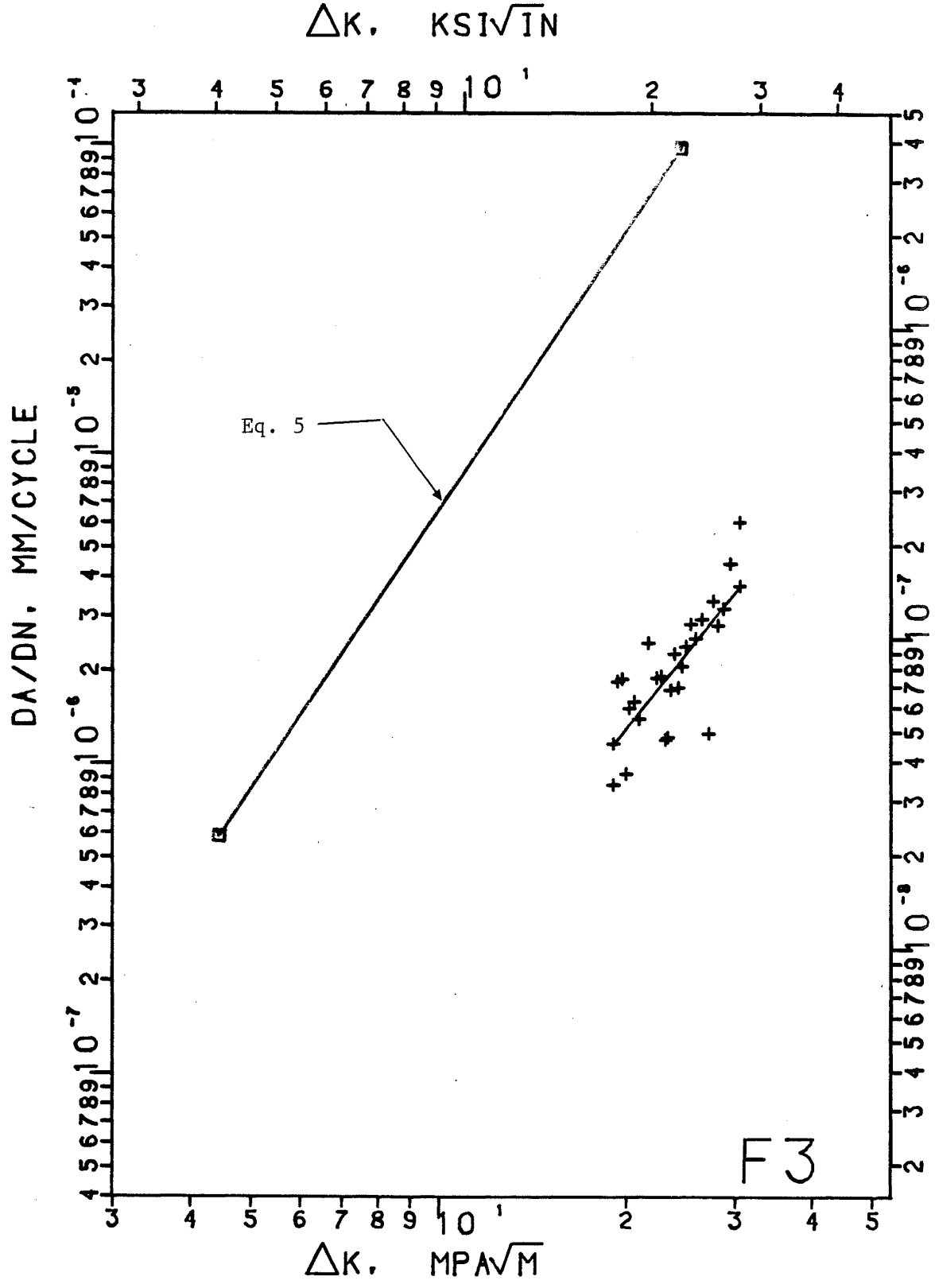

Fig. A3. Fatigue data for specimen F3 with natural cracks at the fusion line.

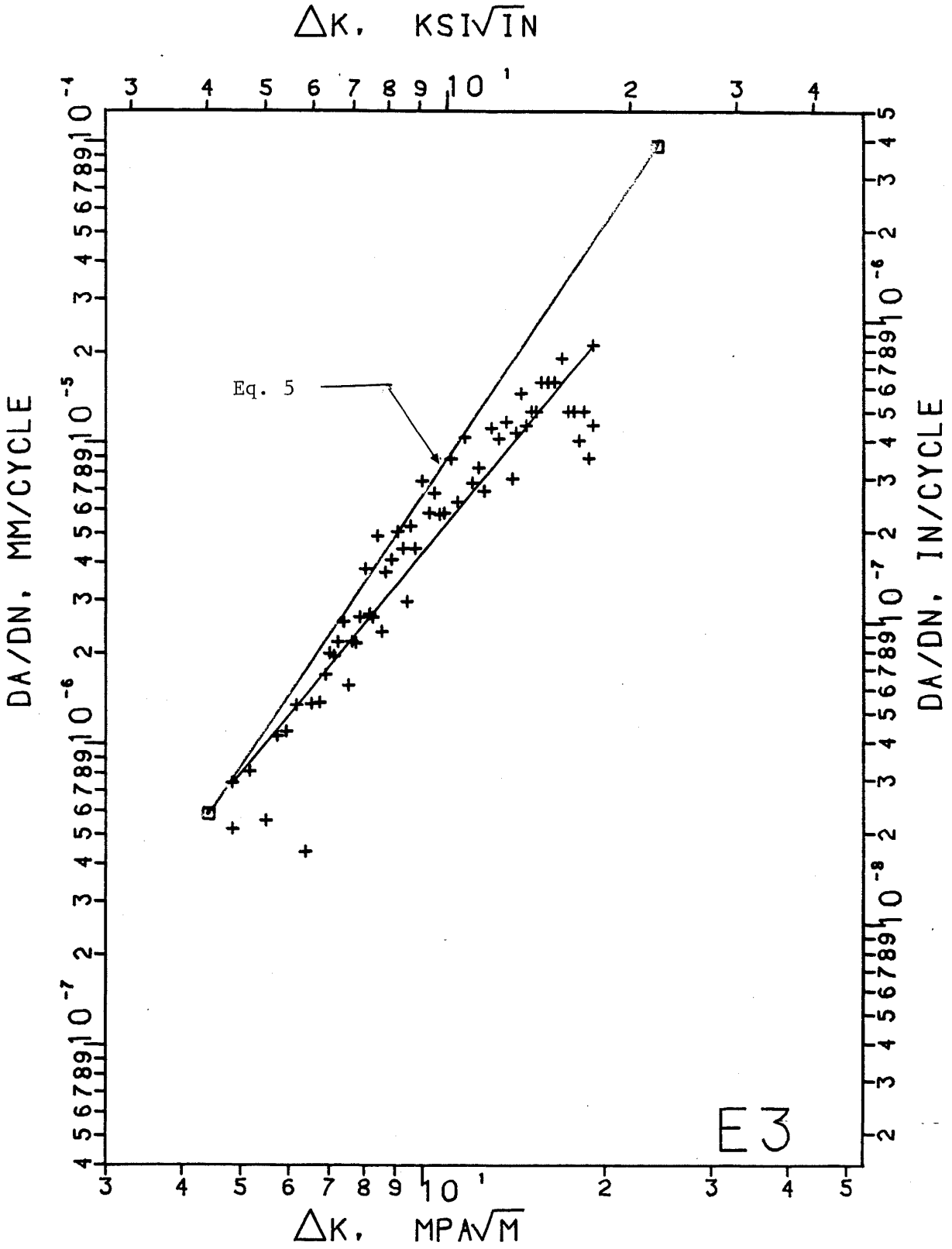

Fig. A4. Fatigue data for specimen E3 EDM notched at fusion line.

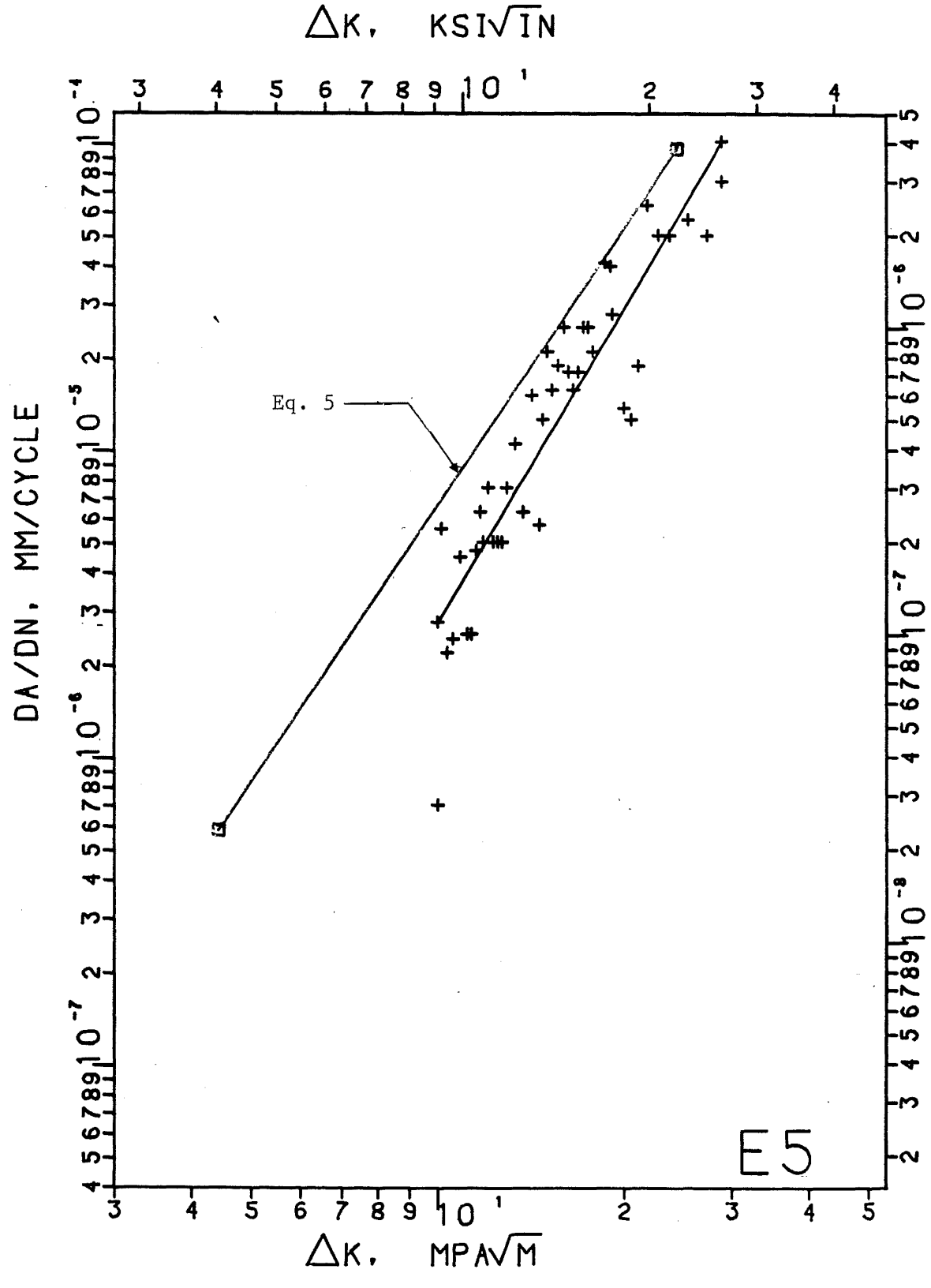

Fig. A5. Fatigue data for specimen E5 EDM notched at fusion line.

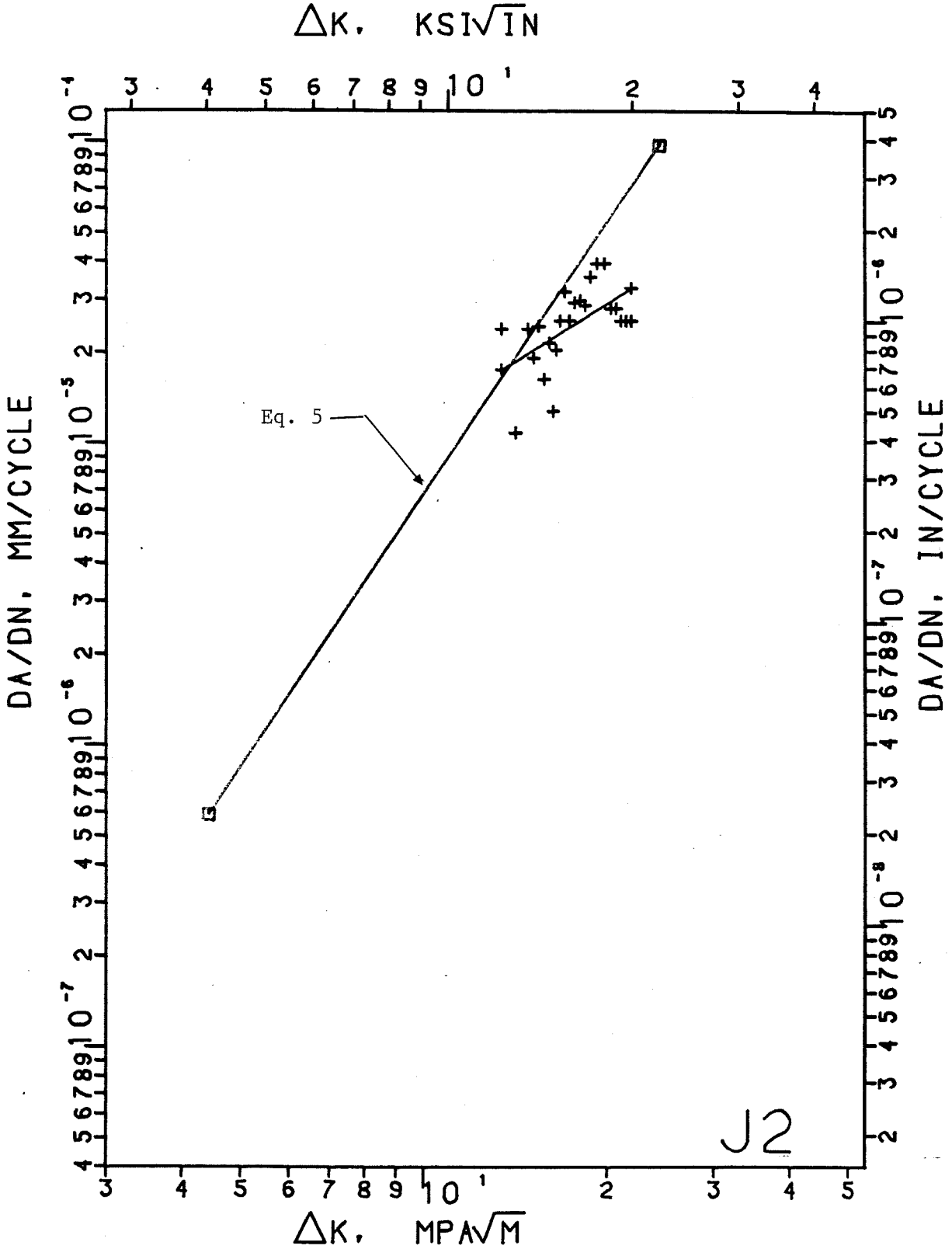

Fig. A6. Fatigue data for specimen J2 EDM notched at fusion line.

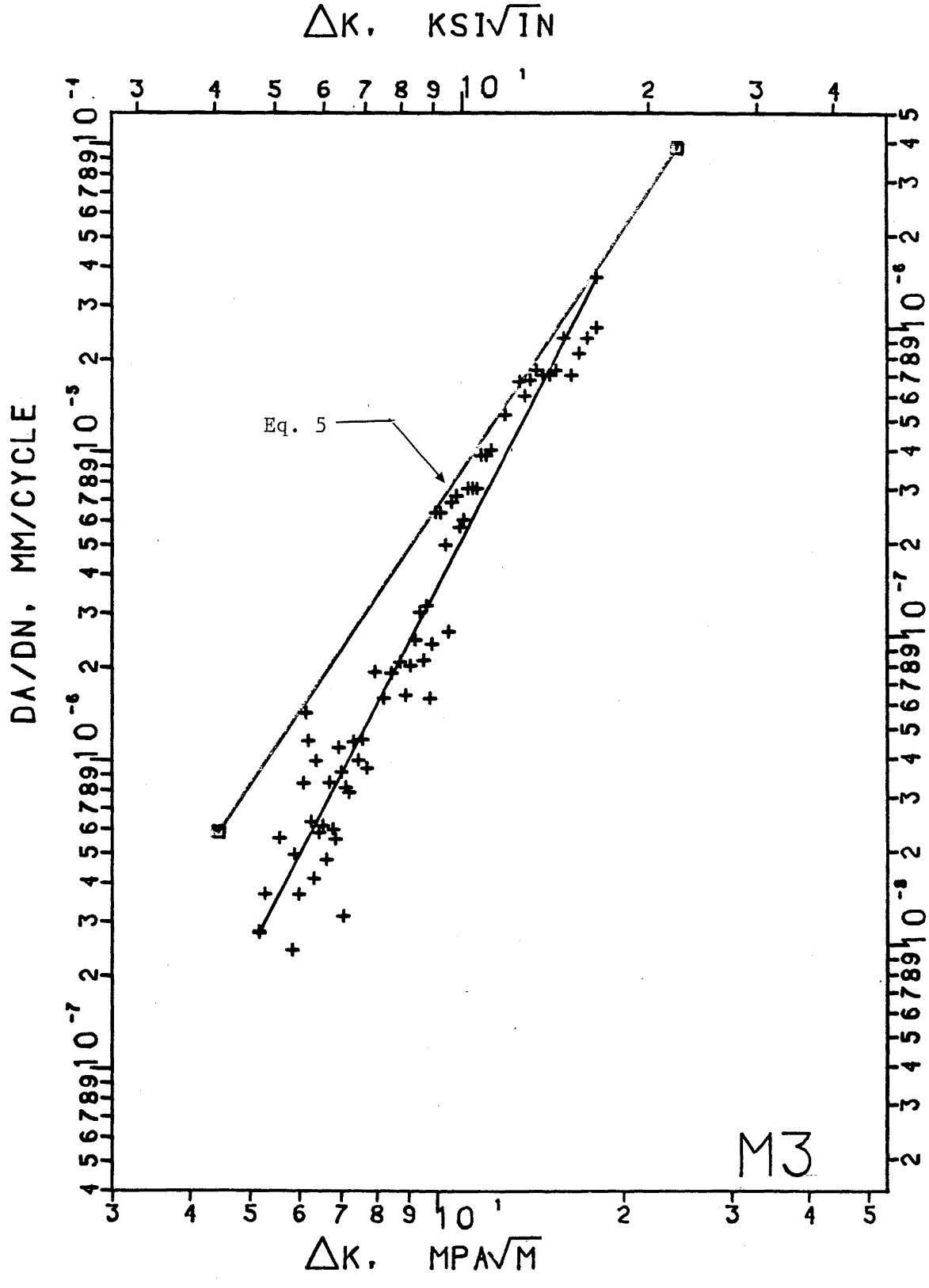

Fig. A7. Fatigue data for specimen M3 EDM notched at fusion line.

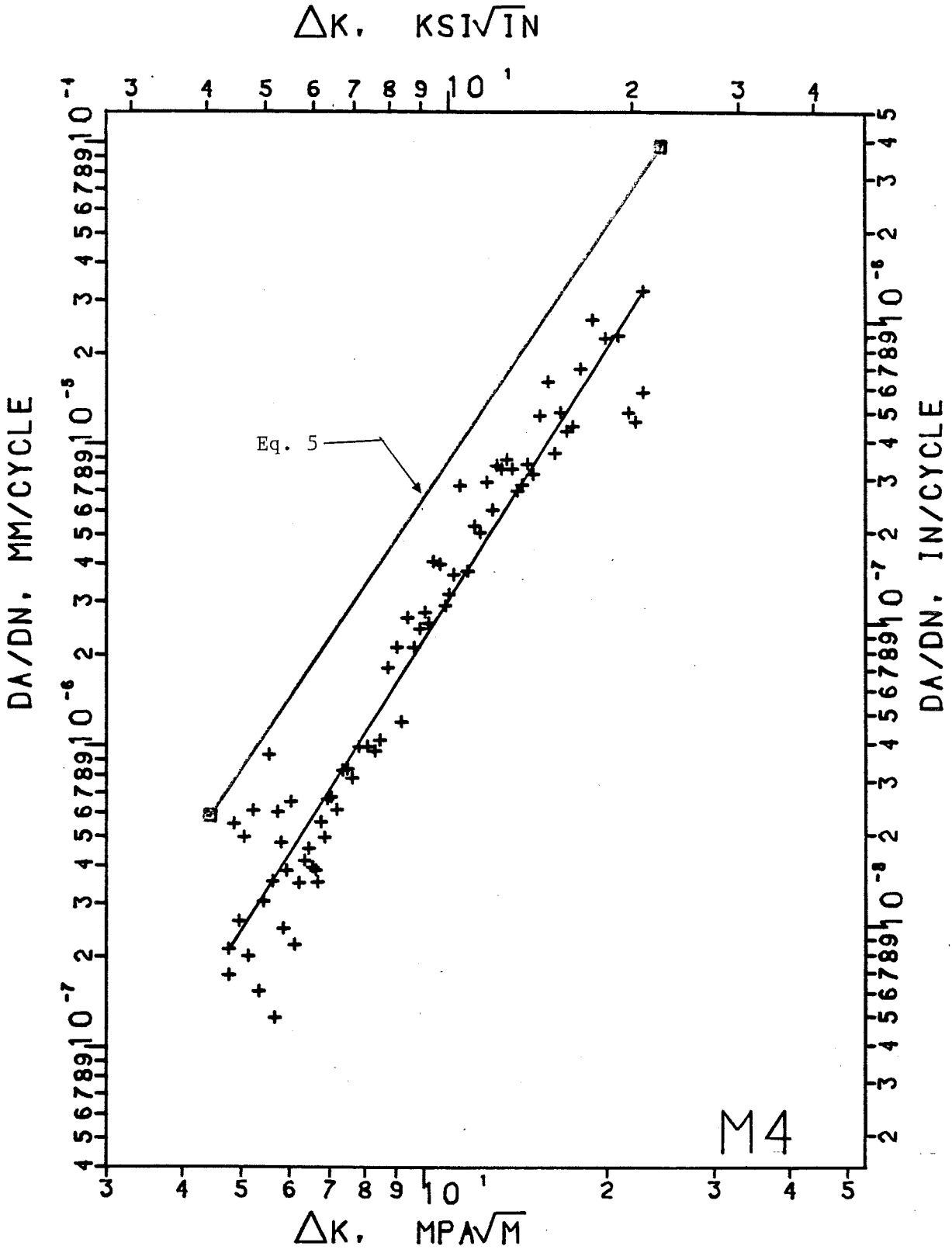

Fig. A8. Fatigue data for specimen M4EDM notched at fusion line.

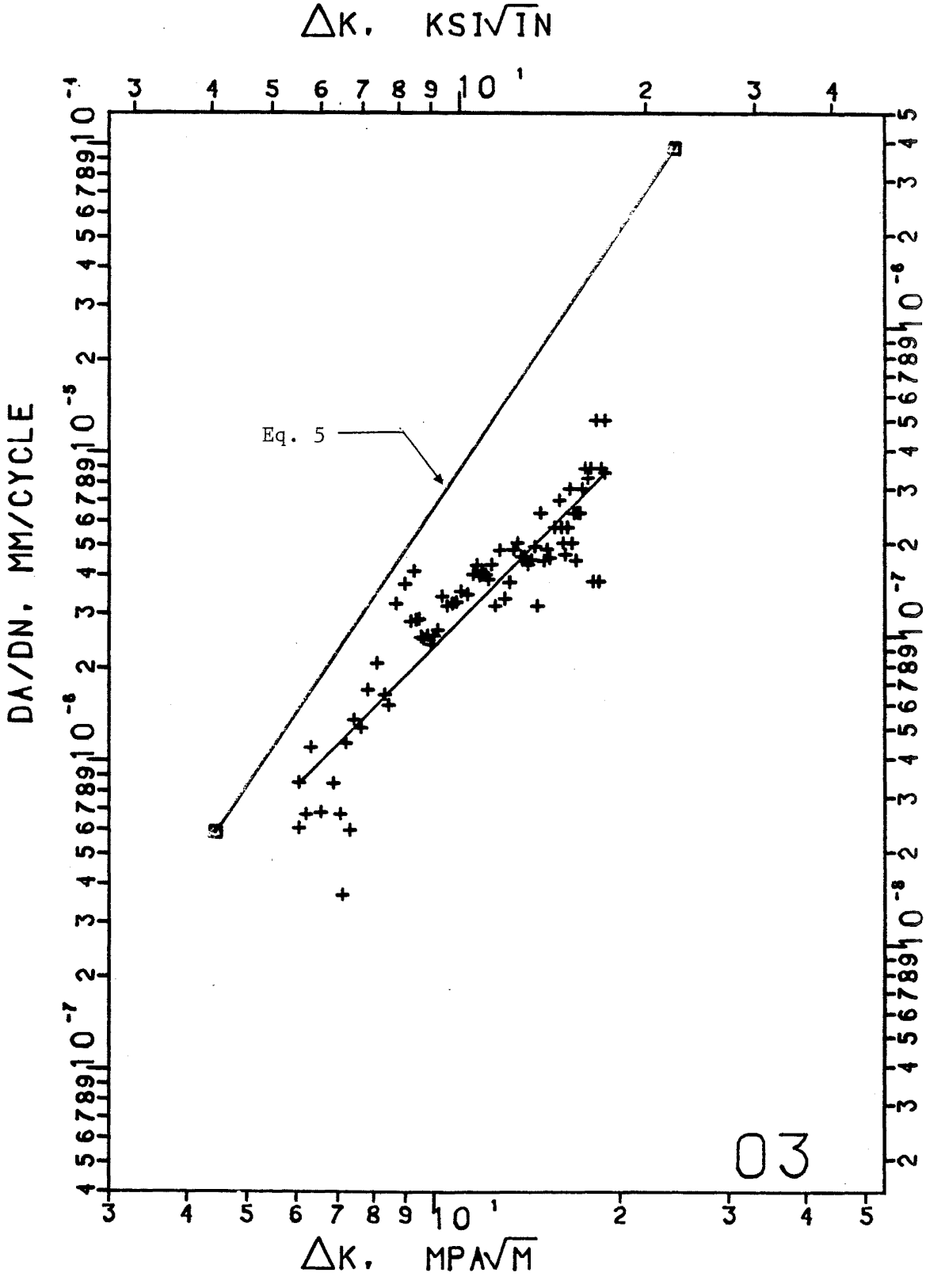

Fig. A9. Fatigue data for specimen 03 EDM notched at fusion line.